In Situ Mass Spectrometry of Polymerising Pulsed Plasmas

CARLETTO, ANDREA

In Situ Mass Spectrometry of Polymerising Pulsed Plasmas

Andrea Carletto

PhD Thesis

Department of Chemistry

Durham University

2019

DECLARATION

The work described in this thesis was carried out in the Department of Chemistry at Durham University between April 2014 and March 2017. The funding for this research was granted by P2i Ltd. It is the original work of the author except where otherwise acknowledged, and has not been previously submitted for a degree in this or any other university.

STATEMENT OF COPYRIGHT

ACKNOWLEDGMENTS

I would like to thank: Professor Jas Pal Badyal FRS for his outstanding yet demanding supervision; Dr. Elina Siokou at P2i Ltd for her insight and useful suggestions; The members from Lab 98 — All of you; The glassblowers, Malcolm and Aaron, for helping me with whatever other people broke, (it wasn't me); Bryan, Kelvin, and Omer from the electronic workshop; Neil and Paul from the mechanical workshop; Dr. Claire Greenwood and Sam Bort at Hiden Analytical helped me fixing the EQP (that was fun). Many thanks to Nicola Menardo; the Italian crew, the Spanish crew, the British crew in Durham.

Thanks to my family.

"If you wait by the river long enough, the bodies of your enemies will float by."

Sun Tzu ,The Art of War

LIST OF PUBLICATIONS

Arising from this Thesis

1 Carletto, A.; Badyal, J. P. S. Mechanistic Reaction Pathway for Hexafluoropropylene Oxide Pulsed Plasma Deposition of PTFE-like Films. *J. Phys. Commun.* **2017**, *1*, 055024.

2 Carletto, A.; Badyal, J. P. S. Ultra-high Selectivity Pulsed Plasmachemical Deposition Reaction Pathways. *Phys. Chem. Chem. Phys.* **2019**, *21*, 16468–16476.

Collaborative Publications

1 von Spreckelsen, R. M.; Harris, M. T.; Wigzell, J. M.; Fraser, R. C.; Carletto, A.; Mosquin, D. P. K.; Justice, D.; Badyal, J. P. S. Bioinspired Breathable Architecture for Water Harvesting. *Sci. Rep.* **2015**, *5*, 16798.

2 Fraser, R. C.; Carletto, A.; Wilson, M.; Badyal, J. P. S. Plasmachemical Double Click Thiol–Ene Reactions for Wet Electrical Barrier. *ACS Appl. Mater. Interfaces* **2016**, *8*, 21832–21838.

3 Gürsoy, M.; Harris, M. T.; Downing, J. O.; Barrientos-Palomo, S. N.; Carletto, A.; Yaprak, A. E.; Karaman, M.; Badyal, J. P. S. Bioinspired Fog Capture and Channel Mechanism Based on the Arid Climate Plant Salsola Crassa. *Colloids Surfaces A Physicochem. Eng. Asp.* **2017**, *529*, 195–202.

4 Gürsoy, M.; Harris, M. T.; Carletto, A.; Yaprak, A. E.; Karaman, M.; Badyal, J. P. S. Bioinspired Asymmetric-Anisotropic (Directional) Fog Harvesting Based on the Arid Climate Plant Eremopyrum Orientale. *Colloids Surfaces A Physicochem. Eng. Asp.* **2017**, *529*, 959–965.

ABSTRACT

Pulsed plasma polymerisation provides an efficient method for the functionalisation of solid surfaces. In comparison to continuous wave plasma conditions, it causes limited monomer fragmentation and leads to high levels of structural retention. Diagnostic studies on such systems have become increasingly common establishing plasma diagnostic techniques as a powerful tool to garner a deeper understanding of the chemistry on which these pulsed plasma deposition processes rely on.

In this work, in situ time-resolved mass spectrometry was employed, operating in both ion and radical species detection mode, to explore the complex nature of the chemical reactions occurring in the plasma phase. The intent of this project is gain insight into reaction pathways of pulsed plasmas, and draw comparisons between conventional step-growth polymerisation (monomer-monomer addition) and pulsed plasma polymerisation routes. Common monomer precursors were investigated under pulsed plasma conditions, namely; 1-decene, allyl glycidyl ether (AGE), hexafluoropropylene oxide (HFPO), glycidyl methacrylate (GMA), maleic anhydride (MAH) and butyl acrylate (BA).

The experimental results confirm that step-growth polymerisation occurs in the plasma phase, via two distinct plasma environments as identified by time-resolved mass spectrometry. Importantly, pulsing electric discharges is demonstrated to limit the monomer fragmentation so that the chemical features of the original monomer precursor remain intact leading to structurally well-defined plasma polymers. Such findings corroborate the results obtained from the characterisation of resulting plasma polymer films that can be found in the literature.

TABLE OF CONTENTS

TABLE OF FIGURES

TABLE OF SCHEMES

TABLE OF STRUCTURES

1 : PLASMA POLYMERISATION

1.1 Plasma Technologies: An Introduction

Plasmas are ionised gases and are often referred to as the fourth state of matter. A plasma is composed of electrons, ions and neutrals which are in fundamental and excited states. These plasma systems are considered electrically neutral from a macroscopic point of view, but they contain free charges and are electrically conductive.[1,2]

Plasma technologies represent a class of industrial processes which make use of a “cloud” of ionised gases (plasmas) that interacts with a surface (or substrate). In fact, the reactive nature of plasma systems can be employed to generate a large number of chemical reactions occurring within the plasma phase or at plasma-surface interfaces. These interactions are usually categorised in three main groups, according to the industrial application: *etching*, or removal of material, often in a selective manner; *surface modification*, when chemical functional groups are incorporated in the outermost surface layer, and *deposition*, wherein a distinct material with a different chemical make-up is formed at the surface.[3,4]

These plasma-based techniques have become increasingly appealing to manufacturing industry as they represent key technological tools for fabricating commodities that can be found in everyday life.[5] For instance, plasmas are heavily utilised in the electronic industry for semiconductor deposition and surface modification.[6,7,8] Industrial plasmas are also employed to deposit low-volume high-value functional layers that can confer optical, electrical, magnetic, mechanical or barrier properties.[9] Among industrial plasmas, polymerising plasmas have generated an immense interest from researchers, because they are relatively inexpensive, solvent-free, and ultimately provide a direct method for the functionalization of solid surfaces with organic thin films. In the following paragraph an overview on plasma polymerisation processes, pioneering mechanistic studies and the evolution to pulsed plasma deposition methods is given.

1.2 Plasma Polymerisation

1.2.1 Principles

Plasma polymerisation techniques are used for the fabrication of thin films and coatings for numerous applications ranging from optics and optoelectronics to aerospace, automotive, biomedical, microelectronics, fabrics, and many others.[10,11,12,13,14] These organic thin films are obtained from the plasma activation of an organic precursor mainly via electron impact collisions, Figure 1.1. This is a solvent-free method which allows to obtain organic thin films with good adhesion properties on many different substrates and the possibility of using an exceptionally wide range of chemical precursors and any volatile compound including saturated ones, may be virtually employed.[15,16] Plasma polymers are characterised by an intrinsic crosslinked structure, due to the chemical bond dissociation of precursors that occurs in the plasma, that confers interesting properties such as excellent mechanical resistance and thermal stability to the final organic film.[17,18] However, because the plasma is operated in continuous wave mode (constant stream of electrons colliding with the molecules in the gas phase), the plasma precursors are randomised, breaking down into radicals or ions and a high level of precursor fragmentation is reached. Therefore, the chemical functional groups derived from the original precursor molecule are lost, leading to a poor chemical control of the plasma polymer composition.[19]

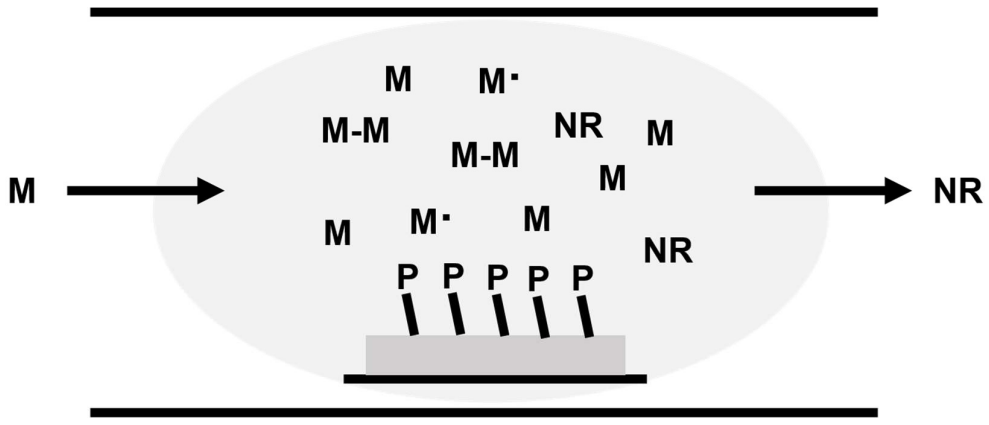

Figure 1.1: Schematic representation of a plasma reaction. M: Monomer, M•: Reactive monomer species, M-M•: Polymerised reactive species, P: Polymer on the surface, NR: non-reactive species.

1.2.2 Proposed Mechanistic Models

Several works on plasma polymerisation mechanisms can be found in the literature, where kinetic aspects and radical/ionic character appear to be the main focuses of these studies. In the following paragraph, some of the pioneering studies aiming at achieving a better understanding the chemistry and physics behind plasma polymerisation are reported and briefly described.

Early models for plasma polymerisation were mainly based on ionic mechanism within the adsorption layer, where the polymerisation rate can be written as $m=\alpha \cdot I \cdot t$, with m being the deposited polymer mass per area, α the adsorption constant, I the current density at the electrodes and t the deposition time.[20] Other fundamental works on glow discharge polymerisation, described the reaction pathway as the result of activated radical species, generated by plasma excitation, which then recombine to form the organic polymer film. The radical plasma reaction proceeds by sequential addition of monomer units resulting in chain growth ($R_n\bullet + M \rightarrow R_{n+1}\bullet$) and radical recombination processes ($R_n\bullet + R_m\bullet \rightarrow P_{n+m}$). The kinetic model can be expressed analytically by the relationship between the radical formation rate and the pressure of the monomer precursor.[21,22] Later on a similar approach was used, introducing the concept of inert gas and its capability to transfer energy to organic monomers.[23] This improved and widely accepted kinetic model assumes that the monomer precursors can be activated by both plasma and inert gas at the same time (energy transfer), this is followed by the initiation step with subsequent radical formation ($M^* \rightarrow M\bullet$) and chain propagation ($R_n\bullet + M \rightarrow R_{n+1}\bullet$). Relevant information about the plasma phase chemistry and reaction pathways can also be obtained by studying different classes of reactive monomer precursors in relation to the behavior shown in a plasma environment and to the resulting polymer film.[24] Several categories can be identified according to retention of monomer structure, fragmentation of large unsaturated species or polymerization of large fragments.

1.2.3 Pulsed Plasma Polymerisation

In view of its high potential for material surface modification, plasma polymerisation has been further improved, in the search for organic deposits with stable and selective chemistry.[25,26,27,28] Over the years researchers have developed a new technique that consists in pulsing the plasma, in order to reduce the overall power input. This new method offers the possibility to overcome the main drawback of continuous wave plasma deposition where the monomer precursors undergo excessive fragmentation levels. Pulsed plasma polymerization techniques have been proven to be very effective; in fact the chemical process is remarkably enhanced due to a better control of the energy dissipation in the gas.[29,30]

Operating in pulsed conditions, the plasma is intermittently generated according to the pulse frequency, which is strictly dependent on the duty cycle. The duty cycle (*DC*) indicates the relationship between the plasma on-time (t_{on}) that represents the time frame in which the plasma is on and the off-time (t_{off}) where the plasma is absent.[31] This physical quantity is expressed analytically by Equation (1.1):

$$DC = \frac{t_{on}}{(t_{on} + t_{off})} \tag{1.1}$$

The mean power *P* is then defined as the average energy dissipated in the plasma over the pulse period (t_{on}+t_{off}), with P_{on} being the continuous wave power introduced in the system during t_{on} time frame, Equation (1.2):

$$P = P_{on} \frac{t_{on}}{(t_{on} + t_{off})} \tag{1.2}$$

The duty cycle is often modulated, in order to control the retention of the chemical group hosted by the chemical precursor in the organic film deposited, although it has been shown that the amount of power input P_{on} is also crucial to obtain well-defined plasma polymers.[2,32,33] The retention of the chemical structure associated with the precursor molecule is a key factor to take in account in pulsed plasma polymerisation processes and this can be seen in terms of amount of preserved chemical functionalities of original precursor in the final organic deposit, Figure 1.2.[34,35]

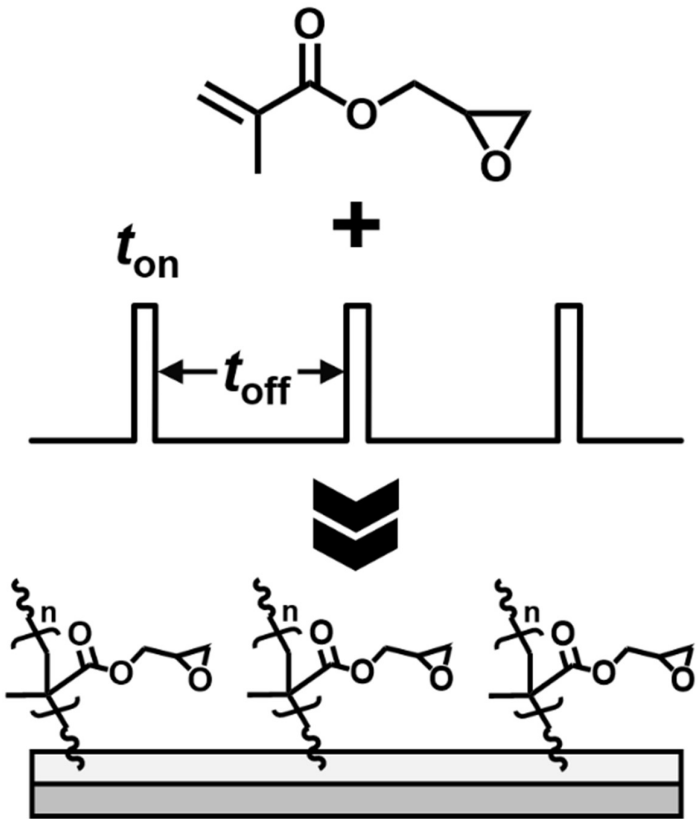

Figure 1.2: Example of pulsed plasma deposition of glycidyl methacrylate (GMA) on a silicon substrate. High selectivity and improved monomer retention can be attained by using low duty cycle pulsed electrical discharges.

REFERENCES

1 Boenig, H. V. Fundamentals of Plasma Chemistry and Technology, Technomic Publishing Co., Inc.: Lancaster, PA, 1988.

2 Yasuda H., Plasma Polymerization, Academic Press, Orlando, Florida, 1986.

3 d'Agostino, R. Plasma Deposition, Treatment and Etching of Polymer Films, Academic Press, Inc.: San Diego, CA, 1990.

4 Stillahn, J. M.; Trevino, K. J.; Fisher, E. R. Plasma Diagnostics for Unraveling Process Chemistry. *Annu. Rev. Anal. Chem.* **2008**, *1* (1), 261–291.

5 Lieberman A. M.; Lichtenberg A. J.; Principles of Plasma Discharges and Materials Processing, John Wiley & Sons, Inc., Hoboken, New Jersey, 2005.

6 Cunge, G.; Vempaire, D.; Ramos, R.; Touzeau, M.; Joubert, O.; Bodard, P.; Sadeghi, N. Radical Surface Interactions in Industrial Silicon Plasma Etch Reactors. *Plasma Sources Sci. Technol.* **2010**, *19*, 034017.

7 Williams, K. L.; Butoi, C. I.; Fisher, E. R. Mechanisms for Deposition and Etching in Fluorosilane Plasma Processing of Silicon. *J. Vac. Sci. Technol. A Vacuum, Surfaces, Film.* **2003**, *21*, 1688–1701.

8 Kushner, M. J. A Model for the Discharge Kinetics and Plasma Chemistry during Plasma Enhanced Chemical Vapor Deposition of Amorphous Silicon. *J. Appl. Phys.* **1988**, *63*, 2532–2551.

9 Martinu, L.; Zabeida, O.; Klemberg-Sapieha, J. E. Plasma-Enhanced Chemical Vapor Deposition of Functional Coatings. In *Handbook of Deposition Technologies for Films and Coatings*; Elsevier, 2010; pp 392–465.

10 Biederman H.; Osada Y., Plasma Technology, Elsevier Science, Amsterdam 1992.

11 Shishoo, R.; Plasma Technologies for Textiles; Woodhead Publishing Limited, 2007.

12 Harris, L. G.; Schofield, W. C. E.; Badyal, J. P. S. MultiFunctional Molecular Scratchcards. *Chem. Mater.* **2007**, *19*, 1546–1551.

13 Friedrich, J. Mechanisms of Plasma Polymerization - Reviewed from a Chemical Point of View. *Plasma Process. Polym.* **2011**, *8*, 783–802.

14 Panchalingam, V.; Poon, B.; Huo, H.-H.; Savage, C. R.; Timmons, R. B.; Eberhart, R. C. Molecular Surface Tailoring of Biomaterials via Pulsed RF Plasma Discharges. *J. Biomater. Sci. Polym. Ed.* **1994**, *5*, 131–145.

15 Biederman, H.; Slavínská, D. Plasma Polymer Films and Their Future Prospects. *Surf. Coatings Technol.* **2000**, *125*, 371–376.

16 Yang, G. H.; Kang, E. T.; Neoh, K. G. Surface Modification of Poly(Tetrafluoroethylene) Films by Plasma Polymerization of Glycidyl Methacrylate and Its Relevance to the Electroless Deposition of Copper. *J. Polym. Sci. Part A Polym. Chem.* **2000**, *38*, 3498–3509.
17 Limb, S. J.; Edell, D. J.; Gleason, E. F.; Gleason, K. K. Pulsed Plasma-Enhanced Chemical Vapor Deposition from Hexafluoropropylene Oxide: Film Composition Study. *J. Appl. Polym. Sci.* **1998**, *67*, 1489–1502.
18 Martinu, L.; Zabeida, O.; Klemberg-Sapieha, J. E. Plasma-Enhanced Chemical Vapor Deposition of Functional Coatings. In *Handbook of Deposition Technologies for Films and Coatings*; Elsevier, 2010; pp 392–465.
19 Denis, L.; Marsal, P.; Olivier, Y.; Godfroid, T.; Lazzaroni, R.; Hecq, M.; Cornil, J.; Snyders, R. Deposition of Functional Organic Thin Films by Pulsed Plasma Polymerization: A Joint Theoretical and Experimental Study. *Plasma Process. Polym.* **2010**, 7, 172–181.
20 D.T. Williams, M. W. Hayes, Polymerization in a Glow Discharge, *Nature* ,**1966**, 209, 769–773.
21 Denaro, A. R.; Owens, P. A.; Crawshaw, A. Glow Discharge Polymerization-Styrene. *Eur. Polym. J.* **1968**, *4*, 93–106.
22 Tibbitt, J. M.; Jensen, R.; Bell, A. T.; Shen, M. A Model for the Kinetics of Plasma Polymerization. *Macromolecules* **1977**, *10*, 647–653.
23 Yasuda, H.; Hsu, T. Some Aspects of Plasma Polymerization Investigated by Pulsed R.F. Discharge. *J. Polym. Sci. Polym. Chem. Ed.* **1977**, *15*, 81–97.
24 A. Bradley, Organic Reactions in Gas Discharges Leading to Polymer Deposits, *J. Electrochem. Soc.* **1972**, 119, 1153–1157.
25 Savage, C. R.; Timmons, R. B.; Lin, J. W. Molecular Control of Surface Film Compositions via Pulsed Radio-Frequency Plasma Deposition of Perfluoropropylene Oxide. *Chem. Mater.* **1991**, *3*, 575–577.
26 Ryan, M. E.; Hynes, A. M.; Badyal, J. P. S. Pulsed Plasma Polymerization of Maleic Anhydride. *Chem. Mater.* **1996**, *8*, 37–42.
27 Fahmy, A.; Mix, R.; Schönhals, A.; Friedrich, J. Structure of Plasma-Deposited Copolymer Films Prepared from Acrylic Acid and Styrene: Part I Dependence on the Duty Cycle. *Plasma Process. Polym.* **2012**, *9*, 273–284.
28 Carletto, A.; Badyal, J. P. S. Ultra-High Selectivity Pulsed Plasmachemical Deposition Reaction Pathways. *Phys. Chem. Chem. Phys*. **2019**, *9*, 273–284.
29 Andreeva, A. V.; Kutsarev, I.; Shatsky, A. V.; Shterenberg, A. M.; Zyn, V. I. Pre-Polymerization Kinetics in Continuous and Pulsed Glow Discharge in Tetrafluoroethylene. *Plasma Process. Polym.* **2012**, *9*, 772–781.

30 Debarnot, D.; Mérian, T.; Poncin-Epaillard, F. Film Chemistry Control and Growth Kinetics of Pulsed Plasma-Polymerized Aniline. *Plasma Chem. Plasma Process.* **2011**, *31*, 217–231.
31 Hynes, M.; Shenton, M. J.; Badyal, J. P. S. Pulsed Plasma Polymerization of Perfluorocyclohexane. *Macromolecules* **1996**, *29*, 4220–4225.
32 Zhang, J.; van Ooij, W.; France, P.; Datta, S.; Radomyselskiy, A.; Xie, H. Investigation of Deposition Rate and Structure of Pulse DC Plasma Polymers. *Thin Solid Films* **2001**, *390*, 123–129.
33 Han, L. M.; Timmons, R. B. Pulsed-Plasma Polymerization of 1-Vinyl-2-Pyrrolidone: Synthesis of a Linear Polymer. *J. Polym. Sci. Part A Polym. Chem.* **1998**, *36*, 3121–3129.
34 Friedrich, J.; Kühn, G.; Mix, R.; Unger, W. Formation of Plasma Polymer Layers with Functional Groups of Different Type and Density at Polymer Surfaces and Their Interaction with Al Atoms. *Plasma Process. Polym.* **2004**, *1*, 28–50.
35 Kumar, V.; Pulpytel, J.; Arefi-Khonsari, F. Fluorocarbon Coatings Via Plasma Enhanced Chemical Vapor Deposition of 1H,1H,2H,2H-Perfluorodecyl Acrylate-1, Spectroscopic Characterization by FT-IR and XPS. *Plasma Process. Polym.* **2010**, *7*, 939–950.

2 : EXPERIMENTAL METHODS

2.1 Introduction

In the present chapter, the experimental set-up that has been employed for this project, is described in detail. The set-up consists of a vacuum vessel with a plasma apparatus used for the generation of polymerising plasmas, coupled to an electrostatic quadrupole mass spectrometer for the purpose of in situ diagnostic studies.

2.2 Plasma Apparatus

The plasma apparatus is a cylindrical glass reactor (volume 2943 cm^3) pumped down to a base pressure of 8 $\times 10^{-3}$ mbar (Scheme 2.1). This is attained by evacuating the glass chamber via the main vacuum line, which comprises a turbomolecular drag pump (model TPD 022, Pfeiffer Vacuum Technology AG) backed by a diaphragm pump (model N813.4 ANE, KNF Neuberger GmbH). A liquid nitrogen cold trap is fitted in between the main vacuum line and the glass reactor to prevent any pump contamination. For rough vacuum operations, the vessel can be pumped down through an additional vacuum line using a second diaphragm pump. All pressure values across the different sections of the apparatus are monitored with a system of thermocouple pressure gauges (model ATC-E, Edwards Ltd), additionally each section can be isolated using a sequence of shut-off valves, to facilitate ordinary maintenance of the equipment (Scheme 2.1). The glass reactor is fitted with an inlet valve system which is used to feed the plasma chamber with the desired precursor, pressure and flow rate are monitored using a thermocouple gauge pressure and meter valve (fine control needle valve model 145–217–4P4PC, Meggitt Avionics Ltd.). A copper coil (7 mm diameter, 4 turns, spanning 10.5 cm) is wrapped around the glass chamber and connected to a 13.56 MHz radio frequency (RF) power supply (model RFG 600SE, Coaxial Power Systems Ltd.) in conjunction with a LC circuit matching unit (to minimise reflected power). A pulse signal generator (model TG503 5 MHz pulse, Thurlby Thandar Instruments Ltd.) was used to trigger the RF power supply and monitored using an oscilloscope (model OX 530 20 MHz, Metrix Ltd.).

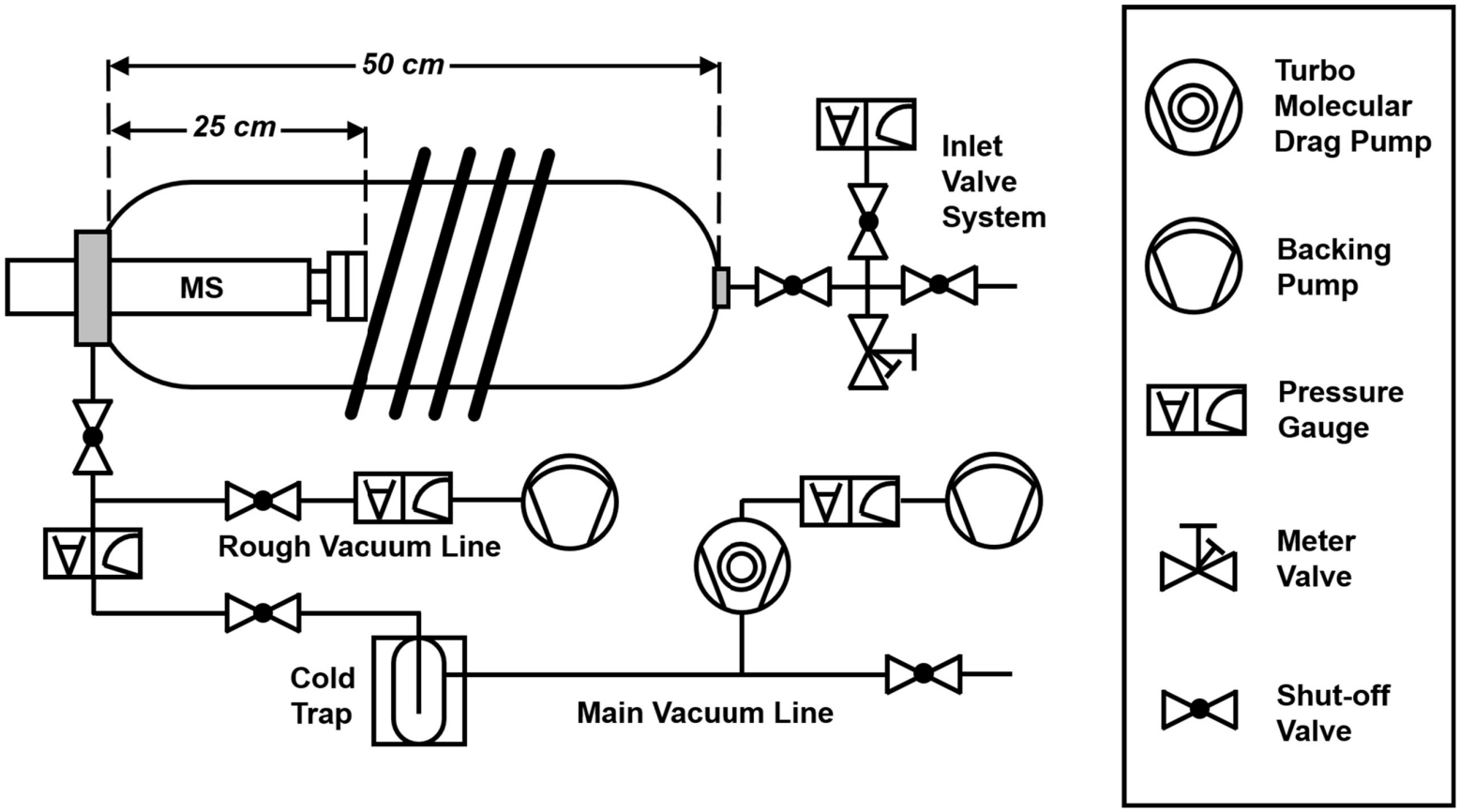

Scheme 2.1: Plasma apparatus utilised for mass spectrometry in situ diagnostic studies of plasma deposition experiment

2.3 Electrostatic Quadrupole Probe: EQP

The instrument used in this work for plasma diagnostic studies, is an electrostatic quadrupole probe (EQP) mass spectrometer (model HAL EQP 2500 manufactured by Hiden Analytical Ltd.), shown in Figure 2.1. The EQP is essentially a 45° sector field ion energy analyser coupled to a triple quadrupole mass filter which is capable of acquiring energy- and mass-resolved spectra, allowing analysis of positive and negative ions from an external ionising source (plasma), or neutrals which are ionised by an internal ion source.[1,2] The ions that make it through the energy and mass filters, are subsequently channelled into a secondary electron multiplier (SEM) detector for data collection. The probe head is immersed in the plasma, protruding 25 cm inside the glass chamber (Figure 2.1) so that ionised gaseous species (plasma ions) and neutrals can be sampled directly from the electrical discharge through a pin-hole sized orifice (50 or 200 μm in diameter), located at the end of it. The EQP has a mass range of 0.4 to 2500 amu and energy range of 1–100 eV. To do so, a set of electrodes throughout the probe, is operated at adjustable high voltages (up to ± 1kV) to optimise ion detection sensitivity, EQP electrodes are governed by variable voltage settings that can be altered by the user to achieve the desired EQP performances (EQP tuning). Plasma diagnostic EQP studies can be carried out utilising two fundamental operating modes: *RGA mode*, which is used as residual gas analysis of neutral/radical detection (internal ion source), and *SIMS mode,* that consists in the positive and negative ions extraction straight from the plasma phase (plasma ions).[3,4] Mass spectrometry measurements entail accurate manipulation of charged particle trajectories applying electromagnetic fields, hence, gas-particle collisions inside the mass spectrometer must be minimised to ensure that ion molecules to be analysed, possess the longest ion mean free path achievable. For this reason, the electrostatic quadrupole probe is housed in an ultra-high vacuum (UHV) chamber where operating pressures are typically below 10^{-6} mbar. In our case, the EQP analyser is evacuated by a turbomolecular pump (model TMU 260, Pfeiffer Vacuum Technology AG) backed by a rotary vane pump (model DUO 2.5, Pfeiffer Vacuum Technology AG) to give a mass spectrometer base pressure of better than 2×10^{-9} mbar,

and operating in the pressure range of 10^{-8} mbar, during plasma experiments, as shown in Figure 2.1.[5,6]

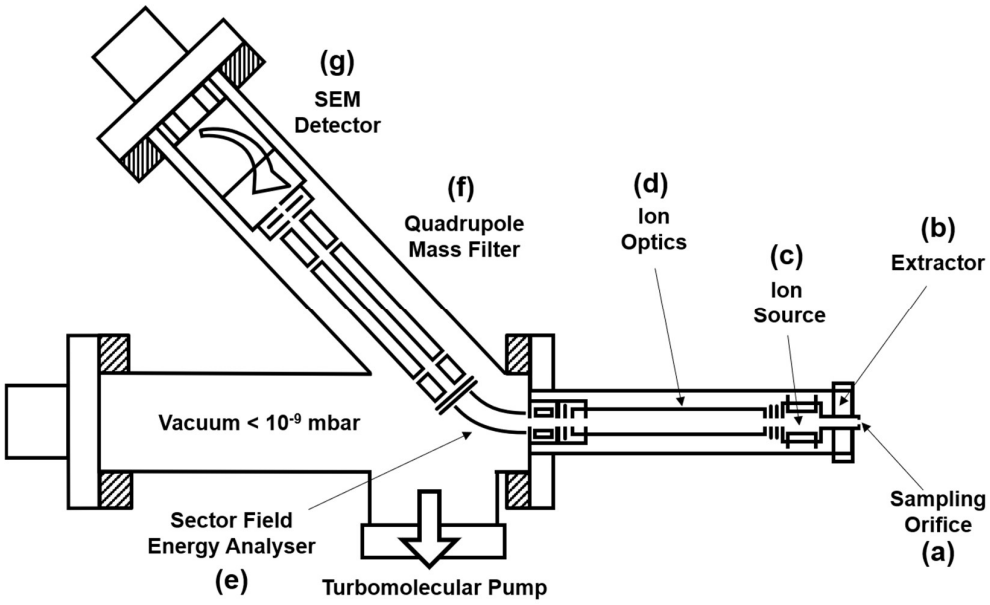

Figure 2.1: Hiden Analytical electrostatic quadrupole probe (EQP) mass spectrometer schematic. Plasma species are sampled from the electrical discharge through the orifice (a), filtered by the extractor electrode (b) in the case of plasma ionised species, or ionised via electron impact by the internal ion source (c). Ions are subsequently focused and decelerated by the ion optics (d) and filtered out according to their energy and mass by the energy analyser (e) and quadrupole mass filter (f) respectively. Ions are then collected by the secondary electron multiplier (g) and converted into count signals.

2.4 Electrodes

As anticipated in the previous section, the electrostatic quadrupole probe (EQP) mass spectrometer is designed for the energy and mass analysis of ions and neutrals generated in a plasma, and this involves the transfer of charged species through the different elements composing the spectrometer. In order to perform these tasks, the EQP has an array of about twenty electrodes (or ion electromagnetic lenses), each of which can be adjusted. The EQP electrodes, shown in Figure 2.2a, can be grouped into five sections; **EXTRACTION, SOURCE, SECTOR, QUAD** and **DETECTOR**. [7,8,9]

Hereafter a brief description of each section and the associated electrodes, is given:

- **EXTRACTION:** *extractor* and *lens1* are the first electrodes that the incident plasma ions encounter, consequently these voltage settings can be quite critical for plasma operation. The *extractor* electrode pulls inside the probe the ion species originated within the plasma phase while *lens1* is used to refocus the ion beam into the internal ion source exit aperture. When the EQP is being operated in RGA mode, the *extractor* potential is normally set to prevent the ingress of ions from the plasma and ensure that only neutrals are analysed.

- **SOURCE:** *emission*, *electron-energy* and *cage* voltages control the EQP electron-impact ionisation source; therefore, these electrodes are only operating when the EQP is running in RGA mode. *The emission* variable controls the electron current (20–5000 μA) and *electron-energy* is used to set the kinetic energy of the electrons generated by the filaments (0–150 eV). Ions are formed by electron impact at a potential energy set by the variable *cage*. If the EQP is fitted with a negative ion RGA the *source-focus* electrode will also be available.

- **SECTOR:** *axis*, *lens2*, *vert*, *horiz*, *D.C. quad*, *plates, energy* and *transit-energy* are the electrodes associated with the sector field energy filter. From the ion source, the ions are accelerated into the drift space, which they transit with an energy set by *axis* electrode (also known as drift space

potential). *Axis* is also responsible for the energy at which ions transit the energy filter. The potential on *lens2* matches the ion source to the energy filter allowing efficient ion transfer. *Vert* and *horiz* are beam alignment controls, *D.C. quad* is used to correct for beam astigmatism, (*vert*, *horiz* and *D.C. quad* electrodes are often referred to as the quadrupole lens). The *plates, energy* and *transit-energy* electrodes govern the voltages at the energy filter.

- **QUAD:** *focus2*, *resolution*, *delta-m*, and *transit energy* constitute the quadrupole section. *Resolution* and *delta-m* allow to control the high mass and low mass resolving powers, respectively. The *focus2* operates at approximately -250 V (for positive ion analysis) and is used to match the energy filter to the quadrupole mass filter. This electrode requires no further tuning once it has been set by the manufacturer.

- **DETECTOR:** *1st-dynode*, *multiplier* and *discriminator* are the variables associated with the secondary electron multiplier (SEM) detector. The *1-st dynode* voltage is usually operated at its maximum of -1200 V for positive ions or +800 V for negative ions. The *multiplier* is the voltage across the electron multiplier and should be set to operate just on the plateau region for all modes. The *discriminator* sets a threshold level at which an ion event is counted.

In order to achieve maximum performance from the EQP, altering the electrodes voltages is often required, this operation is known as tuning. EQP tuning is primarily governed by the application and usually performed by the user in a number of cases, such as: use of different plasma parameters or plasma precursors; change of the ion/neutral mass under investigation; looking at several ions with different mass and energy and after major maintenance operations or alterations made to the plasma system.

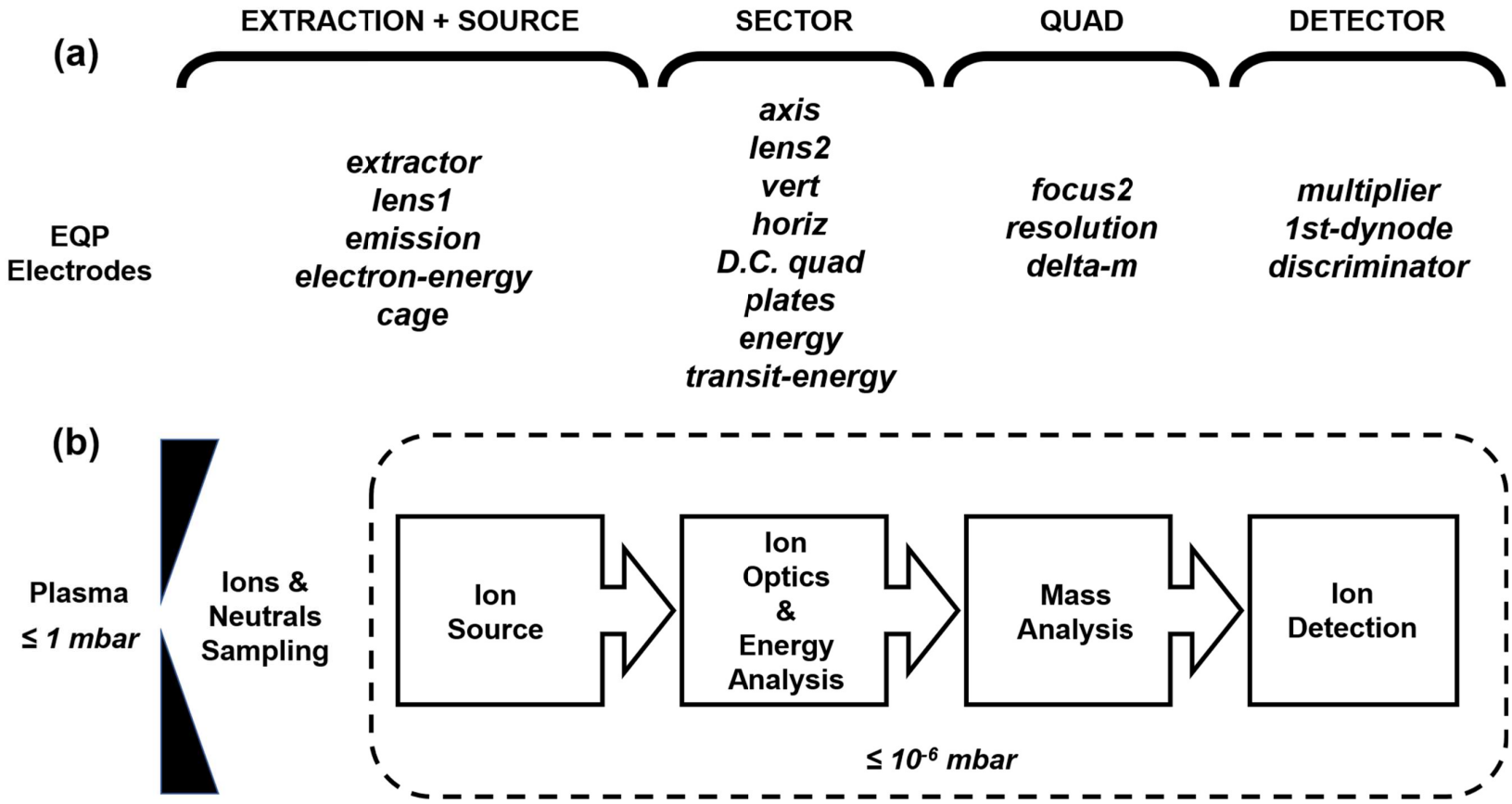

Figure 2.2: The different EQP electrodes are grouped by sections at the top (a), with the associated EQP operations at the bottom (b).

2.5 Main Components

2.5.1 Internal Ion Source

Mass spectrometry requires ionisation of chemical species, for this reason, neutral species sampled by the probe orifice need to carry a charge in order for the EQP to perform mass analysis on RGA mode. Neutrals diffusing into the ion source are subjected to electron bombardment, this leads to ion generation.[10,11]

This phenomenon is known as electron-impact (EI) ionisation, eq. (2.1):

$$\mathrm{M} + \mathrm{e}^- \rightarrow \mathrm{M}^+ + 2\mathrm{e}^- \qquad (2.1)$$

The EQP internal ion source relies on a dual-filament system. The filaments are coated with iridium oxide and can be used in conjunction or one at the time.[12] For RGA mode (which consists in the analysis of radicals or neutrals), one (or both) filament are energised. The current-heated filament gives off electrons generated by thermionic emission (with a specific kinetic energy set by the *electron-energy* variable). The latter are accelerated through a potential (applied across the filament and the cage) and collide with gaseous molecule to form ions at the potential energy set by the *cage* variable, as illustrated in Figure 2.3. Filament current is controlled by the electron emission current. The resulting ions are then focussed and transferred by electromagnetic lenses to the following section of the EQP.[13]

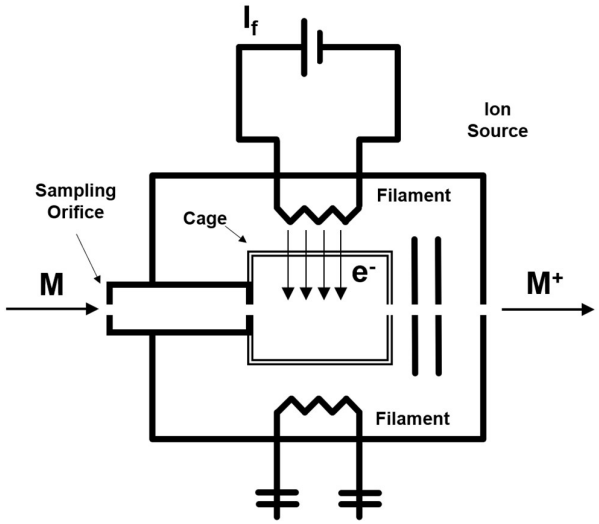

Figure 2.3: Ion Source.

2.5.2 Energy Filter

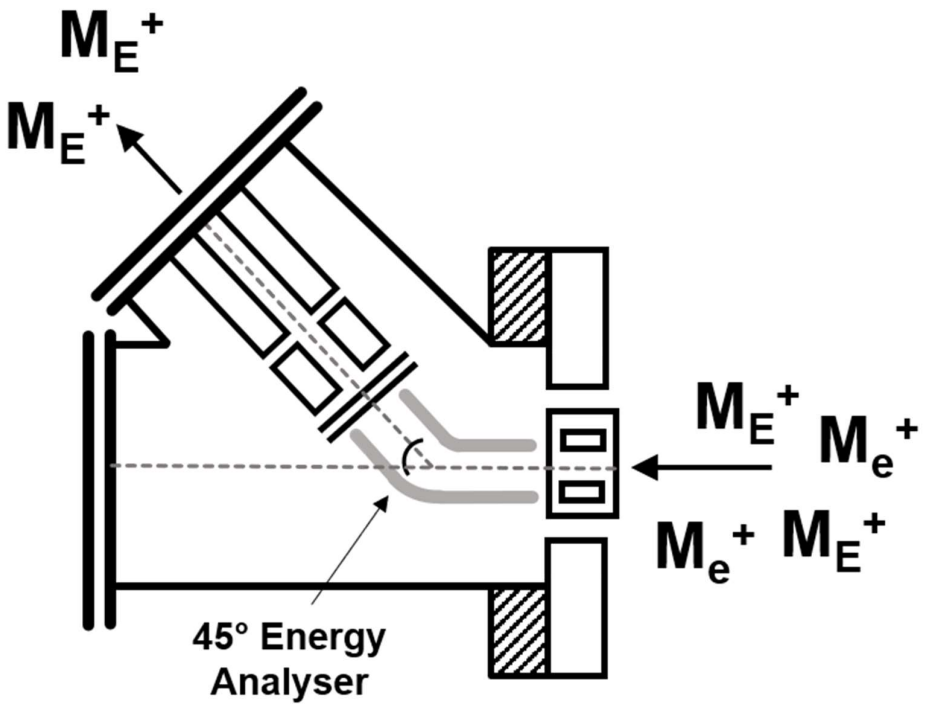

Figure 2.4: EQP sector field electrostatic energy analyser.

The EQP is fitted with an electrostatic sector field energy analyser (ESA) for ion energy analysis placed right before the quadrupole mass filter. The energy analyser consists in two parallel electrodes with a 45° curvature, which are capable of filtering ions out according to their energy, Figure 2.4. Charged particles are sampled from the plasma and accelerated through the energy filter where the kinetic energy of the ions (E_{ion}) can be measured balancing the centripetal force (generated by the potential between the electrodes) with the centrifugal force ($E_0=2E_{ion}/zer_e$).[1,9] The sector field energy analyser on the EQP has an energy range of 0 – 100 eV and energy resolution of 0.1 eV.[3]

2.5.3 Mass Filter

The EQP triple section quadrupole mass filter is responsible for the ion separation according to their mass-to-charge (*m/z*) ratio, this is achieved by using the stability of the ion trajectories in an oscillating electric field.[10,14]

The quadrupole itself consists in four molybdenum parallel rods, Figure 2.5a. A combination of AC (oscillating in the RF region) and DC (static) voltages is applied to the quadrupole; one opposing rod pair receives a positive potential, on the other one the same potential with negative sign is applied, as per Figure 2.5b. The quadrupole generates an electric field composed by an oscillating field (Vcos(ωt)) superimposed to a static one (U), equations (2.2) and (2.3) represent the two potentials with opposite sign applied to the quadrupole elements:

$$\Phi_0 = +[\mathrm{U} + \mathrm{V}cos(\omega \mathrm{t})] \tag{2.2}$$

$$-\Phi_0 = -[\mathrm{U} + \mathrm{V}\cos(\omega \mathrm{t})] \tag{2.3}$$

where, Φ_0 is the potential applied to the rods, ω the angular frequency (expressed in radians per second=2πv, v is the frequency of the RF field), V is the amplitude of the AC voltage and U is the direct potential (U will vary from 0.5 to 2 kV and V from 0 to 3 kV). The charged species travelling along the *z* axis (ions entering the filter) move following trajectories modulated by the varying quadrupole electric field, by exploiting this principle the AC/DC ratio can be adjusted in such way that only ions with the desired *m/z* ratio possess stable trajectories (limited oscillations) and make it through the quadrupole. All other ions will be deflected and collide on the quadrupole rods, losing their charge. This is because the amplitude of their oscillations exceeds r_0, making the ion trajectories unstable along the *x* and *y* axis (Figure 2.5b).

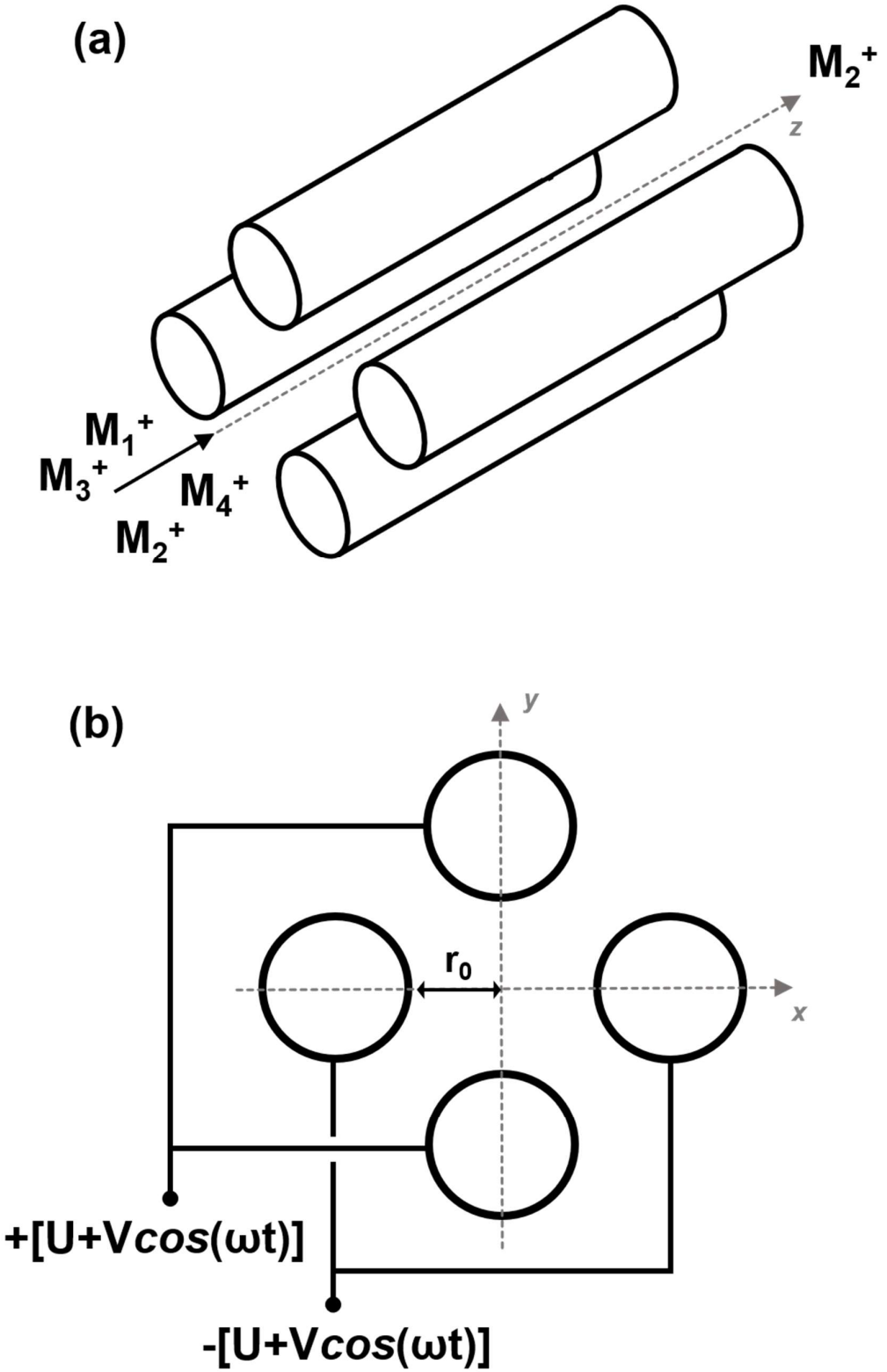

Figure 2.5: Quadrupole cylindrical elements (a), Quadrupole mass filter cross-section with electrical wiring and applied potentials (b).

The physics behind the ion trajectories inside the quadrupole, can be described using the equations of motion along x-axis (2.4) and y-axis (2.5) as a function of the potential Φ, the ion mass and the force induced by the electric field:

$$F_x = m\frac{d^2x}{dt^2} = -ze\frac{\partial^2\Phi}{\partial x} \tag{2.4}$$

$$F_y = m\frac{d^2y}{dt^2} = -ze\frac{\partial^2\Phi}{\partial y} \tag{2.5}$$

Combining the potential equations (2.2) and (2.3) with the equations of motions (2.4) and (2.5), the ion motion equations can be rewritten in the following differential form, known as Paul equations:

$$\frac{d^2x}{dt^2} + \frac{2ze}{mr_0^2}\big(U - Vcos(\omega t)\big)x = 0 \tag{2.6}$$

$$\frac{d^2y}{dt^2} + \frac{2ze}{mr_0^2}\big(U - Vcos(\omega t)\big)y = 0 \tag{2.7}$$

As long as x and y values do not reach the critical radius r_0, the ion trajectories inside the quadrupole are stable, hence the charged particles will not come into contact with the rods. In order to better evaluate the ion stability inside the quadrupolar electric field, the Mathieu differential equation (2.8) should be used in combination with Paul equations (2.6) and (2.7):

$$\frac{d^2u}{d\xi^2} + \big(a_u - q_u cos(2\xi)\big)u = 0 \tag{2.8}$$

Where u is the ion position along the coordinate axes (x or y), and ξ is defined as ωt/2. Replacing t^2 by ξ^2 and changing the variables, Paul equations can be rearranged in the form:

$$a_u = a_x = -a_y = \frac{8zeU}{m\omega^2 r_0^2} \quad or \quad U = a_u\frac{m}{z}\frac{\omega^2 r_0^2}{8e} \tag{2.9}$$

$$q_u = q_x = -q_y = \frac{4zeV}{m\omega^2 r_0^2} \quad or \quad V = q_u\frac{m}{z}\frac{\omega^2 r_0^2}{4e} \tag{2.10}$$

(it should be noted that in any quadrupole filter, r_0 is fixed, the RF frequency ($\omega=2\pi v$) is maintained constant, the only variables are U and V).[15]

The variables a_u and q_u in the equations (2.9) and (2.10) are crucial, as they can be used to represent the stability areas as shown in Figure 2.6.

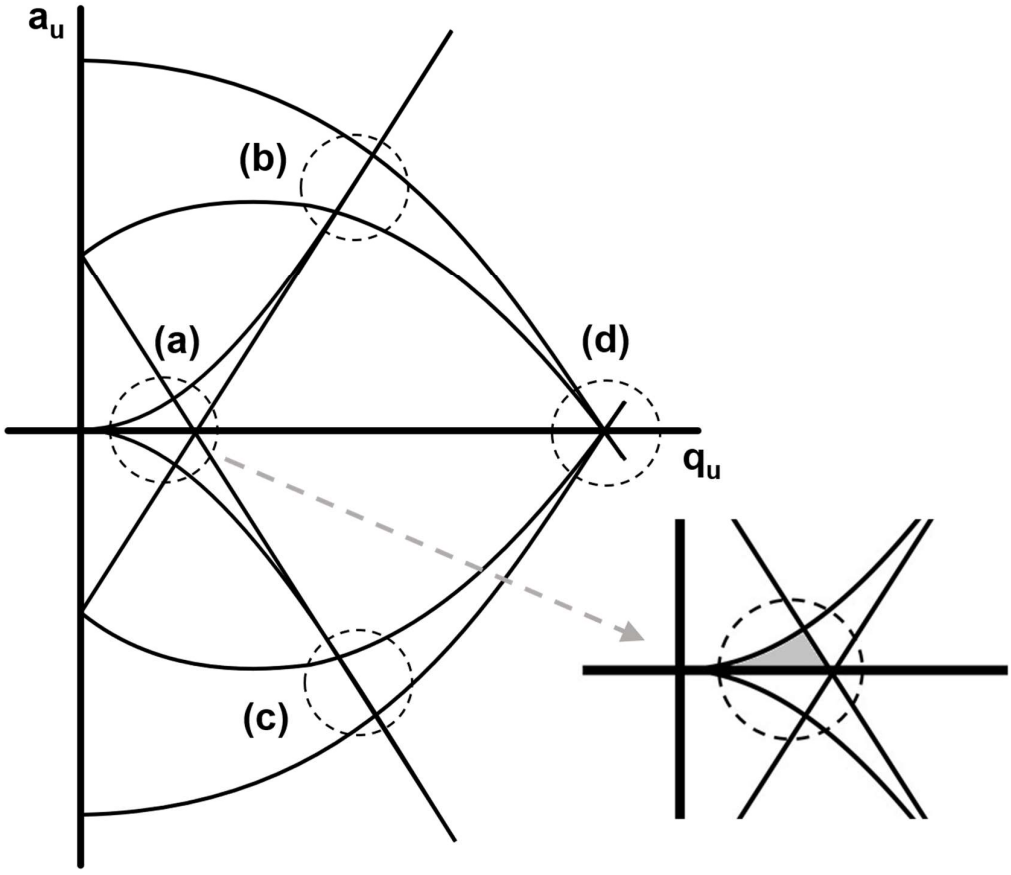

Figure 2.6: Stability areas for an ion along x and y. The four stability areas are circled and labelled as (a), (b), (c) and (d). The area labelled as (a), illustrated in the enlarged plot, is the one commonly used in mass spectrometers. The positive DC potential is represented by the grey area.

In the stability areas (a), (b), (c) and (d) the values of U and V are such that coordinates x and y never reach the critical radius r_0, consequently the passing ion do not touch the quadrupole electrodes. In fact, these operating regions on the plot identify where the ions will have stable trajectories. The area labelled as (a) is the stability region used in quadrupole mass spectrometry, and the grey triangular area in Figure 2.6 (bottom right) represent the positive static potential U.

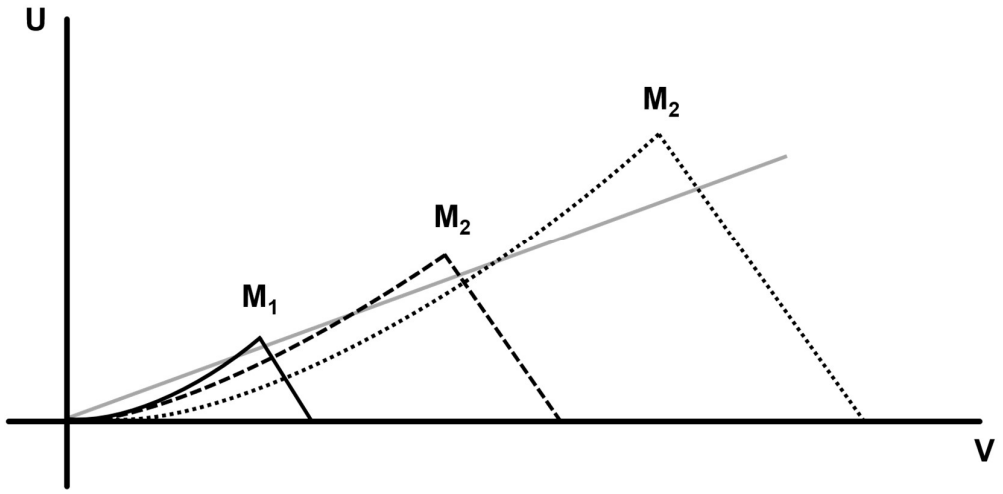

Figure 2.7: Stability areas as a function of U and V for ions with different masses (with $M_1 < M_2 < M_3$).

Changing U linearly as a function of V, we obtain a straight operating line that allows us to observe those ions successively, Figure 2.7. A line with a higher slope would give us a higher resolution, so long as it goes through the stability areas. Keeping U=0 (no direct potential) we obtain zero resolution. All of the ions have a stable trajectory so long as V is within the limits of their stability area.

2.5.4 Detector

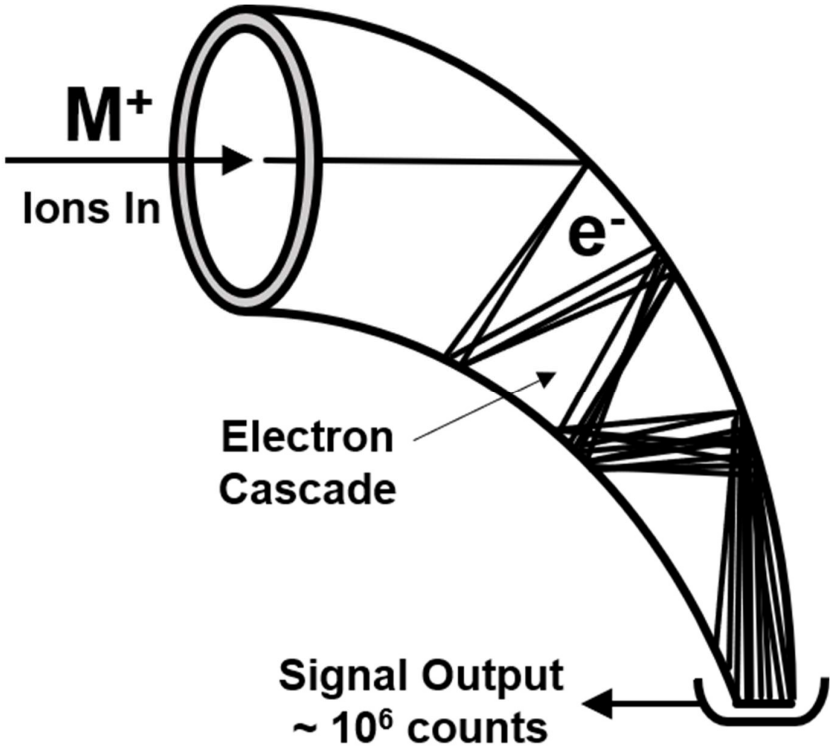

Figure 2.8: Secondary electron multiplier (SEM) ion detector.

The ions that make it through the mass filter are collected by the secondary electron multiplier (SEM) ion detector. The secondary electron multiplier is a continuous dynode which relies on the electron cascade effect generated by ions striking the surface of the electrode (secondary electron emission). The ion signal is then amplified and recorded by the instrument (Figure 2.8).[1,3,6] The secondary electron multiplier (SEM) is usually operated at -1200 V for positive ion or +800 V for negative ion modes.

2.6 Time-resolved Measurements

For time-resolved pulsed plasma measurements, signal gating of the mass spectrometer detector allowed for any specified time window (t_{on} or t_{off}) to be monitored, Figure 2.9. This was achieved by using an additional pulse signal generator (model TGP110 10 MHz, Thurlby Thandar Instruments Ltd.) connected to the mass spectrometer interface unit (MSIU) through a transistor-transistor logic (TTL) acquisition input. One pulse signal generator was employed to trigger both the plasma duty cycle ignition and the other pulse signal generator, where the latter was set to trigger the mass spectrometer ion counting detector during the whole duty cycle or either the t_{on} or t_{off} time windows. [7,16,17,18,19]

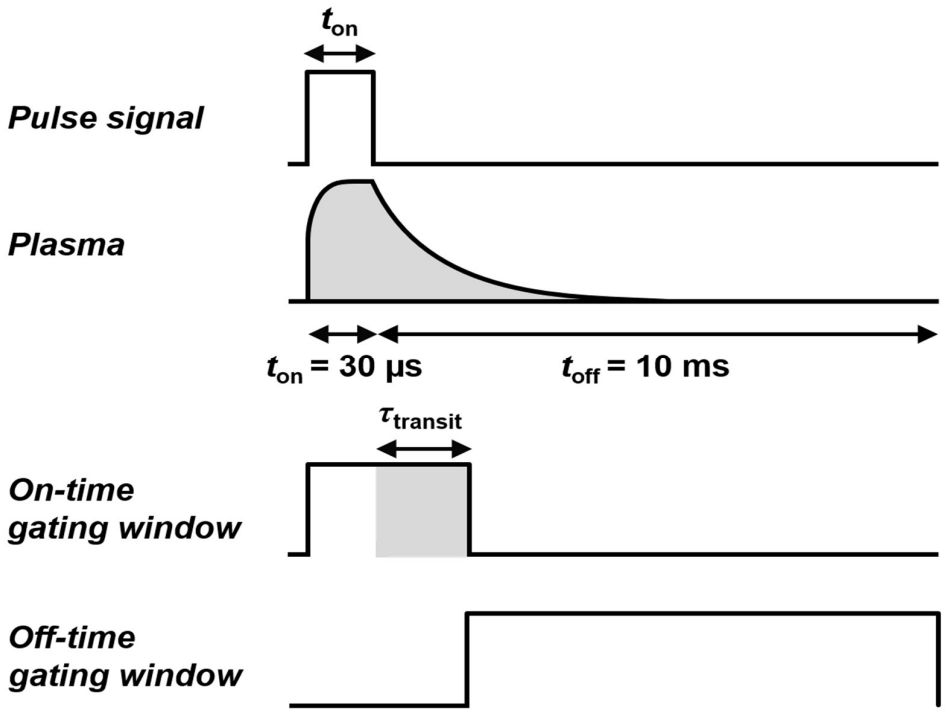

Figure 2.9: Time-resolved pulsed plasma gating measurements (t_{on} = 30 µs, t_{off} = 10 ms).

For the time-resolved mode of analyser operation, the time taken for ions to transit the probe and reach the mass spectrometer detector is defined as the transit time ($\tau_{transit}$). This parameter is dependent on the ion mass (m), the path length of the ion transit (s), and the electrical potential across the region (V) which gives $\tau_{transit}$ as proportional to $s\sqrt{m/2eV}$.[20,21,22,23]

As indicated by the manufacturer, the overall transit time is calculated as the sum of the partial transit times for each region of the probe, namely the extractor, energy analyser, mass filter, and detector.[24,25,26]

The mass spectrometer required a transit time of 300 μs in order to probe up to a mass of 450 *m/z*. Therefore, the detector signal gating window was chosen to be the summation of the on-time and the transit time ($t_{on} + \tau_{transit}$) for on-time measurements whilst for off-time scans this window was shifted to begin detecting 300 μs after the t_{on} and allowed to continue detection until the end of the cycle, as shown in Figure 2.9.[27]

REFERENCES

1 Benedikt, J.; Hecimovic, A.; Ellerweg, D.; von Keudell, A. Quadrupole Mass Spectrometry of Reactive Plasmas. *J. Phys. D. Appl. Phys.* **2012**, *45*, 403001.

2 Muratore, C.; Moore, J. J.; Rees, J. a. Electrostatic Quadrupole Plasma Mass Spectrometer and Langmuir Probe Measurements of Mid-Frequency Pulsed DC Magnetron Discharges. *Surf. Coatings Technol.* **2003**, *163–164*, 12–18.

3 Hiden Analytical Electrostatic Quadrupole Analyser EQP Technical Specifications.https://www.hidenanalytical.com/products/for-thin-films-plasma-and-surface-engineering/eqp/, (accessed June 2, 2019).

4 Stillahn, J. M.; Trevino, K. J.; Fisher, E. R. Plasma Diagnostics for Unraveling Process Chemistry. *Annu. Rev. Anal. Chem.* **2008**, *1*, 261–291.

5 Shishoo, R. *Plasma Technologies for Textiles*; 1st ed.; Elsevier Scientific Publishing Company, Amsterdam, The Netherlands; 2007; p 16.

6 Batey, J. H. The Physics and Technology of Quadrupole Mass Spectrometers. *Vacuum* **2014**, *101*, 410–415.

7 Hiden Analytical, EQP Analyser User Manual, http://www.HidenAnalytical.com. (accessed May 15, 2019).

8 Beck, A. J.; Jones, F. R.; Short, R. D. Mass Spectrometric Study of the Radiofrequency-Induced Plasma Polymerisation of Styrene and Propenoic Acid. *J. Chem. Soc. Faraday Trans.* **1998**, *94*, 559–565.

9 Hamers, E. a. G.; van Sark, W. G. J. H. M.; Bezemer, J.; Goedheer, W. J.; van der Weg, W. F. On the Transmission Function of an Ion-Energy and Mass Spectrometer. *Int. J. Mass Spectrom. Ion Process.* **1998**, *173*, 91

10 De Hoffman, E.; Stroobant, V; *Mass spectrometry : Principles and applications*, 3rd ed.; John Wiley & Sons Ltd, The Atrium, Southern Gate, Chichester, West Sussex, England, 2007; p 16.

11 Große-Kreul, S.; Hübner, S.; Schneider, S.; Ellerweg, D.; Von Keudell, A.; Matejčík, S.; Benedikt, J. Mass Spectrometry of Atmospheric Pressure Plasmas. *Plasma Sources Sci. Technol.* **2015**, *24*.

12 Koller, L. R. Electron Emission From Oxide Coated Filaments. *Phys. Rev.* **1925**, *25*, 671–676.

13 Chait, E. M. Ionization Sources in Mass Spectrometry. *Anal. Chem.* **1972**, *44*, 77A-91a.

14 Dawson, H.P.; Quadrupole *mass spectrometry and its applications*, 1st ed.; Elsevier Scientific Publishing Company, Amsterdam, The Netherlands, 1967; p46.
15 Miller, P. E.; Denton, M. B. The Quadrupole Mass Filter: Basic Operating Concepts. *J. Chem. Educ.* **1986**, *63*, 617.
16 Bradley, J. W.; Bryant, P. M. The Diagnosis of Plasmas Used in the Processing of Textiles and Other Materials. In Plasma Technologies for Textiles; Elsevier, 2007; pp 25–63.
17 Steiner, R. E.; Lewis, C. L.; King, F. L. Time-of-Flight Mass Spectrometry with a Pulsed Glow Discharge Ionization Source. *Anal. Chem.* **1997**, 69, 1715–1721.
18 Lewis, C. L.; Moser, M. A.; Dale, D. E.; Hang, W.; Hassell, C.; King, F. L.; Majidi, V. Time-Gated Pulsed Glow Discharge: Real-Time Chemical Speciation at the Elemental, Structural, and Molecular Level for Gas Chromatography Time-of-Flight Mass Spectrometry. *Anal. Chem.* **2003**, 75, 1983–1996.
19 Li, L.; Millay, J. T.; Turner, J. P.; King, F. L. Millisecond Pulsed Radio Frequency Glow Discharge Time of Flight Mass Spectrometry: Temporal and Spatial Variations in Molecular Energetics. *J. Am. Soc. Mass Spectrom.* **2004**, 15, 87–102.
20 Kawamura, E.; Vahedi, V.; Lieberman, M. A.; Birdsall, C. K. Ion Energy Distributions in Rf Sheaths; Review, Analysis and Simulation. *Plasma Sources Sci. Technol.* **1999**, 8, R45–R64.
21 Voronin, S. A; Alexander, M. R.; Bradley, J. W. Time-Resolved Measurements of the Ion Energy Distribution Function in a Pulsed Discharge Using a Double Gating Technique. *Meas. Sci. Technol.* **2005**, 16, 2446–2452.
22 Voronin, S. A.; Alexander, M. R.; Bradley, J. W. Time-Resolved Mass and Energy Spectral Investigation of a Pulsed Polymerising Plasma Struck in Acrylic Acid. *Surf. Coatings Technol.* **2006**, 201, 768–775.
23 Voronin, S.; Zelzer, M.; Fotea, C.; Alexander, M. R.; Bradley, J. W. Pulsed and Continuous Wave Acrylic Acid Radio Frequency Plasma Deposits: Plasma and Surface Chemistry. *J. Phys. Chem. B* **2007**, 111, 3419–3429.
24 EQP and EQS Analysers Hiden Analytical Technical Information, https://www.hiden.de/wpcontent/uploads/pdf/EQP_and_EQS__Hiden_Analytical_Techinical_Inofrmation.pdf (Accessed: 15 January 2018).
25 Bohlmark, J.; Lattemann, M.; Gudmundsson, J. T.; Ehiasarian, A. P.; Aranda Gonzalvo, Y.; Brenning, N.; Helmersson, U. The Ion Energy Distributions and Ion Flux Composition from a High Power Impulse Magnetron Sputtering Discharge. *Thin Solid Films* **2006**, 515, 1522–1526.
26 Hecimovic, A.; Ehiasarian, A. P. Time Evolution of Ion Energies in

HIPIMS of Chromium Plasma Discharge. *J. Phys. D. Appl. Phys.* **2009**, 42, 135209.

27 Mishra, A.; Clarke, G.; Kelly, P.; Bradley, J. W. High Temporal Resolution Ion Energy Distribution Functions in HIPIMS Discharges. *Plasma Process. Polym.* **2009**, 6, S610–S614.

3 : PLASMA PRECURSORS CONTAINING DOUBLE BONDS

3.1 Introduction

Conventional addition polymerisation is the process of repeated addition of monomer units that possess double bonds, to form polymers. However, the presence of double bonds may not always be a sufficient condition to obtain a polymer. This may be due to various factors, such as monomer reactivity, operating conditions, solvent, process temperature and initiators.[1]

Operating in plasma conditions introduces a further challenge, as these processes rely on a complex set of chemical reactions that are difficult to understand on a molecular level. Unsaturated hydrocarbons, such as α-olefins and allyl compounds are known to give organic deposits when their vapour precursors are exposed to a plasma environment, and several studies can be found in the literature where the obtained plasma polymer thin films are extensively characterised.[2,3,4,5,6] However, the actual repeated addition of monomer units (oligomerisation leading to polymer formation) is rarely observed within the plasma phase.

For the set of experiments reported in this chapter, we have chosen two plasma precursors namely, 1-decene and allyl glycidyl ether (AGE), illustrated in Structure 1. These functional monomers undergoing pulsed plasma conditions were investigated, by in situ mass spectrometry, in the attempt to elucidate the plasma phase chemistry and observe the polymer formation by sequential monomer addition occurring in the ionised gas.

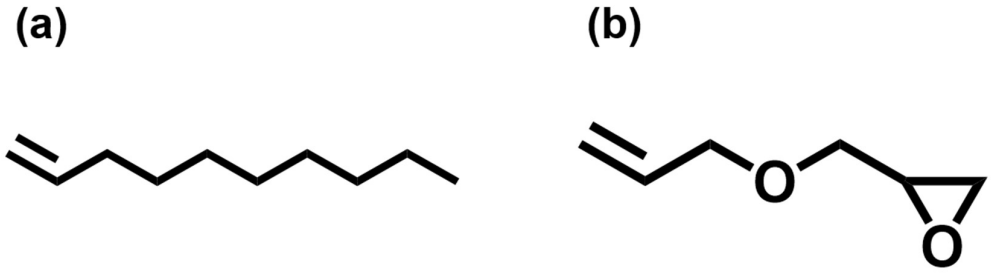

Structure 1: 1-decene (a) and allyl glycidyl ether (b) monomer structures

3.2 Experimental

In situ mass spectrometry experimental set-up is described in details in paragraph 2.2 and 2.3 (Chapter 2). Prior to each experiment, the chamber was cleaned with a 50 W oxygen plasma (0.2 mbar pressure). All monomers, 1-decene precursor (+95%, Sigma Aldrich Co.) and allyl glycidyl ether (AGE +97%, Sigma Aldrich Co.) were loaded in a monomer tube and purified using several freeze-pump-thaw cycles prior to use. For all experiments, the cylindrical glass reactor was purged with the monomer for 20 min at a pressure of 0.1 mbar using a fine control needle valve and pressure was monitored using a thermocouple gauge. For pulsed plasmas, an on-period (t_{on}) of 30 µs and an off-period (t_{off}) of 10 ms were used in conjunction with 15 W of continuous wave power input during the on-period (P_{on}).[7,8] A 200 µm orifice was used. The electron impact ionisation source of the mass spectrometer was operated at low energy (20 eV) for the detection of neutral and radical plasma species whilst avoiding excessive fragmentation. Also ionised gaseous species (plasma ions) were sampled directly from the electrical discharge through the 200 µm end cap orifice.

For time-resolved measurements and detector gating operations, the transit time was calculated using the procedure described in section 2.6 (Chapter 2).

3.3 Results

In the present section, experimental results for 1-decene and allyl glycidyl ether (AGE) gas precursors and pulsed plasmas mass spectrometry measurements are reported. For all experiments, the mass spectrometer was tuned on different masses to ensure consistency with the results.

3.3.1 1-Decene Electron-Impact Mass Spectrometry

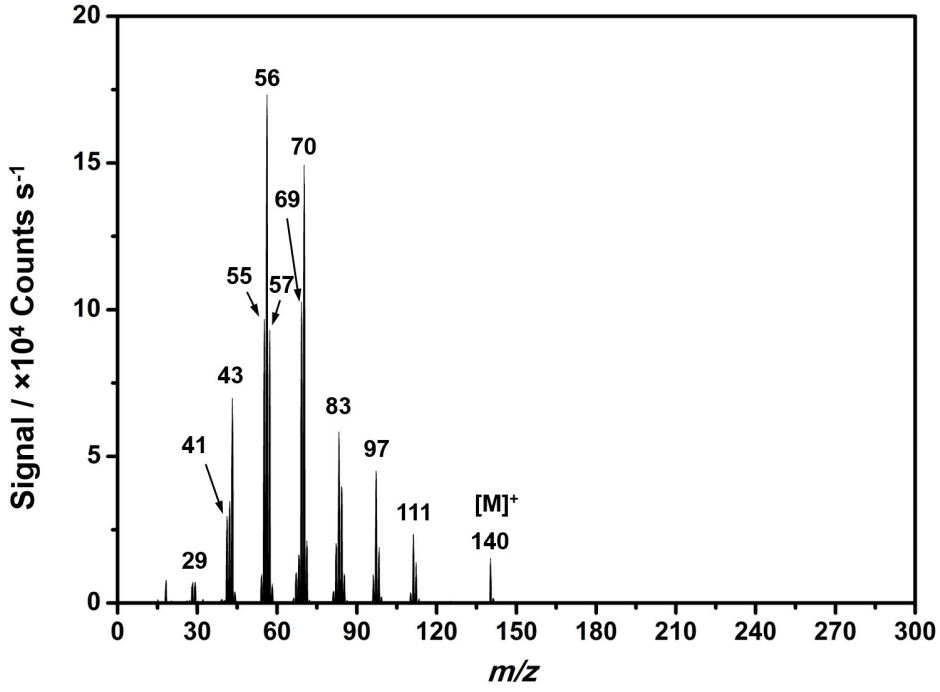

Figure 3.1: 20 eV electron-impact ionisation mass spectrum of 1-decene monomer, (0.1 mbar). Mass spectrometer tuning on 54 *m/z*.

The electron-impact ionisation of 1-decene vapour monomer was carried out at 20 eV, Figure 3.1. The molecular ion ($[M]^+$) is present at 140 *m/z* and the fragment distribution is characterised by ions of the general formula C_nH_{2n-1}. This is usually observed in electron-impact mass spectrometry of mono-olefins and is found to be in good accordance with the NIST reference electron-impact mass spectrum.[21,22] The base peak at 56 *m/z* arises from two main fragmentation pathways: (1) the cleavage of the C_4–C_5 bond with the addition of a proton and (2) the C_6–C_7 bond cleavage with the loss of a proton.

The 1-decene fragment series is shown in, Figure 3.2.

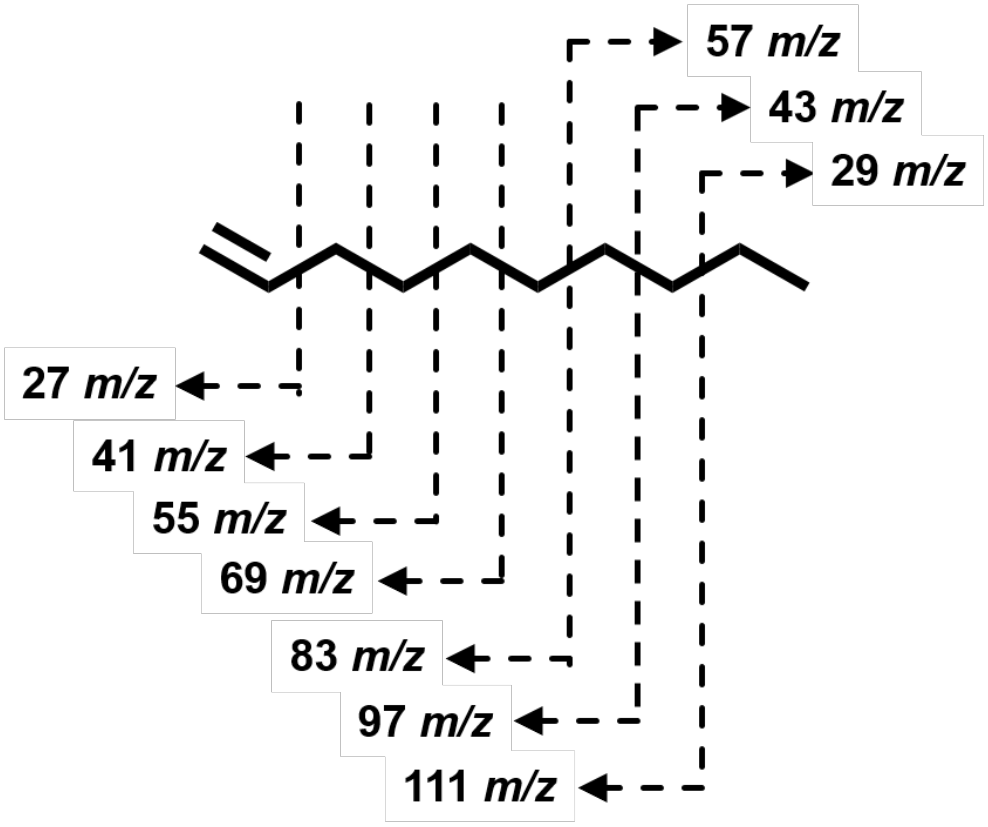

Figure 3.2: 1-decene 20 eV electron impact mass spectroscopy fragmentation pattern.

3.3.2 1-Decene Plasma Ions

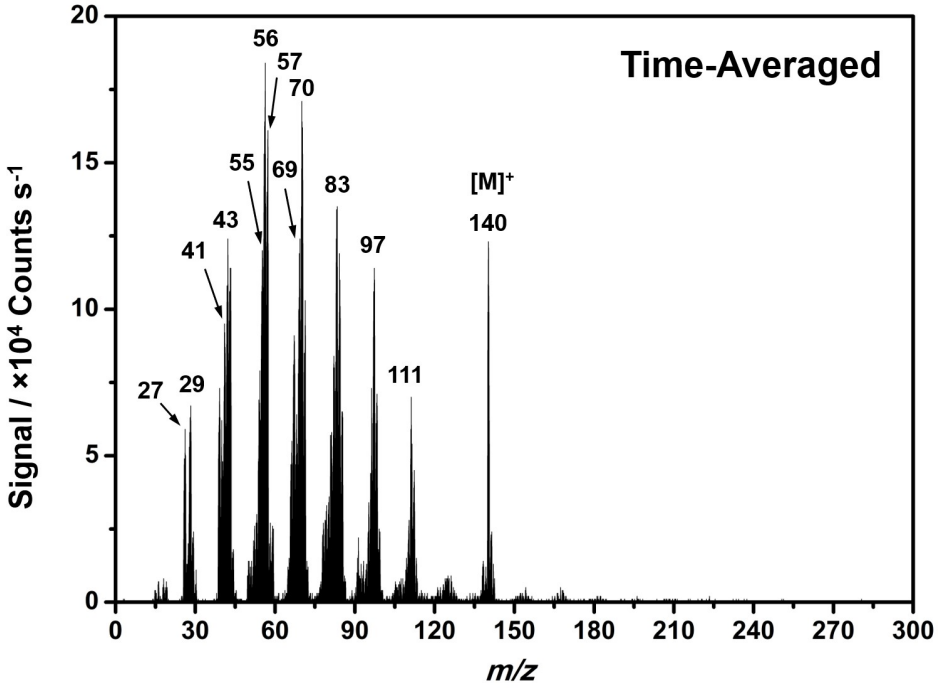

Figure 3.3: Time-averaged positive plasma ion mass spectrum of 1-decene pulsed plasma (t_{on} = 30 µs, t_{off} = 10 ms, P_{on} = 15 W, and 0.1 mbar). Mass spectrometer tuning on 57 *m/z* mass signal.

The ion mass population observed for time-averaged positive plasma spectrometry (Figure 3.3) mirrors the experimental results obtained for electron-impact mass spectrometry of the precursor vapours. Plasma ion high mass signals are often more intense relatively to the base peak, when compared to the mass signal population observed in Figure 3.1. This outcome can be explained by the soft plasma ionisation the monomer precursors undergo when exposed solely to the plasma electron bombardment; the direct consequence is a greater amount of monomer precursor units ($[M]^+$ = 140 *m/z*) being left intact. Additionally, weak signals are observed above the molecular ion peak, indicating high mass molecular species formation due to partial monomer addition, while no dimer species were detected.

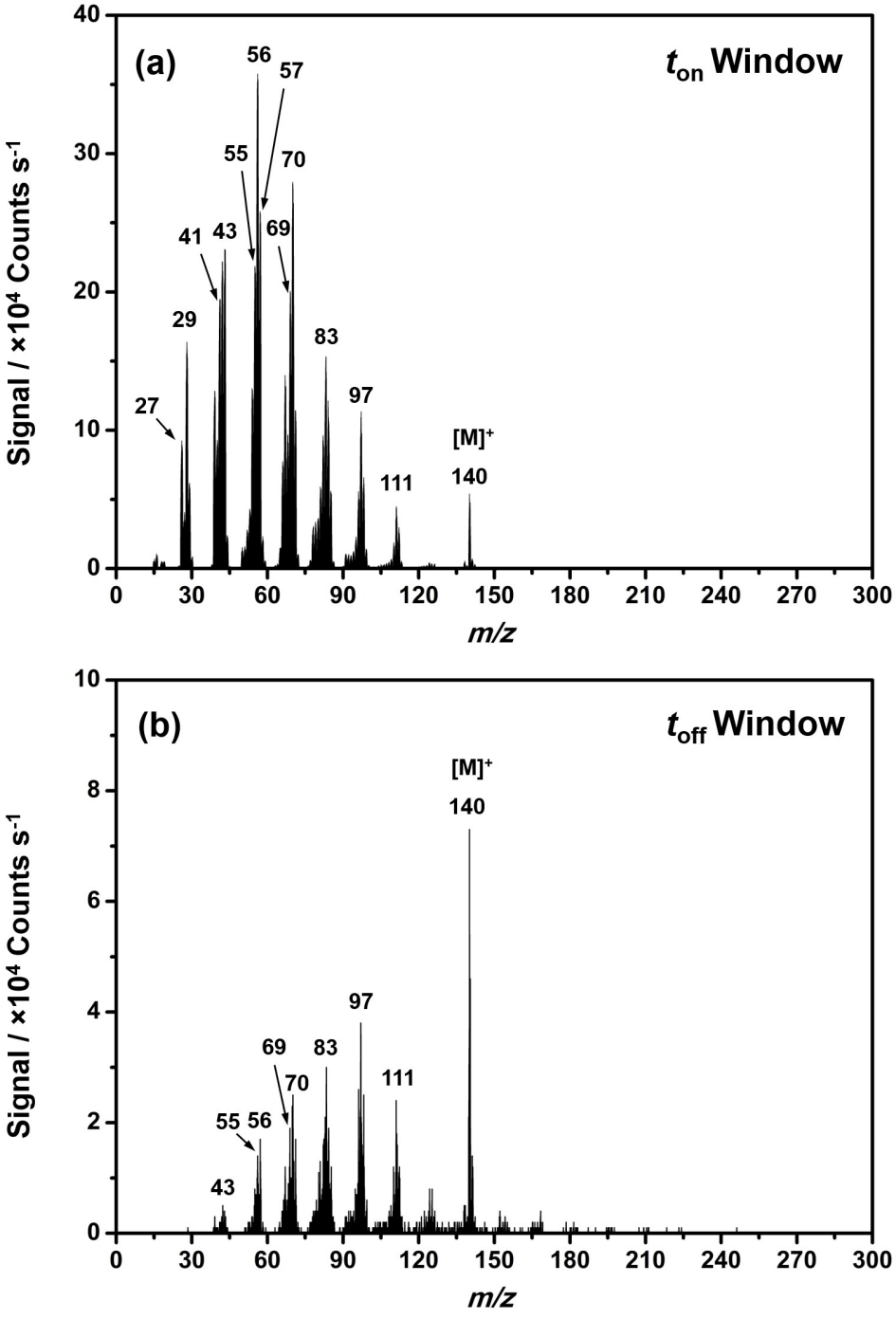

Figure 3.4: Time-resolved positive plasma ion mass spectra of 1-decene pulsed plasma (t_{on} = 30 µs, t_{off} = 10 ms, P_{on} = 15 W, and 0.1 mbar).

Time-resolved positive plasma ion measurements established the existence of two plasma regimes (t_{on} and t_{off} windows) characterised by distinct ion populations. During the electrical discharge (t_{on}), high ion counts for low mass ion fragments were recorded, which is explained by the elevated degree of

fragmentation due to high energy ion bombardment and electron collisions (Figure 3.4a). The off-period features a relatively less intense set of positive ion signals within the low mass region (0–100 *m/z*), with the base peak corresponding to the molecular ion signal $[M]^+$ at 140 *m/z*. This is due to the low fragmentation environment within the extended off-period, leading to the generation of higher mass plasma ion species. In addition, low signals are observed for masses above the molecular ion, indicating the formation of partially polymerised high mass positive ion fragments, however no oligomer fragments are observed (Figure 3.4b).

3.3.3 1-Decene Plasma Radicals

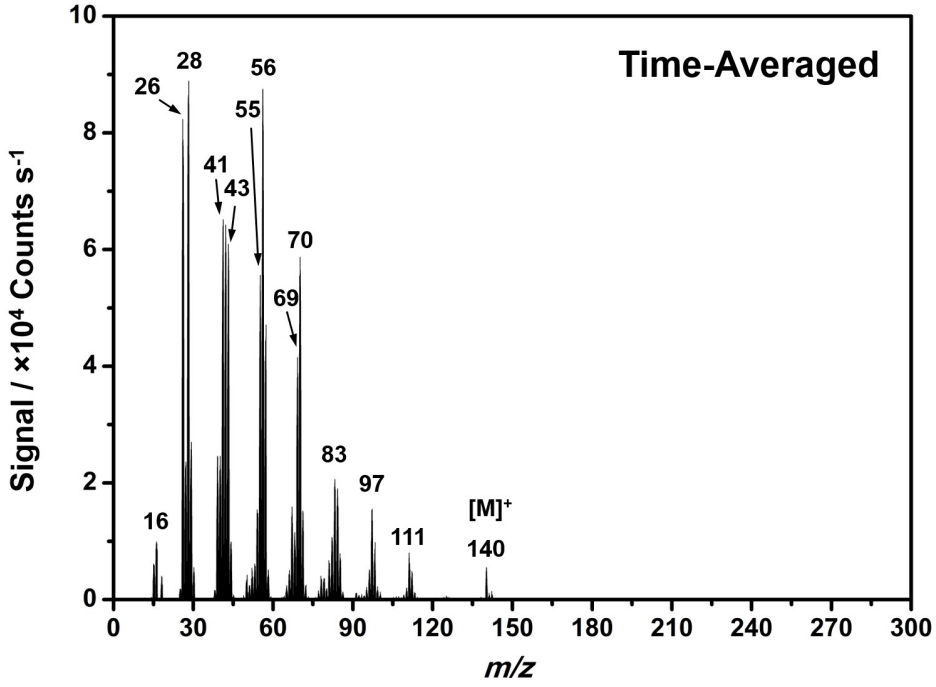

Figure 3.5: Time-averaged electron-impact ionisation mass spectrum of 1-decene pulsed plasma (t_{on} = 30 µs, t_{off} = 10 ms, P_{on} = 15 W, and 0.1 mbar).

Electron-impact ionisation mass spectroscopy operated in time-averaged mode exhibited high fragmentation of 1-decene monomer precursor species within the pulsed plasma phase. The combination of the plasma discharge ionisation together with the 20 eV electron-impact ionisation, produces an elevated degree of fragmentation observed in Figure 3.5, a further confirmation is the presence of intense mass signals in the lower mass region

of the spectrum (0–60 *m/z*). It is also noticeable that, the molecular ion signal is weak compared to the overall mass signal intensities.

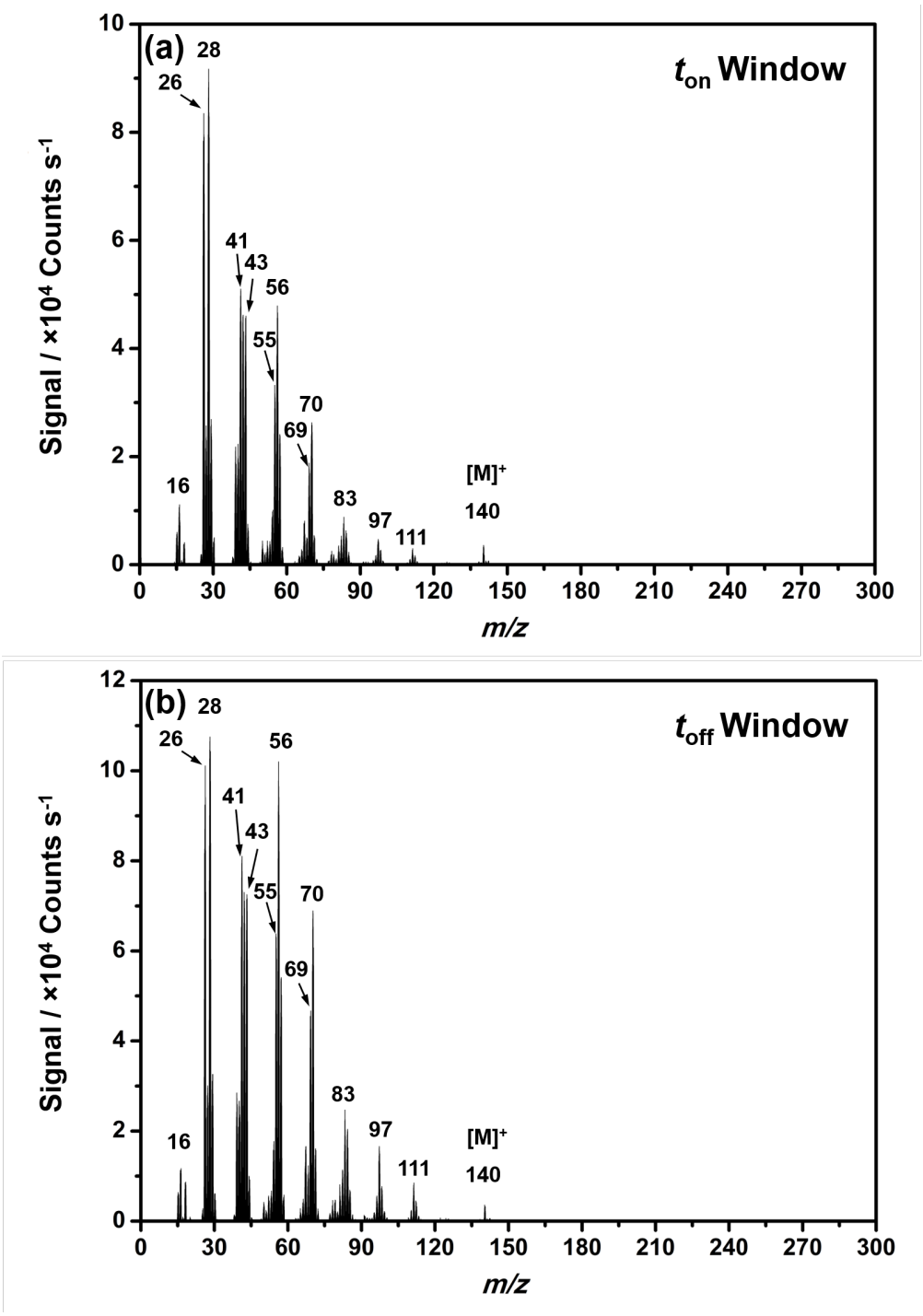

Figure 3.6: Time-resolved electron-impact ionisation mass spectra of 1-decene pulsed plasmas (with t_{on} = 30 µs, t_{off} = 10 ms, P_{on} = 15 W, and 0.1 mbar).

For time-resolved analysis, electron-impact ionisation mass spectrometry shows some minor differences between the two time periods. The signal

intensities for masses between 40 *m/z* and 100 *m/z* (off-time period, Figure 3.6b) are more prominent compared to those recorded during the pulsed plasma discharge in the on-time period, Figure 3.6a, where a greater degree of monomer fragmentation occurs. This can be attributed to the combined effect of the mass spectrometer electron-impact ionisation source and plasma electron bombardment. Moreover, for both plasma periods (t_{on} and t_{off}), the molecular parent ion signal appears to be very weak, additionally no mass signals above the molecular ion peak were detected, due to excessive combined fragmentation.

3.3.4 Allyl Glycidyl Ether Electron-Impact Mass Spectrometry

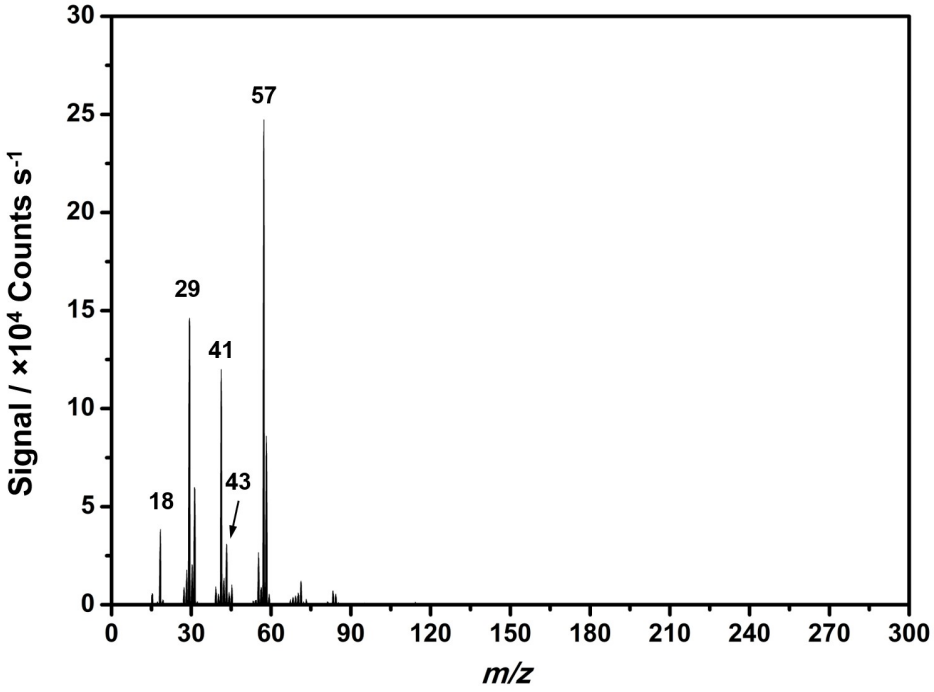

Figure 3.7: 20 eV electron-impact ionisation mass spectrum of AGE monomer, (0.1 mbar). Mass spectrometer tuning on 57 *m/z*.

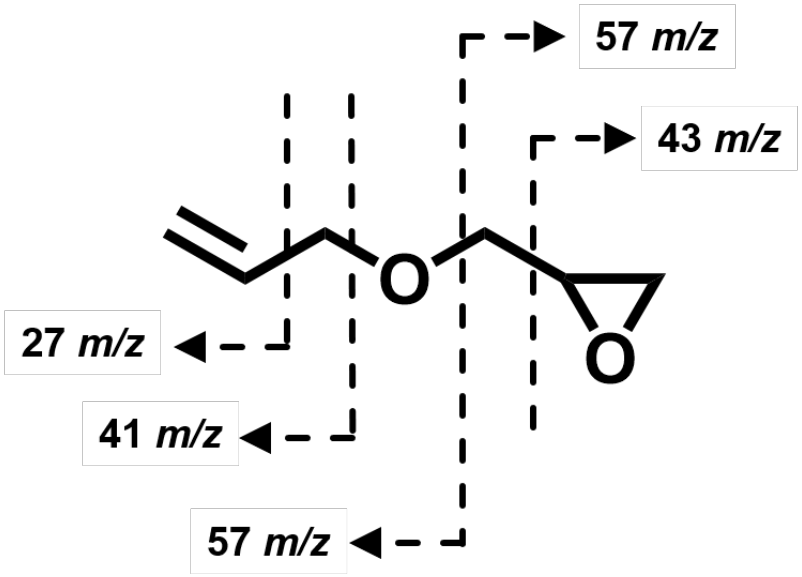

Figure 3.8: Allyl glycidyl ether precursor fragmentation pattern.

The electron-impact ionisation of allyl glycidyl ether (AGE) vapour monomer was carried out at 20 eV (soft ionisation regime), to avoid excessive fragmentation, Figure 3.7. The base peak is found at 57 *m/z* and originates from the bond cleavage between the ether oxygen and the glycidyl group, Figure 3.8 which gives rise to two different fragments with equal molecular mass. The other main fragments observed such as mass 41 and 43 *m/z* correspond to the epoxide ring and the allyl group, as reported in Figure 3.8.[5,23,24]

3.3.5 Allyl Glycidyl Ether Plasma Ions

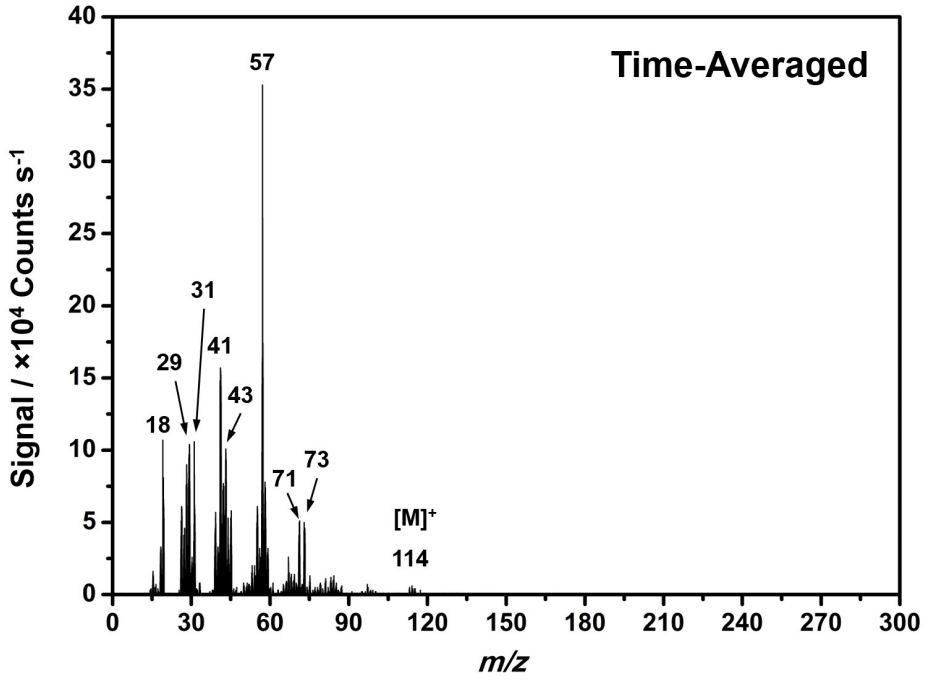

Figure 3.9: Time-averaged positive plasma ion mass spectrum of allyl glycidyl ether pulsed plasma (t_{on} = 30 µs, t_{off} = 10 ms, P_{on} = 15 W, and 0.1 mbar). Mass spectrometer tuning on 57 *m/z* mass signal.

In time-averaged positive ion spectrometry Figure 3.9, the ion mass population observed for AGE pulsed plasma, shows a greater number of mass signals compared to the precursor electron-impact ionisation spectrum (as per Figure 3.7). Particular attention should be paid to signals 71 and 73 *m/z* signals, resulting from the heterogeneous cleavage and loss of the epoxide ring (43 *m/z*) and allyl group (41 *m/z*) respectively. The molecular parent ion is also visible at 114 *m/z*. This additional mass signals are not observed in the 20 eV electron-impact ionisation spectrum, given the lower fragmentation degree.

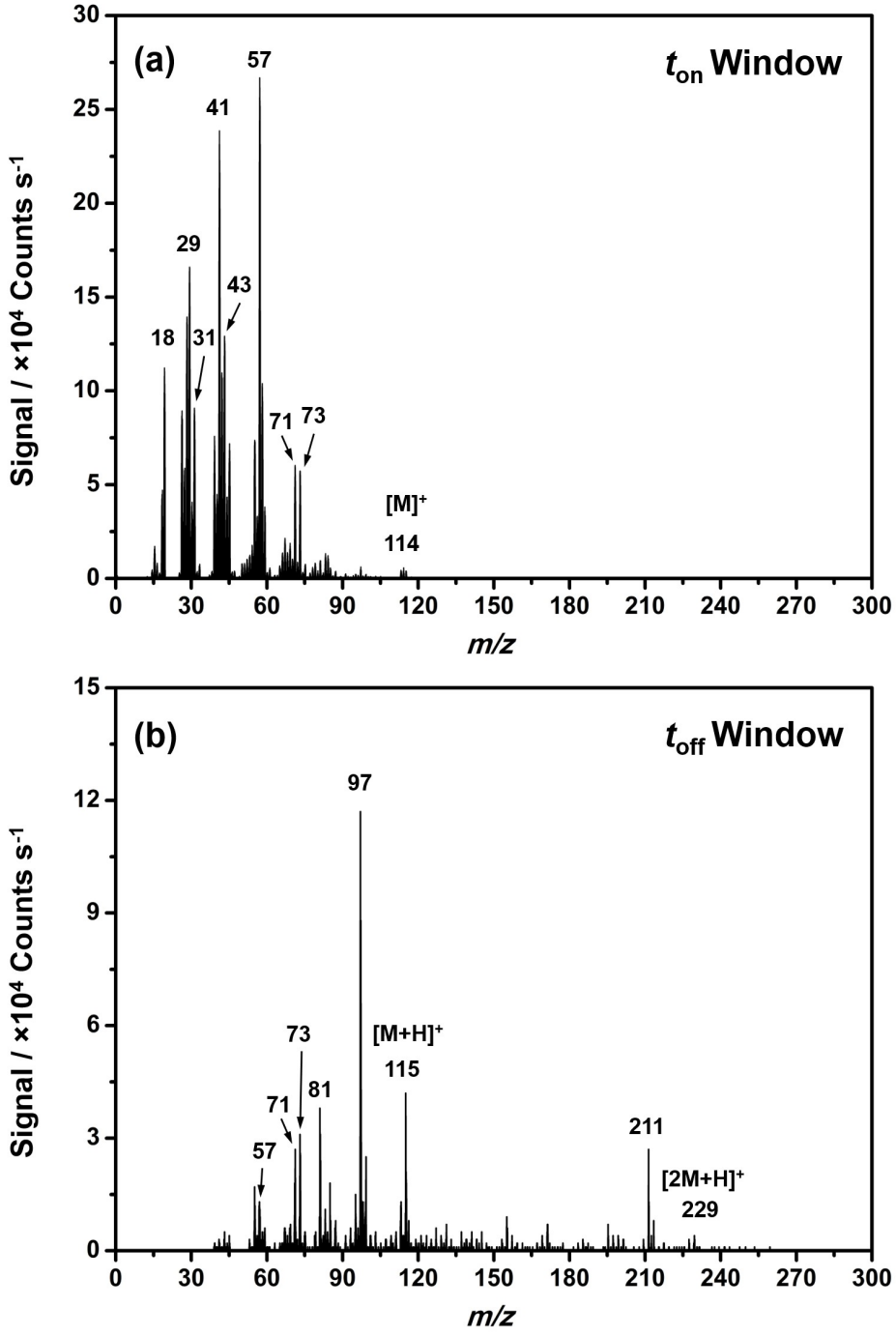

Figure 3.10: Time-resolved positive plasma ion mass spectra of allyl glycidyl ether pulsed plasma (t_{on} = 30 µs, t_{off} = 10 ms, P_{on} = 15 W, and 0.1 mbar). Mass spectrometer tuning on 57 *m/z* mass signal.

Two different plasma environments (t_{on} and t_{off} windows) were observed during in situ time-resolved positive plasma ion mass spectrometry. During the electrical discharge (t_{on}), the mass spectrum recorded (Figure 3.10a) is remarkably similar to the analogous time-averaged mass scan (Figure 3.9),

with high intensity mass signals (~10^{-4} counts s^{-1} range) mainly found in the lower range of the mass spectrum (18–114 *m/z*). As previously mentioned, this is due to the elevated degree of fragmentation together with the high energy ion and electron collisions occurring during the plasma on-period (t_{on}). Conversely, throughout the off-period a greater number of low intensity (~10^{-3} counts s^{-1} range) large mass fragment signals (mass peaks above the molecular ion) are observed. The protonated molecular ion ($[M+H]^+$) is present at 115 *m/z*, as well as the protonated dimer signal ($[2M+H]^+$) visible at 229 *m/z,* which is a clear indication of gas phase plasma polymerisation occurring in the off-period, as shown in Figure 3.10b. Other relevant fragments are 97 and 211 *m/z* which originates from the subtraction of an $[OH]^+$ group from the monomer precursor and the monomer dimer respectively ($[M-OH]^+$ and $[2M-OH]^+$).

3.3.6 Allyl Glycidyl Ether Plasma Radicals

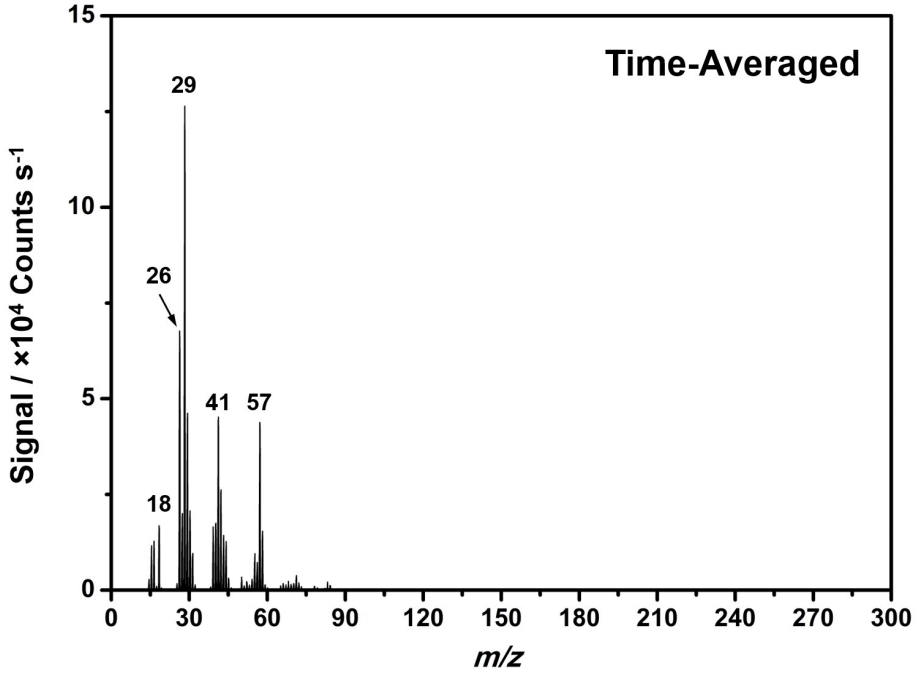

Figure 3.11: Time-averaged electron-impact ionisation mass spectrum of allyl glycidyl ether pulsed plasma (t_{on} = 30 µs, t_{off} = 10 ms, P_{on} = 15 W, and 0.1 mbar). Mass spectrometer tuning on 57 *m/z* mass signal.

Time-averaged electron-impact ionisation mass spectroscopy revealed very high fragmentation of the monomer precursor species within the pulsed plasma phase, Figure 3.11. The mass scan is characterised relatively low mass signals (up to 57 *m/z*) of very high intensity (~10^{-4} counts s^{-1} range), this

can be explained (as observed before) by the combination of the plasma discharge and the electron-impact ionisation giving rise to a large number of ionised particles with low mass. The main mass fragments observed are (26, 29, 41, 57 *m/z*) with no molecular ion signal presence.

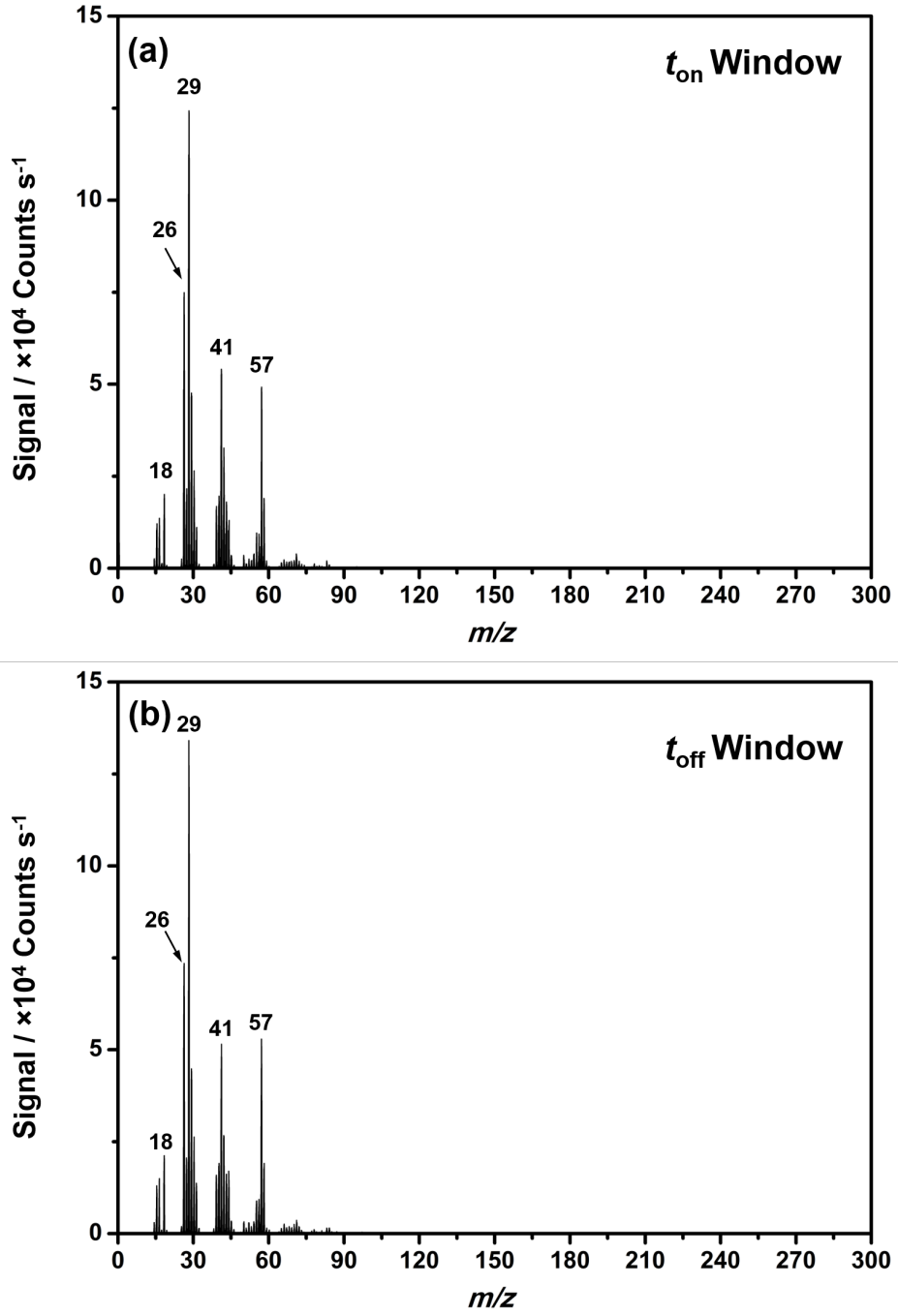

Figure 3.12: Time-resolved electron-impact ionisation mass spectra of allyl glycidyl ether pulsed plasmas (with t_{on} = 30 µs, t_{off} = 10 ms, P_{on} = 15 W, and 0.1 mbar). Mass spectrometer tuning on 57 *m/z* mass signal.

In the case of time-resolved electron-impact ionisation mass spectroscopy, no major differences are observed between the on-time (Figure 3.12a) and off-time (Figure 3.12b) period. Both spectra show very intense signals mainly present in the low mass range. As observed in average-mode (Figure 3.11) the main mass fragments observed are (26, 29, 41, 57 *m/z*) with no molecular ion signal presence, due to an elevated fragmentation degree.

3.4 Discussion

3.4.1 1-Decene

Positive plasma ions and radicals generated by 1-decene pulsed plasmas were investigated by in situ mass spectrometry. Experimental studies carried out in time-averaged mode, showed the characteristic fragmentation pattern of mono-olefins generated by plasma electron collisions occurring on different bonds along the carbon chain and strong signal corresponding to the molecular ion at 140 *m/z*. The same mass pattern can be observed during time-resolved operations, however, there are major differences between the two plasma periods; during on-time analysis (Figure 3.4a), the overall degree of fragmentation appears to be higher compared to the off-time plasma window where a greater concentration of intact precursor is present, with limited fragmentation occurring (Figure 3.4b). When 1-decene pulsed plasmas where studied by average and time-resolved electron impact mass spectrometry a similar trend was observed for plasma radicals, although, signal intensity at higher masses was lower compared to that of plasma ions and despite the presence of a double bond no oligomer formation is observed in the gas phase.

3.4.2 Allyl Glycidyl Ether

While average mode detection of allyl glycidyl ether (AGE) plasma ions did not show any oligomer formation (Figure 3.10), time-resolved analysis for plasma ions exhibited several key differences between on-time and off-time plasma periods. Allyl glycidyl ether monomer precursors undergo a high degree of fragmentation during the 30 μs-long plasma pulse ignition, with very intense ion counts recorded for low mass signals, Figure 3.11a. This is not observed during the subsequent plasma phase (10 ms – off-time period), where larger

fragments (i.e. dimers) are generated by addition polymerisation propagating via protonated intermediate species, such as [M+H] and [2M+H], as shown in Figure 3.11b. However, this signals appear to be relatively weak. The presence of low mass radicals indicates high levels of monomer precursor fragmentation (Figure 3.11 and Figure 3.12 a and b), additionally, no radical oligomer species were observed in average and time-resolved operating modes.

3.5 Conclusion

The experimental results obtained from mass spectrometry measurements of 1-decene and allyl glycidyl ether, have shown poor evidence of plasma phase polymerisation. For 1-decene pulsed plasmas, mass spectrometry analysis recorded total absence of large fragment formation (i.e. dimers and trimers) for both ionic and radical species. When allyl glycidyl ether was exposed to pulsed plasma discharges, weak mass signals corresponding to protonated dimers were recorded for ion species in the off-time window (plasma phase polymerisation via monomer unit addition) but no polymerisation was observed for radical species. Such results are consistent with step growth polymerisation predominantly occurring directly at the surface with little intermolecular propagation occurring in the gas phase. Further work is required to unambiguously establish whether this is the only mechanism in operation as previous reports have shown these monomers are capable of deposition of organic films via polymerisation, when exposed to plasma environments.

REFERENCES

1 Odian, G. Principles of Polymerization; John Wiley & Sons, Inc.: Hoboken, NJ, USA, 2004.

2 Kobayashi, H.; Bell, A. T.; Shen, M. Plasma Polymerization of Saturated and Unsaturated Hydrocarbons. *Macromolecules* **1974**, 7, 277–283.

3 Gillon, X.; Houssiau, L. Plasma Polymerization Chemistry of Unsaturated Hydrocarbons: Neutral Species Identification by Mass Spectrometry. *Plasma Sources Sci. Technol.* **2014**, 23, 045010.

4 Rinsch, C. L.; Chen, X.; Panchalingam, V.; Eberhart, R. C.; Wang, J.-H.; Timmons, R. B. Pulsed Radio Frequency Plasma Polymerization of Allyl Alcohol: Controlled Deposition of Surface Hydroxyl Groups. *Langmuir* **1996**, 12, 2995–3002.

5 Thierry, B.; Jasieniak, M.; de Smet, L. C. P. M.; Vasilev, K.; Griesser, H. J. Reactive Epoxy-Functionalized Thin Films by a Pulsed Plasma Polymerization Process. *Langmuir* **2008**, *24*, 10187–10195.

6 Fahmy, A.; Mix, R.; Schönhals, A.; Friedrich, J. F. Structure–Property Relationship of Thin Plasma Deposited Poly(Allyl Alcohol) Films. *Plasma Chem. Plasma Process.* **2011**, *31*, 477–498.

7 Carletto, A.; Badyal, J. P. S. Mechanistic Reaction Pathway for Hexafluoropropylene Oxide Pulsed Plasma Deposition of PTFE-like Films. *J. Phys. Commun.* **2017**, 1, 55024.

8 O'Toole, L.; Short, R. D.; Ameen, A. P.; Jones, F. R. Mass Spectrometry of and Deposition-Rate Measurements from Radiofrequency-Induced Plasmas of Methyl Isoburate, Methyl Methacrylate and N-Butyl Methacrylate. *J. Chem. Soc. Faraday Trans.* **1995**, 91, 1363–1370.

21 Budzikiewicz,H.; Djerassi C.; Williams D.H.; Mass Spectrometry of Organic Compounds,1st ed.; Longman: New York, 2001; pp 17-32.

22 NIST National Institute of Standard and Technology, U.S. Department of Commerce.https://webbook.nist.gov/cgi/cbook.cgi?ID=C872059&Mask=FFF (accessed October 18, 2018)

23 Yildirim, Y.; Balcan, M.; Bass, A. D.; Cloutier, P.; Sanche, L. Electron Stimulated Desorption of Anions and Cations from Condensed Allyl Glycidyl Ether. *Phys. Chem. Chem. Phys.* **2010**, *12*, 7950–7958.

24 Brown, R. M.; Creaser, C. S. The Electron Impact and Chemical Ionization Mass Spectra of Some Glycidyl Ethers. *Org. Mass Spectrom.* **1980**, *15*, 578–581.

4 : MECHANISTIC REACTION PATHWAY FOR HEXAFLUOROPROPYLENE OXIDE PULSED PLASMAS

4.1 Introduction

Hexafluoropropylene oxide (HFPO) is a stable fluorine-containing cyclic molecule.[1,2] Thermal or pulsed plasma excitation of HFPO is employed for the deposition of PTFE-like ($[\text{-}CF_2\text{-}]_n$) thin films for a variety of technological applications; these include liquid repellency, low dielectric constant electronic materials, encapsulation barrier layers, and biologically-implantable devices.[3,4,5]

The HFPO pyrolysis mechanism is understood to proceed via the formation of either fluoro(trifluoromethyl) carbene (II) and carbonyl difluoride (III), or difluorocarbene (VI) and trifluoroacetyl fluoride (VII) species, Scheme 4.1.[6,7,8,9,10,11] Under these conditions, it is the polymerisation of difluorocarbene ($:CF_2$) radicals which is postulated to give rise to the growth of PTFE-like films.[12,13,14,15] In the case of pulsed plasma excitation of HFPO gas, such intermediate difluorocarbene specie, have been detected by time-resolved ultraviolet absorption spectroscopy within the duty cycle on-period (t_{on}); followed by recombination processes predominating during each subsequent off-period (t_{off}).[13] However, the direct growth of perfluorocarbon chains within the electrical discharge has not previously been validated. Rather, X-ray photoelectron spectroscopy (XPS) and infrared analysis of the pulsed plasma deposited films have shown an enhancement in $–CF_2–$ group content with decreasing pulsed plasma duty cycle (i.e. greater structural retention to form PTFE-like films).[4, 16] In this article, the pulsed plasma polymerisation mechanism for HFPO precursor is investigated by time-resolved in situ mass spectrometry, with a particular emphasis on the role played by difluorocarbene species during the growth of PTFE-like perfluoroalkyl chains ($[\text{-}CF_2\text{-}]_n$).

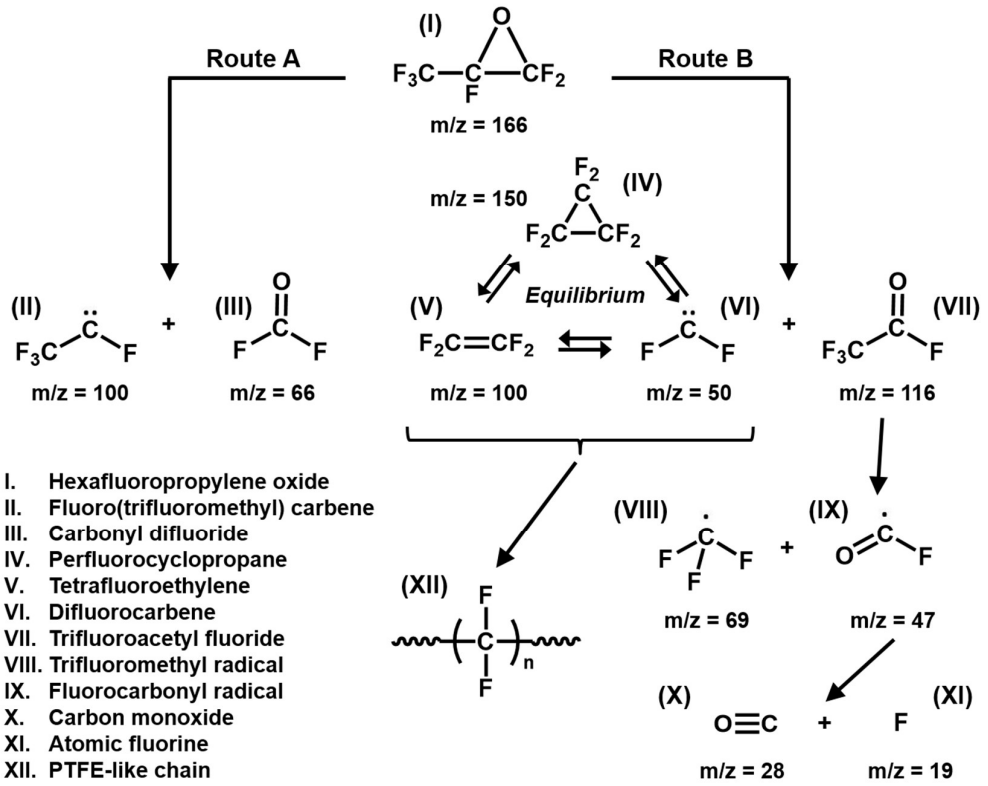

Scheme 4.1: Mechanistic reaction pathways for the fragmentation of hexafluoropropylene oxide (HFPO) and subsequent difluorocarbene polymerisation. The initial fragmentation steps (Route A and Route B) are analogous to reported HFPO thermal decomposition mechanisms.[6,8,9]

4.2 Experimental

In situ mass spectrometry analysis was undertaken during pulsed plasma polymerisation inside a cylindrical glass reactor see section paragraph 2.2 and 2.3 (Chapter 2). For pulsed plasmas, a fixed 500 ms off-period (t_{off}) and variable on-periods (t_{on}) of 10, 5 and 2 ms (corresponding to duty cycles of 2, 1 and 0.4 % approximately) were employed in conjunction with 50 W power input during the on-period (P_{on}). Plasma gaseous species (ions and neutrals) were sampled directly from the electrical discharge through the 200 µm end cap orifice. Mass spectra scans sampled the whole duty cycle, or either the t_{on} or t_{off} (afterglow) time frames, and were averaged over multiple pulse cycles to improve signal-to-noise (typically 2 min total scan time for 0–400 *m/z* range). Prior to each experiment, the chamber was cleaned with a 50 W oxygen plasma (0.2 mbar pressure) and then purged with

hexafluoropropylene oxide gas precursor (HFPO, +98%, Aldrich Chemical Company Inc.) at a pressure of 0.2 mbar via a fine control needle valve (model 145–217–4P4PC, Meggitt Avionics Ltd.) for 20 min, prior to electrical discharge ignition.

A range of standard perfluorocarbon molecules were also analysed in the gas phase (no plasma) using the same instrument in order to provide reference electron-impact ionisation mass fragmentation patterns and cross-checked against the American NIST database.[17,18] These included perfluoro-n-pentane (+99%, Fluorochem Ltd.) and perfluoro(methylcyclohexane) (+90%, Fluorochem Ltd.).

4.3 Results

4.3.1 Time-Averaged Mode Detection of Plasma Species

The parent fragment ion (molecular mass of HFPO = 166 amu), was absent during mass spectrometric analysis of the precursor molecule (t_{on} = 0 ms, i.e. no plasma), with CO^+ (28 *m/z*), CF^+ (31 *m/z*), and CF_3^+ (69 *m/z*) being the predominant peaks, Figure 4.1.[21] Plasma ignition leads to an order of magnitude increase in concentration of neutral species together with the appearance of ionic fragments. In time-averaged mass spectrometry detection mode, the relative concentration of neutral species is several orders of magnitude greater than positive ions, and was found to rise dramatically as the t_{on} period was shortened. Conversely, the number of positive plasma ions detected increased for longer t_{on} values, Figure 4.1. The most intense peaks for electron-impact of neutral plasma species were CO^+ (28 *m/z*), and CF_3^+ (69 *m/z*); whilst the most intense peak for positive plasma ions was CF_3^+ (69 *m/z*). At longer t_{on} values, the mass spectra approached those observed for continuous wave (non-pulsed) HFPO plasmas.[22] Whilst for decreasing t_{on} values, the electron-impact of neutral plasma species CO^+ (28 *m/z*) : CF_3^+ (69 *m/z*) ratio approaches that observed for the HFPO precursor molecule (t_{on} = 0 ms).

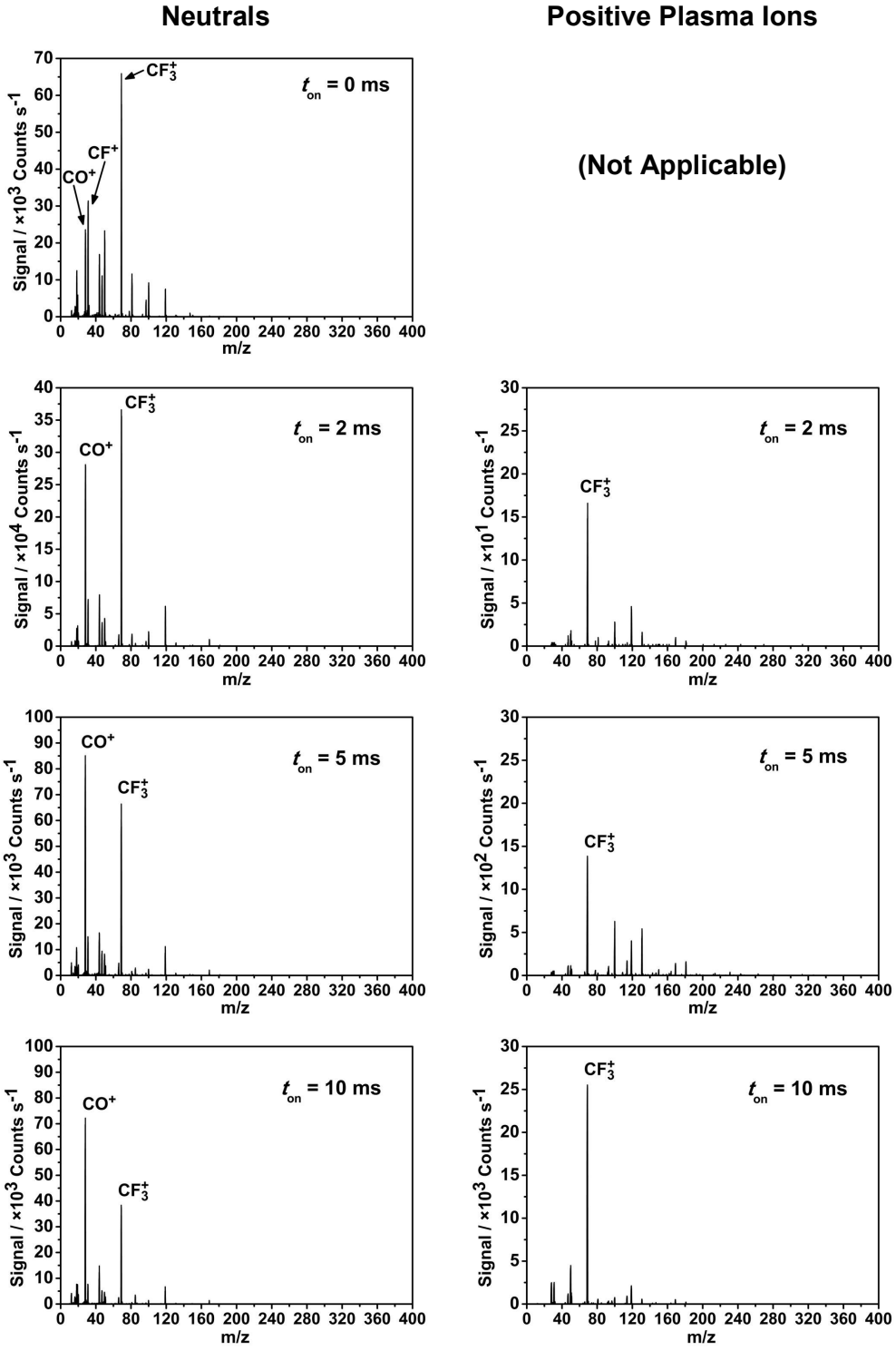

Figure 4.1. Time-averaged positive-mode mass spectra for electron-impact of neutral plasma species and positive plasma ions as a function of duty cycle for HFPO pulsed plasma (t_{off} = 500 ms, P_{on} = 50 W, and 0.2 mbar).

In the absence of electron-impact/attachment ionisation, no negative ion species (including F^- ions) were detected. Whilst for electron-attachment negative-mode mass spectrometry detection of plasma species, only fluorine atoms (19 *m/z*) were measured in all time-frames (time-averaged, resolved on-period and resolved off- period), Figure 4.2.

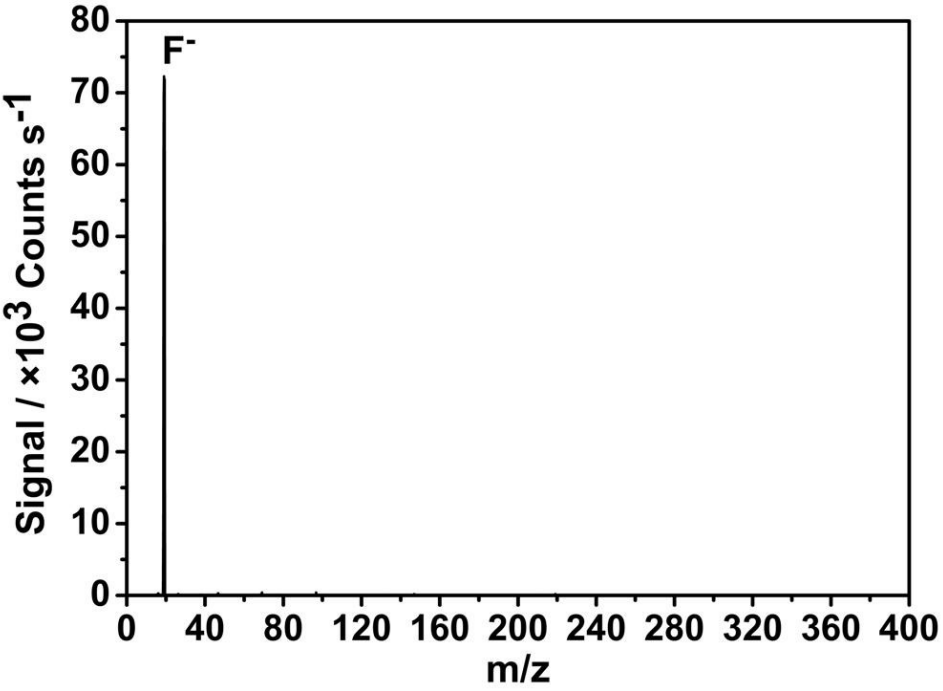

Figure 4.2. Typical time-averaged electron attachment negative-mode mass spectrum of HFPO pulsed plasma (t_{on} = 2 ms, t_{off} = 500 ms, P_{on} = 50 W, and 0.2 mbar).

4.3.2 Time-Resolved Electron-Impact Ionisation Positive-Mode Mass Spectrometry of Neutral Plasma Species

In the case of reference mass spectra taken for standard linear C_nF_{n+2} perfluoroalkane molecules, the CF_2^+ / CF_3^+ ion signal ratio remains fairly constant for n>3. This CF_2^+ / CF_3^+ ion ratio was also found to be steady for the analysis of HFPO pulsed plasma neutral species, which therefore supports the growth of linear C_nF_{n+2} perfluoroalkyl chains (species (XII) in Scheme 4.1), Figure 4.3. Other evidence for the formation of neutral linear chain perfluorocarbon species included the detection of mass spectrometric electron-impact ionisation mass fragments: ($C_2F_4^+$ (100 *m/z*), $C_2F_5^+$ (119 *m/z*), $C_3F_6^+$ (150 *m/z*), $C_3F_7^+$ (169 *m/z*), $C_4F_7^+$ (181 *m/z*), $C_4F_9^+$ (219 *m/z*) and $C_5F_{11}^+$ (269 *m/z*)), Figure 4.3. The signal intensity of these perfluoroalkyl chain fragments was found to increase by an order of magnitude (in both the t_{on} and t_{off} windows) with decreasing t_{on} period, which supports there being less plasma-induced fragmentation of growing polymer chains for shorter t_{on} values.[23] On the other hand, electrical discharge generated fragments arising from HFPO decomposition by-products become relatively more predominant at longer t_{on} values; for instance the CO^+ (28 *m/z*) signal is greater compared to the CF_3^+ (69 *m/z*) intensity at t_{on} = 10 ms and lower for t_{on} = 2 ms. These observations are also consistent with the aforementioned attenuation of extended plasma-induced HFPO molecule breakdown at shorter t_{on} periods (less CO by-product formation).

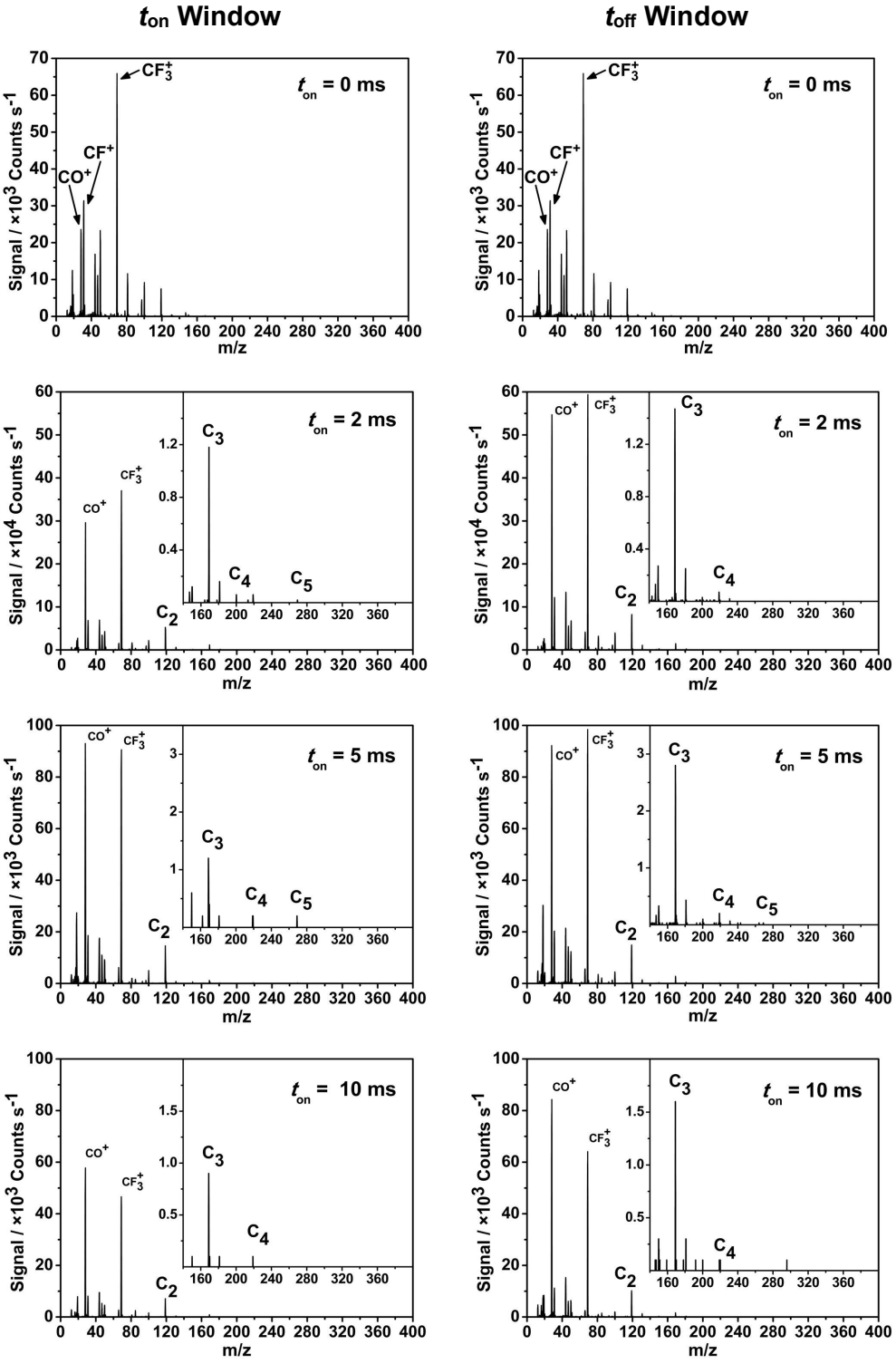

Figure 4.3. Time-resolved electron-impact ionisation positive-mode mass spectra of HFPO pulsed plasma neutral species as a function of duty cycle t_{on} period (t_{off} = 500 ms, P_{on} = 50 W, and 0.2 mbar). The detector was triggered for the whole duration of t_{on} and t_{off} time windows respectively. $C_nF_{2n+1}^+$ fragments are labelled as: C_2 = $C_2F_5^+$ (119 *m/z*), C_3 = $C_3F_7^+$ (169 *m/z*), C_4 = $C_4F_9^+$ (219 *m/z*), and C_5 = $C_5F_{11}^+$ (269 *m/z*). t_{on} = 0 ms corresponds to the fragmentation pattern of HFPO precursor molecule (absence of plasma ignition).

The relative signal intensity of neutral species measured during the t_{off} window was greater compared to either time-averaged or t_{on} period detection modes; which indicates that radical concentrations are highest during the t_{off} window (a prerequisite for polymer chain propagation mechanism involving either difluorocarbene (VI) or tetrafluoroethylene (V) intermediate species, Scheme 1), Figure 4.1 and Figure 4.3.

4.3.3 Time-Resolved Positive-Mode Mass Spectrometry of Positive Ion Plasma Species

In contrast to 70 eV electron-impact mass spectrometry of the HFPO precursor molecule (t_{on} = 0 ms, Figure 4.3), the HFPO parent molecular positive ion (166 *m/z*) was detected in the pulsed plasmas suggesting that the HFPO molecule undergoes much more gentle ionisation within the electrical discharge due to lower energy plasma electron impact collisions[24], allowing the formed HFPO molecule positive ion to remain intact, Figure 4.4. Linear C_nF_{n+2} perfluorocarbon chain positive ion plasma fragments were also detected ($C_2F_4^+$ (100 *m/z*), $C_2F_5^+$ (119 *m/z*), $C_3F_6^+$ (150 *m/z*), $C_3F_7^+$ (169 *m/z*), $C_4F_7^+$ (181 *m/z*), $C_4F_8^+$ (200 *m/z*), $C_4F_9^+$ (219 *m/z*), $C_5F_8^+$ (231 *m/z*), $C_5F_{11}^+$ (269 *m/z*)). The greater visibility of higher mass range fragments in positive-ion detection mode relative to fragments at lower masses is again due to the lower energy plasma electron impact ionisation process (compared to the higher 70 eV energy electron-impact ionisation employed for neutral species detection mode, Figure 4.3)[24]. The relative intensity of these perfluoroalkyl chain positive ion fragments rises with decreasing t_{on} period, which supports there being less plasma-induced fragmentation/damage of growing polymer chains at shorter t_{on} values. Interactions between ions and HFPO is observed with the exchange of an F^- ion with an O^{2-} ion derived from HFPO giving rise to an intense $C_3F_7^+$ peak, Figure 4.4.[25]

The previously described enhancement of neutral plasma species concentration during the t_{off} period at shorter t_{on} values detected in mass spectrometry electron-impact ionisation mode (Figure 4.3) is mirrored by a corresponding drop in intensity of positive-ion plasma species detected during the off-period. Furthermore, the positive-ion signal intensities are an order of

magnitude greater during the t_{on} period (electrical discharge) compared to the t_{off} period, Figure 4.4.

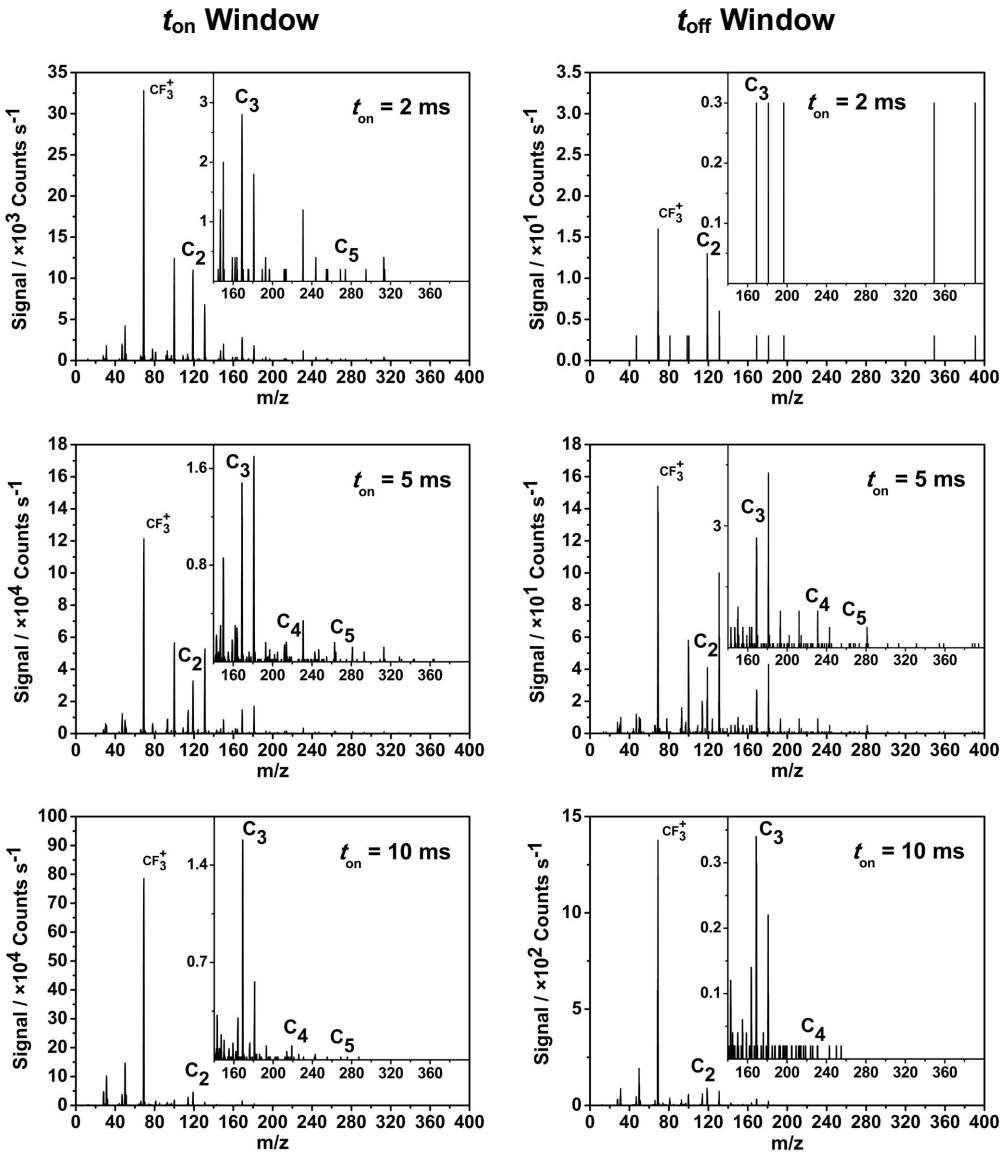

Figure 4.4. Time-resolved positive-mode mass spectra of HFPO pulsed plasma positive ions species as a function of duty cycle t_{on} period (t_{off} = 500 ms, P_{on} = 50 W, and 0.2 mbar). For each duty cycle, the detector was triggered for the whole duration of t_{on} and t_{off} time windows respectively. $C_nF_{2n+1}^+$ fragments are labelled as: $C_2 = C_2F_5^+$ (119 *m/z*), $C_3 = C_3F_7^+$ (169 *m/z*), $C_4 = C_4F_9^+$ (219 *m/z*), and $C_5 = C_5F_{11}^+$ (269 *m/z*).

4.4 Discussion

The detection of perfluoroalkyl chain fragments ($C_2F_4^+$ (100 *m/z*), $C_2F_5^+$ (119 *m/z*), $C_3F_6^+$ (150 *m/z*), $C_3F_7^+$ (169 *m/z*), $C_4F_7^+$ (181 *m/z*), $C_4F_8^+$ (200 *m/z*), $C_4F_9^+$ (219 *m/z*), $C_5F_8^+$ (231 *m/z*), $C_5F_{11}^+$ (269 *m/z*)) is consistent with reaction pathway B (Scheme 4.1) along with the formation of trifluoroacetyl fluoride (VII) by-product. The HFPO decomposition difluorocarbene (VI) product species (observed by time-resolved ultraviolet absorption spectroscopy[13]) exists in gas phase equilibrium with tetrafluoroethylene (V); where the balance between tetrafluoroethylene (CF_2=CF_2) and difluorocarbene (**:**CF_2) radicals lies towards CF_2=CF_2 (–Log K_{eq} ranges between 4.28–5.33).[26,27] A concurrent equilibrium with perfluorocyclopropane (IV) species is consistent with the detection of $C_3F_6^+$ (150 *m/z*) signal, Scheme 4.1, Figure 4.3 and Figure 4.4.[8,9] The rearrangement of perfluorocyclopropane (IV) to perfluoropropane followed by polymerisation can be ruled out due to the lack of expected -CF_3 groups detected by XPS in the deposited PTFE-like films.[4]

On this basis, the proposed mechanism entails HFPO molecules undergoing plasma-induced fragmentation during the t_{on} period to form difluorocarbene (**:**CF_2) species, and these then readily undergo polymerisation via **:**CF_2 or intermediate tetrafluoroethylene (CF_2=CF_2) species to form growing perfluoroalkyl chains ([-CF_2-]$_n$), Scheme 4.1. Shorter t_{on} values (less amount of energetic plasma ion-induced fragmentation) lead to the formation of longer perfluoroalkyl chains—which correlates to the high levels of -CF_2- content found in HFPO pulsed plasma deposited PTFE-like films at low duty cycles (up to 70% measured by X-ray photoelectron spectroscopy[4,14,16]).

4.5 Conclusions

Pulsed plasma polymerisation of hexafluoropropylene oxide (HFPO) proceeds via electrical discharge initiated decomposition of the precursor molecule to yield difluorocarbene (**:**CF_2) radicals during the pulse t_{on} period. These then readily recombine to form tetrafluoroethylene (CF_2=CF_2) intermediate species, which subsequently undergo polymerisation to create perfluoroalkyl PTFE-like chains. Shorter pulsed plasma duty cycles (t_{on}) give rise to a greater concentration of neutral species (including polymerisable tetrafluoroethylene (CF_2=CF_2) molecules), in conjunction with an attenuation of plasma ion concentrations—this leads to the growth of longer perfluoroalkyl PTFE-like chains.

REFERENCES

1 Sargeant, P. B. Fluorocyclopropanes. I. Preparation and Nuclear Magnetic Resonance Spectra. *J. Org. Chem.* **1967**, *35*, 678–682.

2 Sargeant, P. B.; Krespan, C. G. Fluorocyclopropanes. II. Synthesis, Properties, and Reactions of Perfluorocyclopropene. *J. Am. Chem. Soc.* **1969**, *91*, 415–419.

3 Gleason, K. K.; Limb, S. J. H.; Gleason, E. F.; Sawin, H. H.; Edell, D. J., Chemical Vapor Deposition of Fluorocarbon Polymer Thin Films, US6156435, December 5, 2000.

4 Savage, C. R.; Timmons, R. B.; Lin, J. W. Molecular Control of Surface Film Compositions via Pulsed Radio-Frequency Plasma Deposition of Perfluoropropylene Oxide. *Chem. Mater.* **1991**, *51*, 575–577.

5 Timmons, R. B.; Wang, J. Molecular Tailoring of Surfaces, US5876753, March 2, 1999.

6 Eleuterio, H. S. Polymerization of Perfluoro Epoxides. *J. Macromol. Sci. Part A - Chem.* **1972**, *6*, 1027–1052.

7 Ng, M.; Mok, D. K. W.; Dyke, J. M.; Lee, E.P.F. Decomposition Reactions of Hexafluoropropylene Oxide (HFPO): Rate Coefficients Calculated at Different Temperatures Using Ab Initio and DFT Reaction Paths. *J. Fluor. Chem.* **2014**, *159*, 29–37.

8 Craig Kennedy, R.; Levy, J. B. The Pyrolysis of Hexafluoropropylene Oxide. *J. Fluor. Chem.* **1976**, *7*, 101–114.

9 Mahler, W.; Resnick, P. R. The Reversible Difluorocarbene Elimination from Hexafluoropropylene Epoxide. *J. Fluor. Chem.* **1974**, *3*, 451–452.

10 Liu, D.; Martin, I. T.; Fisher, E. R. CF_2 Surface Reactivity during Hot Filament and Plasma-Enhanced Chemical Vapor Deposition of Fluorocarbon Films. *Chem. Phys. Lett.* **2006**, *430*, 113–116.

11 Banks, R. E.; Barlow, M. G. Specialist Periodical Reports: Fluorocarbon and Related Chemistry, Vol. 1; Royal Society of Chemistry, 2007; pp 146–147.

12 Lau, K. K. S.; Gleason, K. K. Pulsed Plasma Enhanced and Hot Filament Chemical Vapor Deposition of Fluorocarbon Films. *J. Fluor. Chem.* **2000**, *104*, 119–126.

13 Cruden, B. A.; Gleason, K. K.; Sawin, H. H. Time Resolved Ultraviolet Absorption Spectroscopy of Pulsed Fluorocarbon Plasmas. *J. Appl. Phys.* **2001**, *89*, 915–922.

14 Butoi, C. I.; Mackie, N. M.; Gamble, L. J.; Castner, D. G.; Barnd, J.; Miller, A. M.; Fisher, E. R. Deposition of Highly Ordered CF_2-Rich Films Using Continuous Wave and Pulsed Hexafluoropropylene Oxide Plasmas. *Chem. Mater.* **2000**, *12*, 2014–2024.

15 Butoi, C. I.; Mackie, N. M.; McCurdy, P. R.; Peers, J. R. D.; Fisher, E. R. Surface Interactions of Radicals During Plasma Processing of Polymers. *Plasmas Polym.* **1999**, *4*, 77–91.

16 Limb, S. J.; Edell, D. J.; Gleason, E. F.; Gleason, K. K. Pulsed Plasma-Enhanced Chemical Vapor Deposition from Hexafluoropropylene Oxide: Film Composition Study. *J. Appl. Polym. Sci.* **1997**, *67*,1489–1502.

17 NIST National Institute of Standard and Technology, U.S. Department ofCommerce.http://webbook.nist.gov/cgi/cbook.cgi?ID=C678262&Units=SI&Mask=200#Mass-Spec. (accessed May 29, 2017).

18 NIST National Institute of Standard and Technology, U.S. Department ofCommerce.http://webbook.nist.gov/cgi/cbook.cgi?ID=C355022&Units=SI&Mask=200#Mass-Spec. (accessed May 29, 2017).

21 NIST National Institute of Standard and Technology, U.S. Department ofCommerce.http://webbook.nist.gov/cgi/inchi?ID=C428591&Mask=200#Mass-Spec. (accessed May 29, 2017).

22 Cuddy, M. F.; Blechle, J. M.; Fisher, E. R. Ion Contributions to Gas–surface Interactions in Inductively-Coupled Fluorocarbon Plasmas. *Int. J. Mass Spectrom.* **2012**, *330–332*, 46–57.

23 Ryan, M. E.; Hynes, A. M.; Badyal, J. P. S. Pulsed Plasma Polymerization of Maleic Anhydride. *Chem. Mater.* **1996**, *8*, 37–42.

24 Grill, A. Cold Plasma Materials Fabrication: From Fundamentals to Applications, 1st ed.; IEEE Press: Piscataway, 1994; pp 8–10.

25 Su, T.; Hammond, G. B.; Morris, R. A.; Viggiano, A. A.; Paulson, J. F.; Liebman, J. F.; Su, A. C. L. Gaseous Ion-Molecule Reactions of F^-, CF_3^-, $C_2F_5^-$, CF_3^+ and $C_2F_5^+$ with Hexafluoropropene Oxide. *J. Fluor. Chem.* **1995**, *74*, 149–157.

26 Lau, K. K. S.; Gleason, K. K.; Trout, B. L. Thermochemistry of Gas Phase CF_2 Reactions: A Density Functional Theory Study. *J. Chem. Phys.* **2000**, *113*, 4103–4108.

27 Zmbov, K. F.; Uy, O. M.; Margrave, J. L. Mass Spectrometric Study of the High Temperature Equilibrium $C_2F_4 \leftrightarrow 2CF_2$ and the Heat of Formation of the CF_2 Radical. *J. Am. Chem. Soc.* **1968**, *90*, 5090–5092.

5 : ULTRA-HIGH SELECTIVITY PULSED PLASMACHEMICAL DEPOSITION REACTION PATHWAYS

5.1 Introduction

High selectivity chemical reaction pathways are of fundamental importance in modern chemistry and have in the past been attained via a variety of conventional approaches, including catalysis (heterogeneous, homogeneous, enzymes), high pressure kinetic methods, mixing techniques, and solvent effects.[1,2,3,4,5,6,7] Although these have proven to be selective towards the formation of specific chemical products, there can be inherent limiting factors. For instance, in the case of catalytic processes where metals are often employed, such systems can be expensive and seldom reusable; whilst high pressure, mixing, and solvent-based syntheses can be environmentally unfriendly as well as involving multiple steps.[8,9,10,11]

Non-equilibrium (low temperature) electrical discharges offer the potential for single-step and low cost chemical syntheses. However, the main drawback has been poor chemical selectivity.[12] Pulsing such plasmas potentially provides means to control the lifetimes of reactive intermediate species, and thereby enable control over reaction pathways. In the case of pulsed plasma excitation of organic monomers, through a careful selection of electrical discharge parameters, it is possible to achieve high levels of molecular control for the deposited film composition and its properties.[13,14] For example, hundreds of millions of smartphones have been protected against water damage using such functional nanocoatings.[15] By using a variety of surface characterisation techniques (including ToF-SIMS, MALDI-MS, XPS, FTIR), strong structural similarities have been found with analogous conventional wet chemical synthesis step-growth polymers.[16,17,18]

However, the underlying mechanism for the growth of such structurally well-defined pulsed plasma functional films is poorly understood. Previous in situ mass spectrometry studies of polymerising plasmas have identified oligomer formation, but an absence of ultra-high selectivity reaction pathways.[19,20,21,22,23,24,25,26]

Time-resolved in situ mass spectrometry studies of pulsed electrical discharges, offer the scope for probing plasmachemical reaction pathways during the respective on- and off-time windows (t_{on} and t_{off}). In this study, glycidyl methacrylate precursor () is investigated following earlier reports of the pulsed plasma deposition of structurally well-defined poly(glycidyl methacrylate) films (as confirmed by XPS and ToF-SIMS).[16,27] Furthermore, glycidyl methacrylate contains two reactive functionalities (acrylate carbon–carbon double bond and epoxide group)—the selective plasmachemical activation of one of these groups (acrylate) highlights the versatility of pulsed plasma deposition as a method for surface functionalisation. Such epoxide-functionalized surfaces are sought for technological applications such as, chemosensors, biosensors, drug delivery, biomolecule arrays, electroless metal deposition, and anti-biofouling surfaces.[28,29,30,31,32,33,34,35]

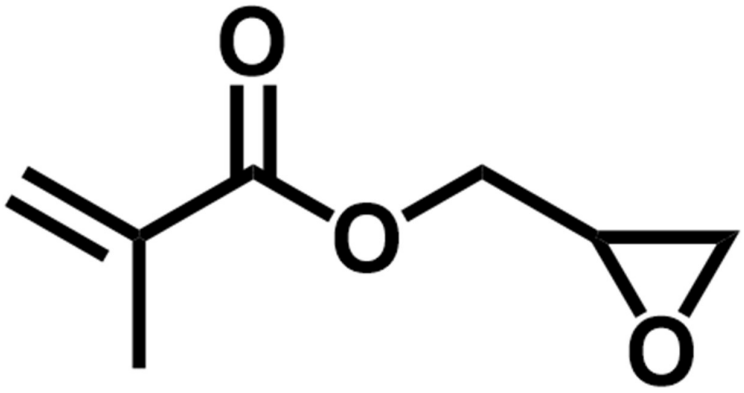

Structure 2: Glycidyl methacrylate

5.2 Experimental

Time-resolved in situ mass spectrometry measurements were performed during pulsed plasma excitation of glycidyl methacrylate precursor (+97%, Sigma Aldrich Co.). Prior to each experiment, the chamber was cleaned by running a 50 W oxygen plasma (0.2 mbar pressure) until no contaminant species were detected by mass spectrometry. Glycidyl methacrylate precursor was loaded into a sealable glass tube, degassed via at least 5 freeze–pump–thaw cycles, and attached to the reactor. The monomer was then purged through the system at a pressure of 0.1 mbar via a fine control needle valve

(model 145-217-4P4PC, Meggitt Avionics Ltd.) for 20 min, followed by electrical discharge ignition. For pulsed plasmas, an on-period (t_{on}) of 30 μs and an off-period (t_{off}) of 10 ms were used in conjunction with 15 W of continuous wave power input during the on-period (P_{on}). These parameters were chosen on the basis of earlier optimisation studies reported for high structural retention of pulsed plasma deposited poly(glycidyl methacrylate) nanolayers.[16] After each experiment, the pulsed plasma poly(glycidyl methacrylate) nanolayer was oxidised off the chamber walls by running a 50 W oxygen plasma (0.2 mbar pressure) until no carbonaceous species were detected by mass spectrometry. The electron impact ionisation source of the mass spectrometer was operated at low energy (20 eV) in order to avoid excessive fragmentation during the detection of neutral and radical plasma species. In addition, ionised gaseous species (plasma ions) were sampled directly from within the electrical discharge through the 200 μm diameter end cap orifice by switching off the electron impact ionisation source and appropriate ion energy tuning was chosen according to the mass range to be investigated.

For time-resolved measurements and detector gating operations, the transit time was calculated using the procedure described in section 2.6 (Chapter 2).

5.3 Results

5.3.1 Glycidyl Methacrylate Electron-Impact Fragmentation

Low energy (20 eV) electron-impact ionisation avoids extensive molecular fragmentation of glycidyl methacrylate precursor vapour, Figure 5.1. The main mass fragments formed are at 41, 43, 57, and 69 *m/z,* which correspond to specific bond cleavages within the molecule.[36,37,38,39] The parent molecular ion mass signal (142 *m/z*) and protonated molecular ion (143 *m/z*) were both absent.[40]

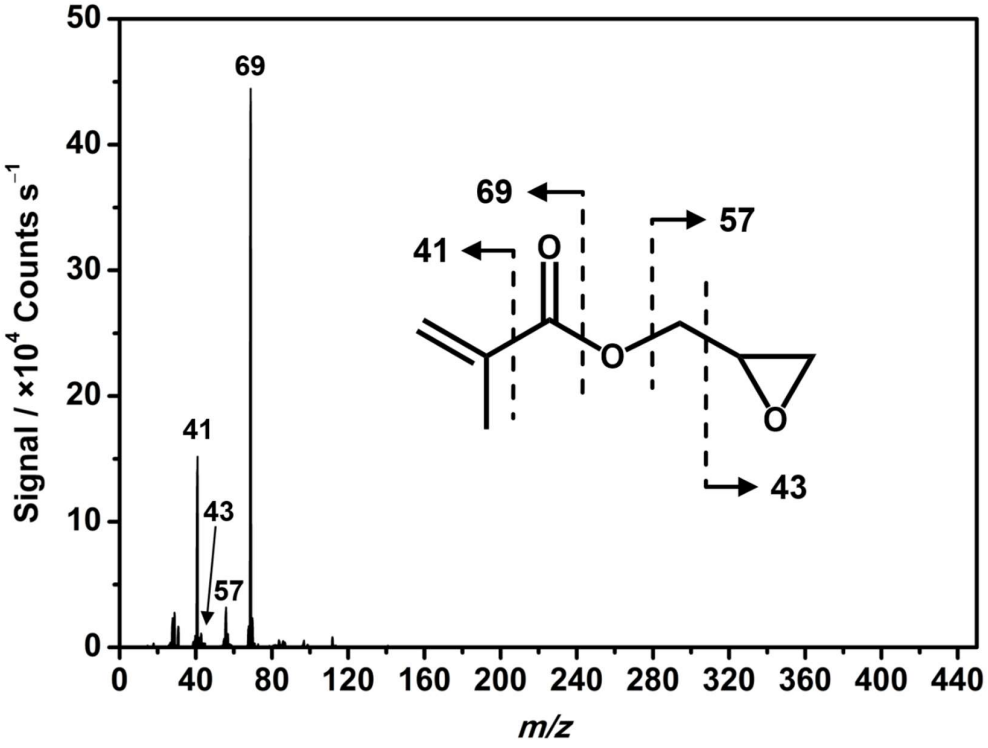

Figure 5.1: 20 eV electron-impact ionisation mass spectrum of glycidyl methacrylate monomer vapour, (0.1 mbar pressure). Mass spectrometer tuning optimised on 69 *m/z* mass signal.

5.3.2 Positive Plasma Ion Species

In contrast to the absence of any parent molecular ion peak in the electron-impact ionisation mass spectrum of glycidyl methacrylate precursor (Figure 5.1), the protonated molecular ion peak (143 *m/z*) is present in the time-averaged positive ion mass spectrum of glycidyl methacrylate pulsed plasma, Figure 5.2. Moreover, the formation of new well-defined oligomer species at

higher masses is evident corresponding to increasing integer number addition of glycidyl methacrylate monomer molecular mass repeat units (demonstrative of high selectivity). These arise as a consequence of step-wise glycidyl methacrylate monomer addition polymerisation from two initiator species—the main low energy electron impact fragmentation ion for glycidyl methacrylate monomer (69 *m/z*) and protonated glycidyl methacrylate precursor (143 *m/z*), Figure 5.1 and Figure 5.2, respectively.

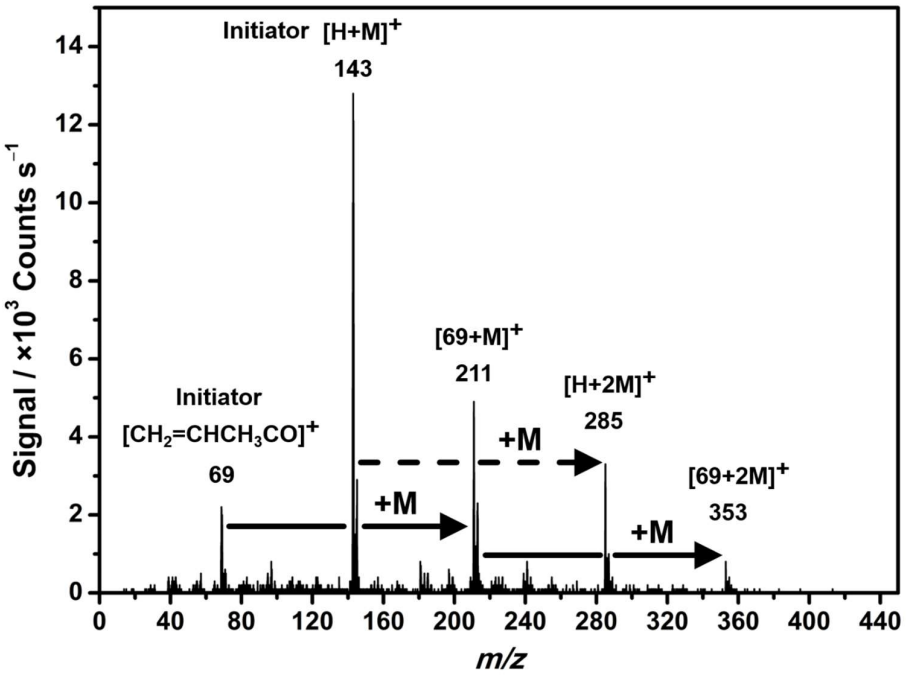

Figure 5.2: Time-averaged positive plasma ion mode mass spectrum of glycidyl methacrylate pulsed plasma (t_{on} = 30 µs, t_{off} = 10 ms, P_{on} = 15 W, and 0.1 mbar pressure). Mass spectrometer tuning optimised on 285 *m/z* mass signal.

Time-resolved mass spectrometry of glycidyl methacrylate pulsed plasmas detected the presence of a variety of positive ions during the electrical discharge on-period (t_{on}), Figure 5.3. These were low mass fragments (19, 28, 41, 43, 57, 69 and 143 *m/z*), with the main electron-impact molecular fragment (69 *m/z*) of glycidyl methacrylate monomer and the protonated precursor ion (143 *m/z*) being predominant within the on-period window, i.e. the formation of initiator species required for subsequent step-wise monomer addition polymerisation during the off-period, Figure 5.3.

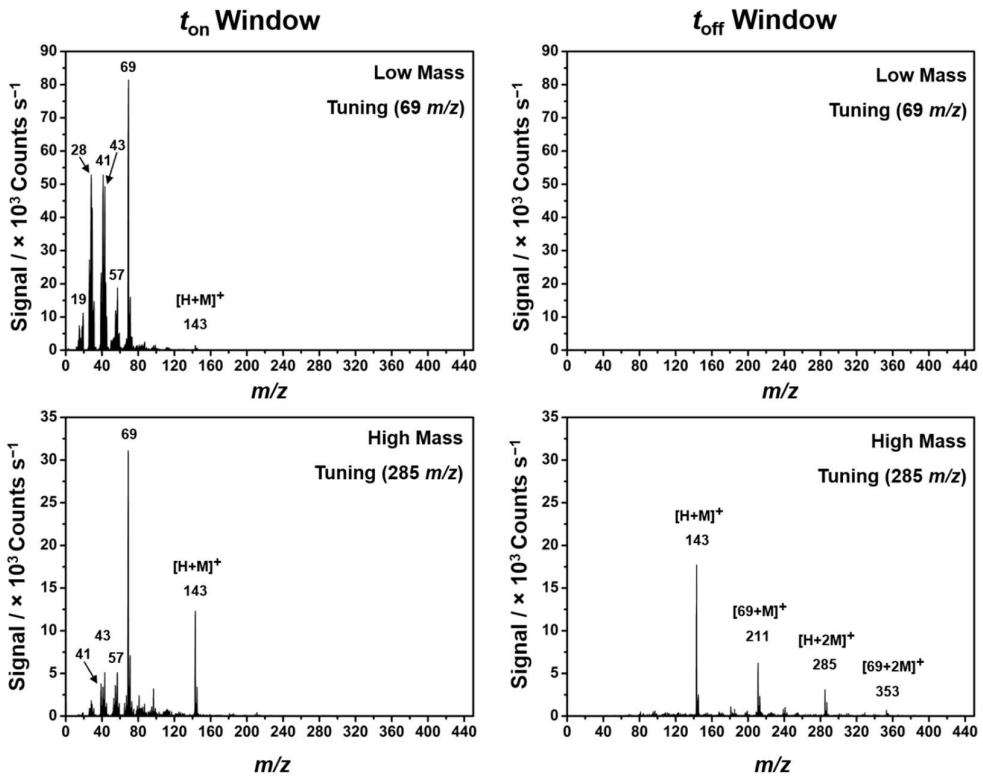

Figure 5.3: Low and high mass tuning time-resolved positive plasma ion mode mass spectra of glycidyl methacrylate pulsed plasma (t_{on} = 30 µs, t_{off} = 10 ms, P_{on} = 15 W, and 0.1 mbar pressure).

Monitoring of the subsequent off-period (t_{off}) window revealed exclusive (high selectivity) step-wise addition of glycidyl methacrylate monomer repeat units to both of the aforementioned on-period (t_{on}) window cation initiator species (69 and 143 *m/z*), leading to well-defined polymer chain growth over a time scale of about 5 ms—with longer (higher mass) polymer chain ions becoming more prominent over time, Figure 5.4. Beyond this time frame of 5 ms, these polymer cations disappear due to recombination processes, film deposition, and decrease in ion energy (detuning of the mass spectrometer). Regardless, it is clear that the polymeric cations do indeed survive beyond the short on-period (t_{on} = 30 µs).

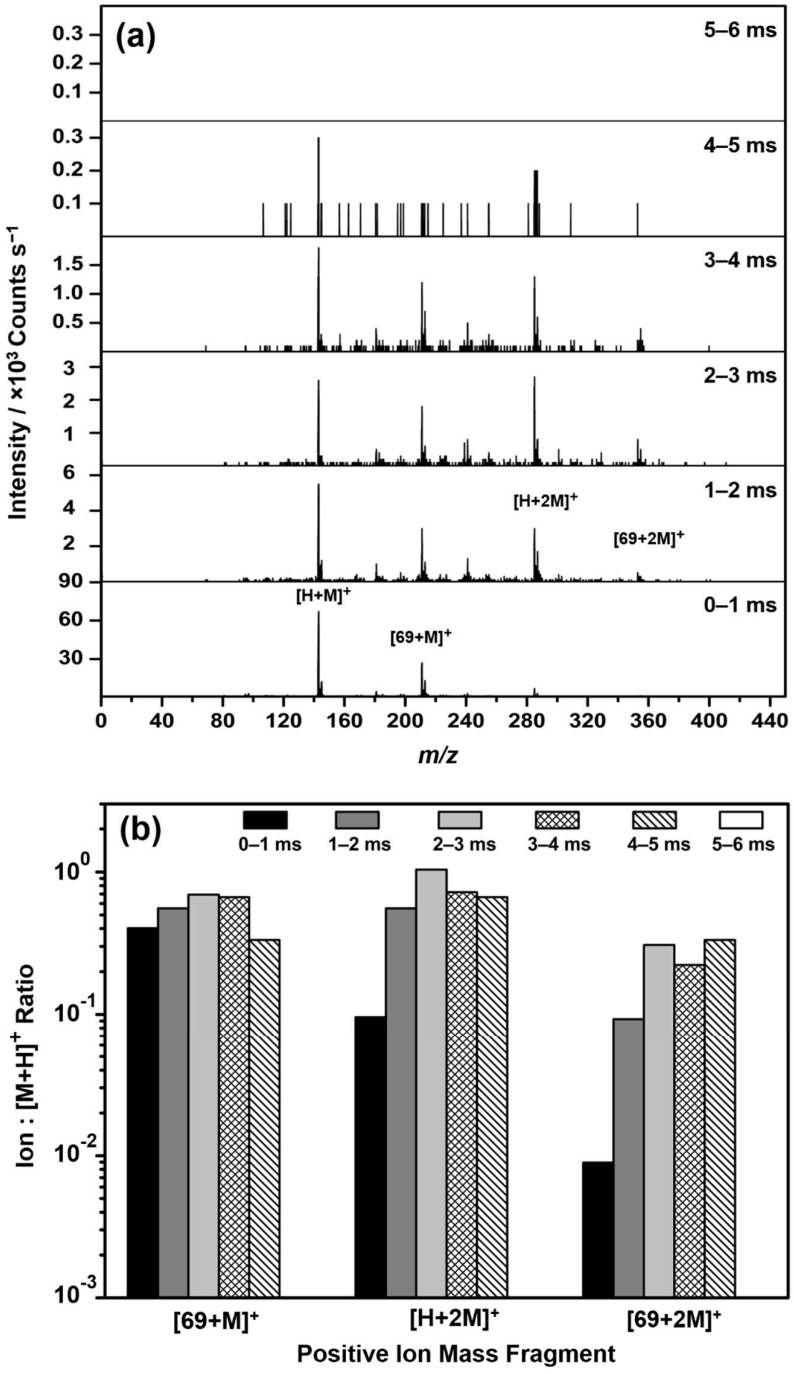

Figure 5.4: (a) Off-period positive ion mass mode spectra taken during consecutive 1 ms sampling time windows for glycidyl methacrylate pulsed plasma (t_{on} = 30 µs, t_{off} = 10 ms, P_{on} = 15 W, and 0.1 mbar pressure); and (b) variation of positive ion mass mode fragments between consecutive 1 ms sampling time windows during the off-period, showing relative positive ion : protonated molecular ion (143 *m/z*) intensity ratios. Note the complete disappearance of positive ion species after 5 ms. Mass spectrometer tuning optimised on 285 *m/z* mass signal.

5.3.3 Neutral Plasma Species

Low energy (20 eV) electron-impact ionisation mass spectrometry of neutral pulsed plasma species (including radicals) detected similar fragments to those observed during positive plasma ion sampling, with the main glycidyl methacrylate electron-impact fragment being 69 *m/z*, Figure 5.1 and Figure 5.5. This species in combination with hydrogen atom addition to monomer (143 *m/z*) act as radical initiators for step-wise monomer addition polymerisation.

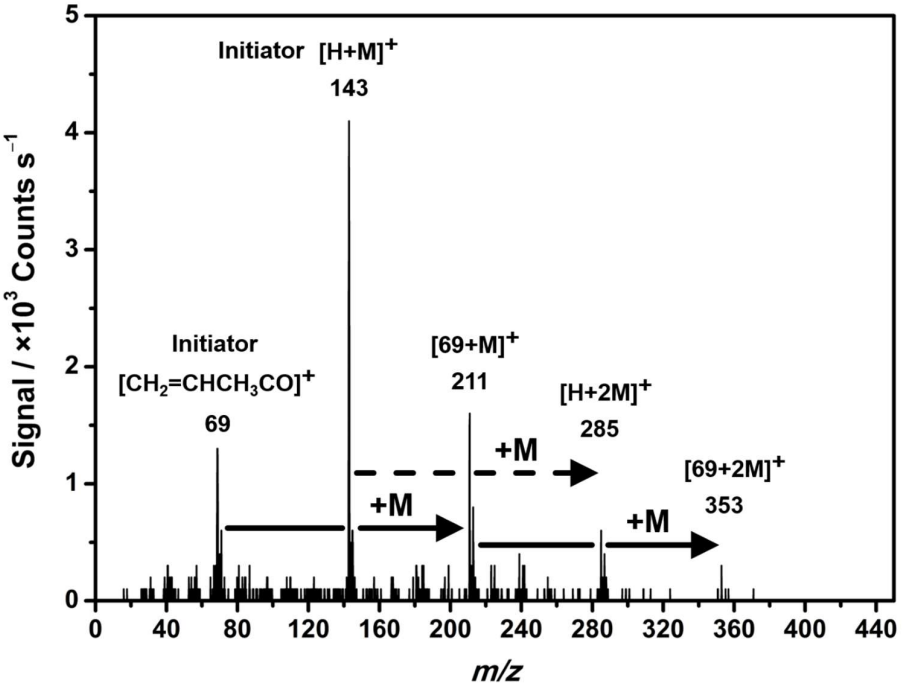

Figure 5.5: Time-averaged 20 eV electron-impact ionisation mass spectrum of glycidyl methacrylate pulsed plasma (t_{on} = 30 µs, t_{off} = 10 ms, P_{on} = 15 W, and 0.1 mbar pressure). Mass spectrometer tuning optimised on 211 *m/z* mass signal.

As observed previously during positive plasma ion mass spectrometer detection mode, 69 *m/z* and 143 *m/z* initiator species are created during the short pulsed plasma time-on (t_{on}) window, Figure 5.6. Polymer chain growth occurs within the extended pulsed plasma off-period (t_{off}) window, with longer growing (higher mass) chain signal intensities rising over time, Figure 5.7. The drop in overall intensity can be attributed to recombination processes as well as film deposition.

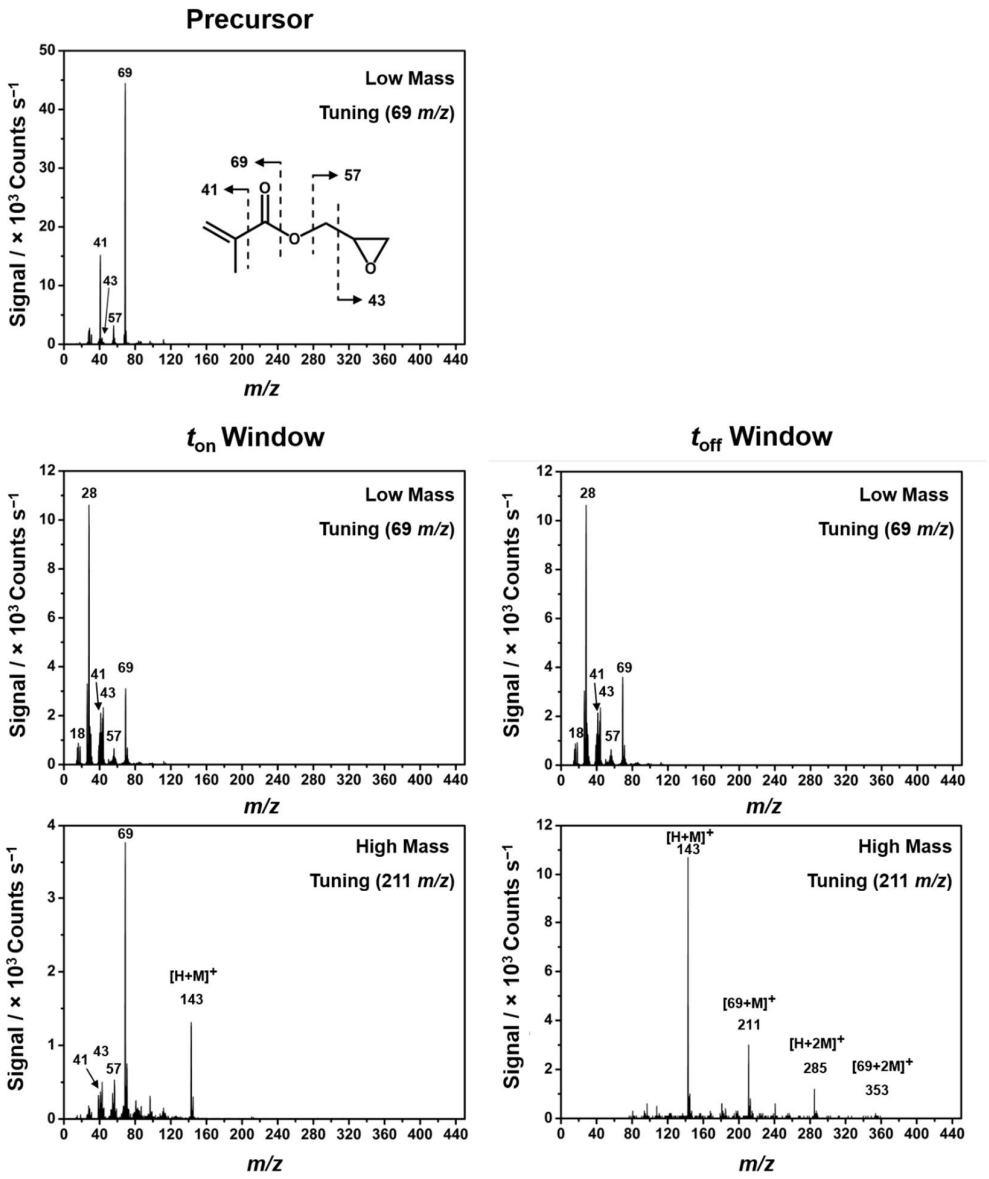

Figure 5.6: Low and high mass tuning time-resolved 20 eV electron-impact ionisation mass spectra of glycidyl methacrylate monomer vapour (top left) and pulsed plasma (middle and bottom spectra, with t_{on} = 30 µs, t_{off} = 10 ms, P_{on} = 15 W, and 0.1 mbar pressure).

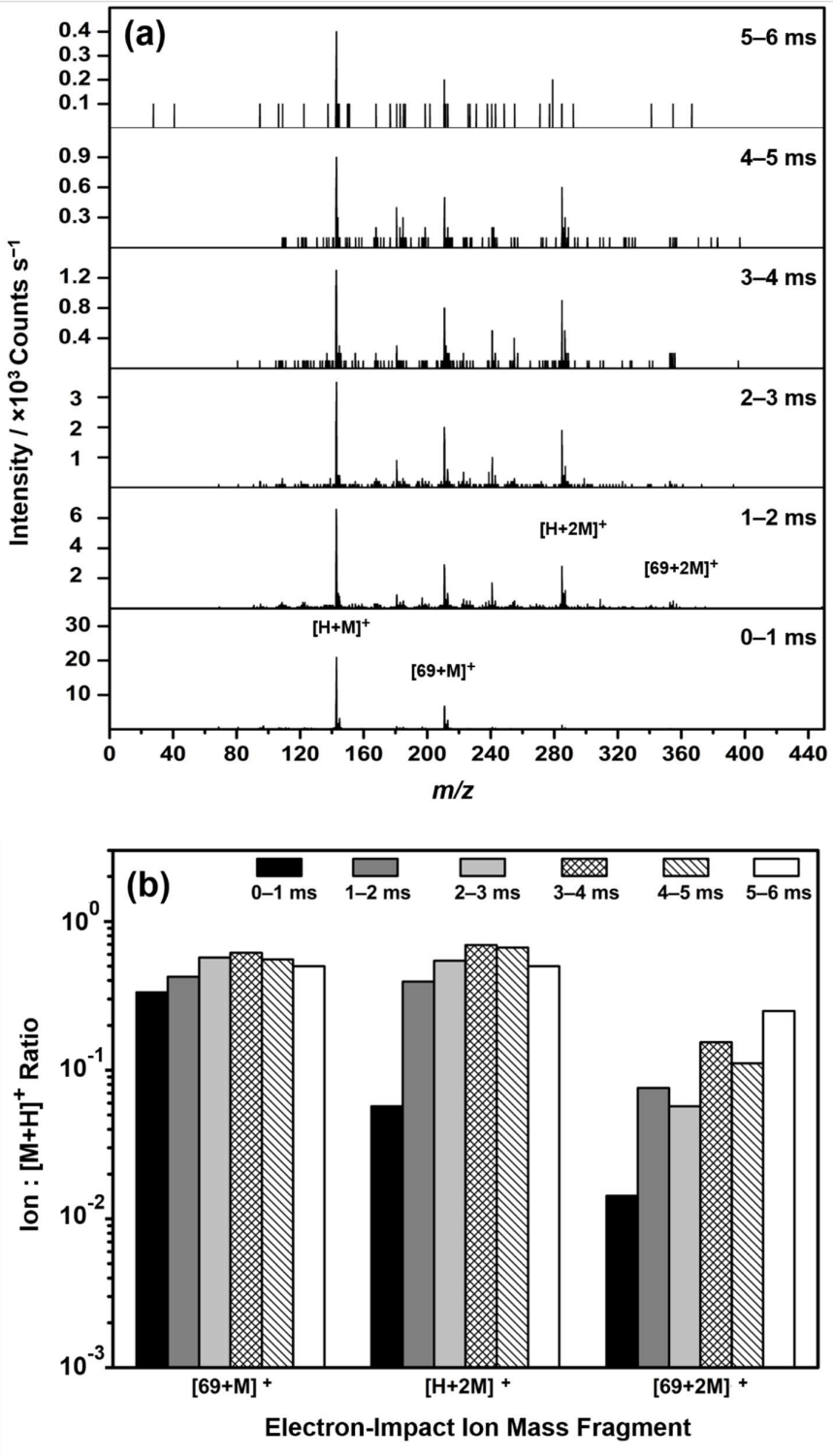

Figure 5.7: (a) Off-period 20 eV electron-impact ionisation mass spectra taken during consecutive 1 ms sampling time windows for glycidyl methacrylate pulsed plasma (t_{on} = 30 µs, ms t_{off} = 10 ms, P_{on} = 15 W, and 0.1 mbar pressure); and (b) variation of mass fragments between consecutive 1 ms sampling time windows during the off-period, showing relative fragment : protonated molecular ion (143 *m/z*) intensity ratios. Mass spectrometer tuning optimised on 211 *m/z* mass signal.

5.4 Discussion

The high levels of plasmachemical reaction pathway selectivity observed by mass spectrometry for the pulsed electrical discharge of glycidyl methacrylate precursor complements the earlier reported time-of-flight secondary ion mass spectrometry (ToF-SIMS) spectra of pulsed plasma deposited poly(glycidyl methacrylate) nanolayers.[16]

This in situ mass spectrometry provides direct evidence for a highly selective step-wise monomer addition polymerisation mechanism occurring during pulsed plasma excitation which underpins the growth of structurally well-defined poly(glycidyl methacrylate) thin films, Figure 5.3 and Figure 5.6. There are two distinct reaction regimes corresponding to the short on-period (t_{on}) and long off-period (t_{off}) time windows, Scheme 5.1. The former corresponds to electrical discharge ignition occurring on the microsecond (μs) timescale to create two initiator species: methacryolyl (69 *m/z*—which is the main fragment formed following low energy electron impact of glycidyl methacrylate precursor, Figure 5.1), and the protonated monomer (143 *m/z*).[16,17,41,42] This is followed by conventional polymerisation reactions proceeding during the subsequent longer millisecond (ms) off-period timescale, with monomer units sequentially adding to the growing polymer chain, Scheme 5.1.17,[24,43,44] Both positive ions and radicals at 69 *m/z* and 143 *m/z* act as initiators for the off-period polymerisation reaction pathway, Figure 5.3 and Figure 5.6 respectively. This is accompanied by an increase in relative intensity of the higher mass oligomeric species during the off-period, Figure 5.4 and Figure 5.7.

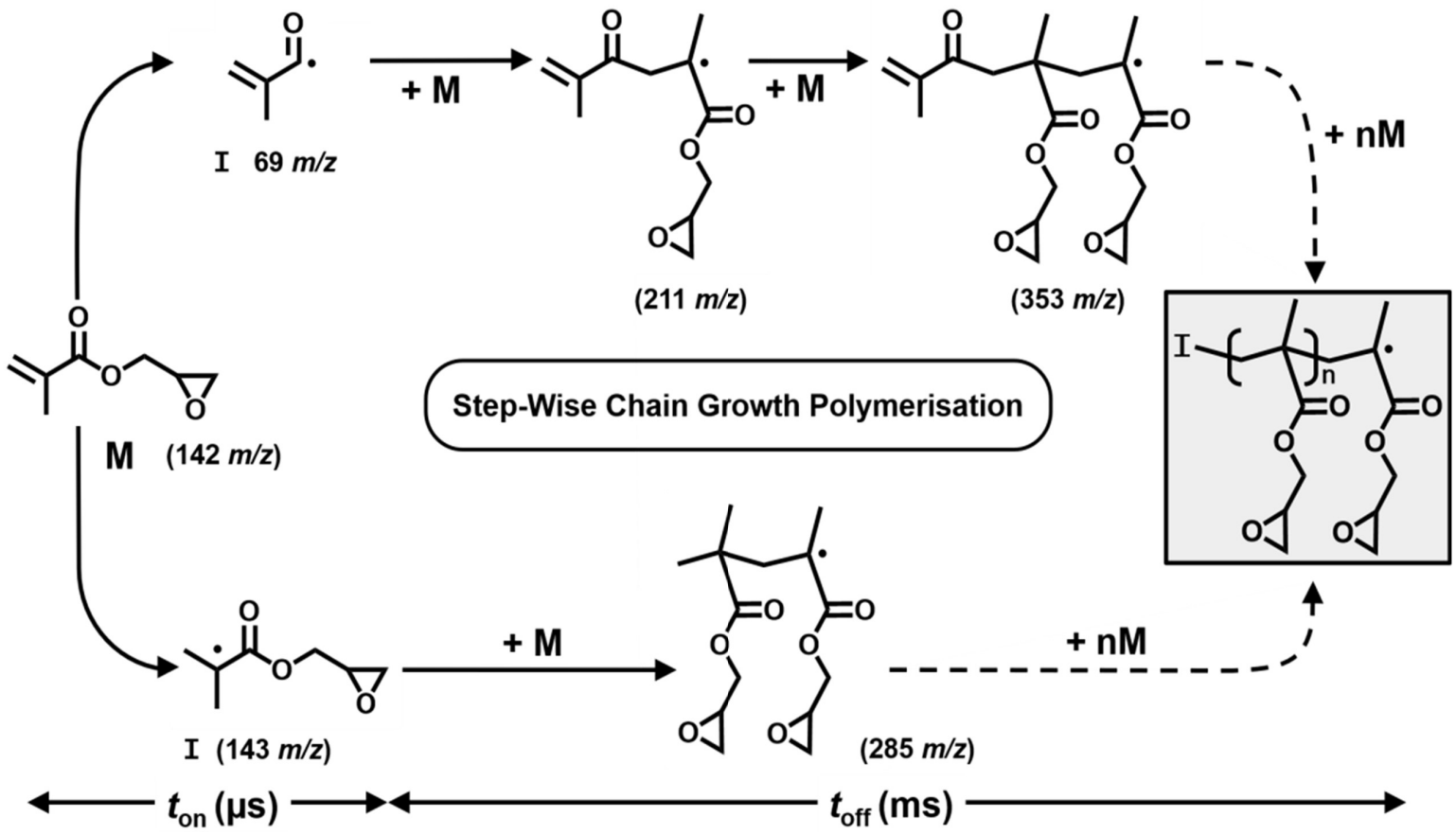

Scheme 5.1: Free radical chain growth polymerisation mechanism for glycidyl methacrylate pulsed plasma deposition (a similar mechanism could be envisaged for the corresponding 69 *m/z* and 143 *m/z* positive plasma ion initiator species).

The ultra-high reaction pathway selectivities observed in the present investigation are in marked contrast compared to previous time-resolved in situ mass spectrometry studies of pulsed plasmas—where highly selective reaction pathways (product formation) have not been reported for monomers such as: acrylic and methacrylic precursors, styrenic monomers, thiols, amines, silanes, terpenoids, or saturated and unsaturated linear hydrocarbons.[19,20,22,23,25,45,46,47] This can be attributed to the earlier use of longer on-periods (t_{on} = milliseconds), whereas in the present study shorter t_{on} values (in the microsecond range) are employed which narrows the time frame for any damaging cascading plasmachemical fragmentation reaction pathways as well as prohibiting the build-up of the plasma sheath potential leading to ion bombardment damage.[48] Growth of well-defined oligomer species is achieved as a consequence of selecting short micro-millisecond pulsed plasma duty cycles and low powers. This is accompanied by the formation of high mass ions via plasma electron-impact ionisation of high mass radicals within the electrical discharge—which accounts for the absence of any significant difference in mass fragments between positive ion versus low energy electron-impact detection modes, Figure 5.2 and Figure 5.5.[49,50] The degree of ionisation in such glow discharge plasmas is very low (10^{-4}–10^{-6}), and hence neutral species are present in much higher concentrations.[51,52] Furthermore, the duration of each plasma pulse is very short (t_{on} = microseconds) relative to the extinction period (t_{off} = milliseconds), hence the concentration of ions is further diluted. On this basis, a cationic polymerisation mechanism is not expected to be predominant.[53]

5.5 Conclusions

High selectivity reaction pathways for low duty cycle pulsed electrical discharges have been identified using in situ time-resolved mass spectrometry. For glycidyl methacrylate precursor, short electrical discharge pulses (t_{on} = microseconds timescale) lead to the creation of initiator species (the main low energy electron-impact fragment of glycidyl methacrylate (69 *m/z*)) and hydrogen atom addition to the molecular precursor (143 *m/z*). These initiator species then undergo sequential monomer addition within the extended off-period window (t_{off} = milliseconds timescale) giving rise to the

growth of well-defined epoxide-functionalised polymer chains. These plasmachemical mechanisms should be applicable to other precursors employed for the low duty cycle pulsed plasma deposition of functional nanolayers.

REFERENCES

1 Gross, E.; Liu, J. H.-C.; Toste, F. D.; Somorjai, G. A. Control of Selectivity in Heterogeneous Catalysis by Tuning Nanoparticle Properties and Reactor Residence Time. *Nat. Chem.* **2012**, *4*, 947–952.

2 Kyriakou, G.; Boucher, M. B.; Jewell, A. D.; Lewis, E. a; Lawton, T. J.; Baber, A. E.; Tierney, H. L.; Flytzani-Stephanopoulos, M.; Sykes, E. C. H. Isolated Metal Atom Geometries as a Strategy for Selective Heterogeneous Hydrogenations. *Science* **2012**, *335*, 1209–1212.

3 Jakuttis, M.; Schönweiz, A.; Werner, S.; Franke, R.; Wiese, K. D.; Haumann, M.; Wasserscheid, P. Rhodium-Phosphite SILP Catalysis for the Highly Selective Hydroformylation of Mixed C4 Feedstocks. *Angew. Chemie - Int. Ed.* **2011**, *50*, 4492–4495.

4 Pindur, U.; Lutz, G.; Otto, C. Acceleration and Selectivity Enhancement of Diels-Alder Reactions by Special and Catalytic Methods. *Chem. Rev.* **1993**, *93*, 741–761.

5 Witte, P. T.; Boland, S.; Kirby, F.; van Maanen, R.; Bleeker, B. F.; de Winter, D. A. M.; Post, J. A.; Geus, J. W.; Berben, P. H. NanoSelect Pd Catalysts: What Causes the High Selectivity of These Supported Colloidal Catalysts in Alkyne Semi-Hydrogenation? *ChemCatChem* **2013**, *5*, 582–587.

6 Jenner, G. High Pressure and Selectivity in Organic Reactions. *Tetrahedron* **1997**, *53*, 2669–2695.

7 Bourne, J. R. Mixing and the Selectivity of Chemical Reactions. *Org. Process Res. Dev.* **2003**, *7*, 471–508.

8 Mellmer, M. A.; Sener, C.; Gallo, J. M. R.; Luterbacher, J. S.; Alonso, D. M.; Dumesic, J. A. Solvent Effects in Acid-Catalyzed Biomass Conversion Reactions. *Angew. Chemie Int. Ed.* **2014**, *53*, 11872–11875.

9 Mushrif, S. H.; Caratzoulas, S.; Vlachos, D. G. Understanding Solvent Effects in the Selective Conversion of Fructose to 5-Hydroxymethyl-Furfural: A Molecular Dynamics Investigation. *Phys. Chem. Chem. Phys.* **2012**, *14*, 2637.

10 Schwartz, T. J.; Bond, J. Q. A Thermodynamic and Kinetic Analysis of Solvent-Enhanced Selectivity in Monophasic and Biphasic Reactor Systems. *Chem. Commun.* **2017**, *53*, 8148–8151.

11 Bayer, T.; Himmler, K. Mixing and Organic Chemistry. *Chem. Eng. Technol.* **2005**, *28*, 285–289.

12 Friedrich, J. Mechanisms of Plasma Polymerization - Reviewed from a Chemical Point of View. *Plasma Process. Polym.* **2011**, *8*, 783–802.

13 Ryan, M. E.; Hynes, A. M.; Badyal, J. P. S. Pulsed Plasma Polymerization of Maleic Anhydride. *Chem. Mater.* **1996**, 8, 37–42.

14 Savage, C. R.; Timmons, R. B.; Lin, J. W. Molecular Control of Surface Film Compositions via Pulsed Radio-Frequency Plasma Deposition of

Perfluoropropylene Oxide. *Chem. Mater.* **1991**, *3*, 575–577.
15 Badyal, J. P. S.; Coulson, S. R.; Willis, C.; Brewer, S. A. Surface Coatings. Patent US6551950B1, April 22, 2003.
16 Tarducci, C.; Kinmond, E. J.; Badyal, J. P. S.; Brewer, S. A.; Willis, C. Epoxide-Functionalized Solid Surfaces. *Chem. Mater.* **2000**, *12*, 1884–1889.
17 Boscher, N. D.; Hilt, F.; Duday, D.; Frache, G.; Fouquet, T.; Choquet, P. Atmospheric Pressure Plasma Initiated Chemical Vapor Deposition Using Ultra-Short Square Pulse Dielectric Barrier Discharge. *Plasma Process. Polym.* **2015**, *12*, 66–74.
18 Kinmond, E. J.; Coulson, S. R.; Badyal, J. P. S.; Brewer, S. A.; Willis, C. High Structural Retention during Pulsed Plasma Polymerization of 1H,1H,2H-Perfluorododecene: An NMR and TOF-SIMS Study. *Polymer* **2005**, *46*, 6829–6835.
19 Haddow, D.; France, R.; Short, R. A Mass Spectrometric and Ion Energy Study of the Continuous Wave Plasma Polymerization of Acrylic Acid. *Langmuir* **2000**, *12*, 5654–5660.
20 Fraser, S.; Short, R. D.; Barton, D.; Bradley, J. W. A Multi-Technique Investigation of the Pulsed Plasma and Plasma Polymers of Acrylic Acid: Millisecond Pulse Regime. *J. Phys. Chem. B* **2002**, *106*, 5596–5603.
21 O'Toole, L.; Beck, A. J.; Ameen, A. P.; Jones, F. R.; Short, R. D. Radiofrequency-Induced Plasma Polymerisation of Propenoic Acid and Propanoic Acid. *J. Chem. Soc. Faraday Trans.* **1995**, *91*, 3907.
22 O'Toole, L.; Short, R. D.; Ameen, A. P.; Jones, F. R. Mass Spectrometry of and Deposition-Rate Measurements from Radiofrequency-Induced Plasmas of Methyl Isoburate, Methyl Methacrylate and N-Butyl Methacrylate. *J. Chem. Soc. Faraday Trans.* **1995**, *91*, 1363–1370.
23 Ahmad, J.; Bazaka, K.; Whittle, J. D.; Michelmore, A.; Jacob, M. V. Structural Characterization of γ-Terpinene Thin Films Using Mass Spectroscopy and X-Ray Photoelectron Spectroscopy. *Plasma Process. Polym.* **2015**, *12*, 1085–1094.
24 Swindells, I.; Voronin, S. A.; Bryant, P. M.; Alexander, M. R.; Bradley, J. W. Temporal Evolution of an Electron-Free Afterglow in the Pulsed Plasma Polymerisation of Acrylic Acid. *J. Phys. Chem. B* **2008**, *112*, 3938–3947.
25 Deschenaux, C.; Affolter, A.; Magni, D.; Hollenstein, C.; Fayet, P. Investigations of CH4, C2H2 and C2H4 Dusty RF Plasmas by Means of FTIR Absorption Spectroscopy and Mass Spectrometry. *J. Phys. D. Appl. Phys.* 1999, *32*, 1876–1886.

26 Coulson, S. R.; Woodward, I. S.; Badyal, J. P. S.; Brewer, S. A.; Willis, C. Ultralow Surface Energy Plasma Polymer Films. *Chem. Mater.* **2000**, *12*, 2031–2038.
27 Oehr, C.; Müller, M.; Elkin, B.; Hegemann, D.; Vohrer, U. Plasma Grafting — A Method to Obtain Monofunctional Surfaces. *Surf. Coatings Technol.* **1999**, *116–119*, 23–25.
28 Schofield, W. C. E.; McGettrick, J. D.; Badyal, J. P. S. A Substrate-Independent Approach for Cyclodextrin Functionalized Surfaces. *J. Phys. Chem. B* **2006**, *110*, 17161–17166.
29 Harris, L. G.; Schofield, W. C. E.; Badyal, J. P. S. MultiFunctional Molecular Scratchcards. *Chem. Mater.* **2007**, *19*, 1546–1551.
30 Thierry, B.; Jasieniak, M.; de Smet, L. C. P. M.; Vasilev, K.; Griesser, H. J. Reactive Epoxy-Functionalized Thin Films by a Pulsed Plasma Polymerization Process. *Langmuir* **2008**, *24*, 10187–10195.
31 Coad, B. R.; Jasieniak, M.; Griesser, S. S.; Griesser, H. J. Controlled Covalent Surface Immobilisation of Proteins and Peptides Using Plasma Methods. *Surf. Coatings Technol.* **2013**, *233*, 169–177.
32 Yang, G. H.; Kang, E. T.; Neoh, K. G. Surface Modification of Poly(tetrafluoroethylene) Films by Plasma Polymerization of Glycidyl Methacrylate and Its Relevance to the Electroless Deposition of Copper. *J. Polym. Sci. Part A Polym. Chem.* **2000**, *38*, 3498–3509.
33 Camporeale, G.; Moreno-Couranjou, M.; Bonot, S.; Mauchauffé, R.; Boscher, N. D.; Bebrone, C.; Van de Weerdt, C.; Cauchie, H.-M.; Favia, P.; Choquet, P. Atmospheric-Pressure Plasma Deposited Epoxy-Rich Thin Films as Platforms for Biomolecule Immobilization-Application for Anti-Biofouling and Xenobiotic-Degrading Surfaces. *Plasma Process. Polym.* **2015**, *12*, 1208–1219.
34 Bonot, S.; Mauchauffé, R.; Boscher, N. D.; Moreno-Couranjou, M.; Cauchie, H.; Choquet, P. Self-Defensive Coating for Antibiotics Degradation—Atmospheric Pressure Chemical Vapor Deposition of Functional and Conformal Coatings for the Immobilization of Enzymes. *Adv. Mater. Interfaces,* **2015**, 2, 1500253.
35 Brown, P. S.; Wood, T. J.; Schofield, W. C. E.; Badyal, J. P. S. A Substrate-Independent Lift-Off Approach for Patterning Functional Surfaces. *ACS Appl. Mater. Interfaces* **2011**, *3*, 1204–1209
36 Zimmerman, P. A.; Hercules, D. M.; Benninghoven, A. Time-of-Flight Secondary Ion Mass Spectrometry of Poly(alkyl Methacrylates). *Anal. Chem.* **1993**, *65*, 983–991.
37 Eccles, A. J.; Vickerman, J. C. The Characterization of an Imaging Time-of-flight Secondary Ion Mass Spectrometry Instrument. *J. Vac. Sci. Technol. A Vacuum, Surfaces, Film.* **1989**, *7*, 234–244.

38 Brown, R. M.; Creaser, C. S. The Electron Impact and Chemical Ionization Mass Spectra of Some Glycidyl Ethers. *Org. Mass Spectrom.* **1980**, *15*, 578–581.
39 Yildirim, Y.; Balcan, M.; Bass, A. D.; Cloutier, P.; Sanche, L. Electron Stimulated Desorption of Anions and Cations from Condensed Allyl Glycidyl Ether. *Phys. Chem. Chem. Phys.* **2010**, *12*, 7950–7958.
40 NIST National Institute of Standard and Technology, US Department of Commerce http://webbook.nist.gov/cgi/cbook.cgi?ID=C106912&Mask=200#Mass-Spec (Accessed: 5 Feb 2018).
41 Ryan, M. E.; Hynes, A. M.; Badyal, J. P. S. Pulsed Plasma Polymerization of Maleic Anhydride. *Chem. Mater.* **1996**, *8*, 37–42.
42 Mishra, G.; McArthur, S. L. Plasma Polymerization of Maleic Anhydride: Just What Are the Right Deposition Conditions? *Langmuir* **2010**, *26*, 9645–9658.
43 Manakhov, A.; Moreno-Couranjou, M.; Boscher, N. D.; Rogé, V.; Choquet, P.; Pireaux, J. J. Atmospheric Pressure Pulsed Plasma Copolymerisation of Maleic Anhydride and Vinyltrimethoxysilane: Influence of Electrical Parameters on Chemistry, Morphology and Deposition Rate of the Coatings. *Plasma Process. Polym.* **2012**, *9*, 435–445.
44 Klages, C.-P.; Höpfner, K.; Kläke, N.; Thyen, R. Surface Functionalization at Atmospheric Pressure by DBD-Based Pulsed Plasma Polymerization. *Plasmas Polym.* **2000**, *5*, 79–89.
45 Beck, A. J.; Jones, F. R.; Short, R. D. Mass Spectrometric Study of the Radiofrequency-Induced Plasma Polymerisation of Styrene and Propenoic Acid. *J. Chem. Soc. Faraday Trans.* **1998**, *94*, 559–565.
46 Thiry, D.; Britun, N.; Konstantinidis, S.; Dauchot, J.-P. J.-P.; Guillaume, M.; Cornil, J.; Snyders, R. Experimental and Theoretical Study of the Effect of the Inductive-to-Capacitive Transition in Propanethiol Plasma Polymer Chemistry. *J. Phys. Chem. C* **2013**, *117*, 9843–9851.
47 Michelmore, A.; Bryant, P. M.; Steele, D. A.; Vasilev, K.; Bradley, J. W.; Short, R. D. Role of Positive Ions in Determining the Deposition Rate and Film Chemistry of Continuous Wave Hexamethyl Disiloxane Plasmas. *Langmuir* **2011**, *27*, 11943–11950.
48 Mackie, N. M.; Dalleska, N. F.; Castner, D. G.; Fisher, E. R. Comparison of Pulsed and Continuous-Wave Deposition of Thin Films from Saturated Fluorocarbon/H2 Inductively Coupled Rf Plasmas. *Chem. Mater.* **1997**, 9, 349–362.
49 Kushner, M. J. A Model for the Discharge Kinetics and Plasma Chemistry during Plasma Enhanced Chemical Vapor Deposition of Amorphous Silicon. *J. Appl. Phys.* **1988**, 63, 2532–2551.

50 Schwarzenbach, W.; Cunge, G.; Booth, J. P. High Mass Positive Ions and Molecules in Capacitively-Coupled Radio-Frequency CF4 Plasmas. *J. Appl. Phys.* **1999**, 85, 7562.
51 Plasma Surface Modification and Plasma Chemistry Schram. D. C.; Bisschops, Th. H. J.; Kroesen, G. M. W.; de Hoog, F. J.; *Plasma Phys. Control. Fusion* **1987**, *29*, 1353–1364.
52 Grill, A. Cold Plasma in Materials Fabrication: From Fundamentals to Applications, IEEE Press: Piscataway, NJ, 1994.
53 Saboohi, S.; Coad, B.; Griesser, H.; Michelmore, A.; Short, R. Synthesis of Highly Functionalised Plasma Polymer Films from Protonated Precursor Ions via the Plasma α–γ Transition. *Physical Chemistry Chemical Physics* **2017**, 19, 5637–5646.

6 : MALEIC ANHYDRIDE PULSED PLASMA POLYMERISATION MECHANISM

6.1 Introduction

Maleic anhydride (MAH) is obtained from dehydration of maleic acid and is the second most important anhydride in commercial use.[1,2] Common examples of maleic anhydride uses are Diels-Alder reaction chemistry,[3] photo and radical reactions,[4,5] copolymers and homopolymers.[6,7,8,9] Although, maleic anhydride is an excellent electron acceptor and can successfully copolymerise with a variety of monomers, homopolymerisation of maleic anhydride has proved to be challenging because of several reasons; steric hindrance factors, unfavourable double bond-double bond interactions (due to its electron-acceptor nature) or high chain transfer activity.[1] Pulsed plasma polymerisation is an alternative approach to obtain functional coatings containing maleic anhydride functionalities.[10] Several works on maleic anhydride plasma polymers are reported in the literature as this type of functional films have a wide range of potential applications such as: biosurfaces, protein immobilisation, controlled radical polymerisation, improving adhesion properties.[11,12,13,14,15,16,17] In this chapter, the chemistry of maleic anhydride precursor exposed to ultra-short (µs range) pulsed electric discharges is investigated by time-averaged and time-resolved mass spectrometry, Figure 6.1, and experimental results are discussed from the mechanistic point of view.

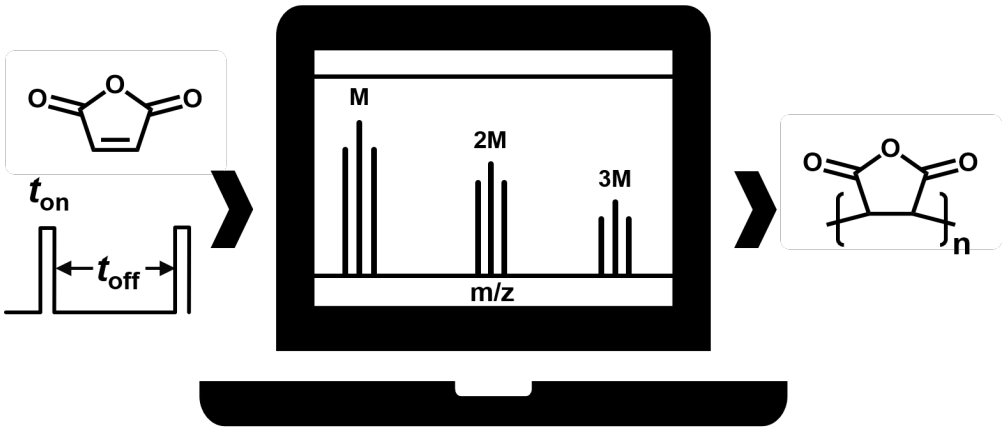

Figure 6.1: Maleic anhydride pulsed plasma mass spectrometric measurements.

6.2 Experimental

Briquettes of maleic anhydride (Aldrich, 99% purity) were ground into a fine powder and loaded into a monomer tube. Maleic anhydride precursor was purged at a pressure of 0.1 mbar for 20 min via a fine control needle valve. For pulsed plasmas, an on-period (t_{on}) of 50 µs and an off-period (t_{off}) of 6 ms were used in conjunction with 7 W of continuous wave power input during the on-period (P_{on}), Figure 2.9.[10,18,19] Ionised gaseous species (plasma ions) were sampled directly from the electrical discharge through the 200 µm end cap orifice. For time-resolved measurements and detector gating operations, the transit time was calculated using the procedure described in section 2.6 (Chapter 2).

6.3 Results

6.3.1 Maleic Anhydride Electron-Impact Mass Spectrometry

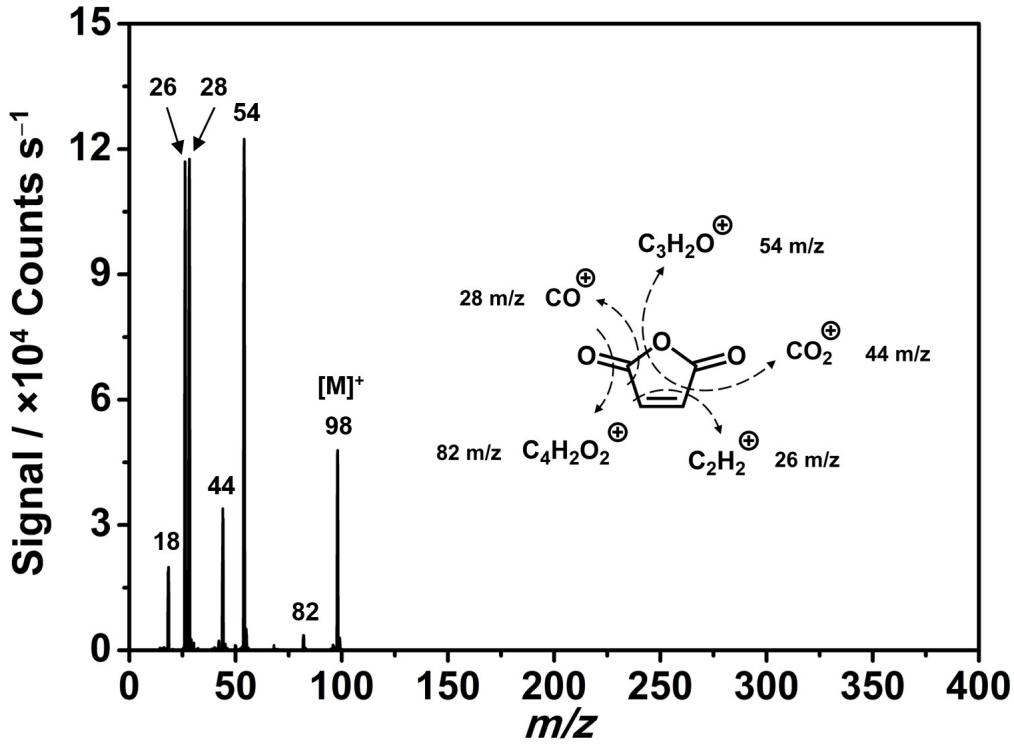

Figure 6.2: 20 eV electron-impact ionisation mass spectrum of maleic anhydride monomer, (0.1 mbar). Mass spectrometer tuning on 54 *m/z*.

The results for electron-impact ionisation of maleic anhydride monomer are in good accordance with the fragmentation pattern reported by NIST database.[20] Maleic anhydride precursor undergoing 20 eV electron-impact ionisation gives rise to a characteristic set of mass fragments, Figure 6.2. The base peak at *54 m/z* = $[C_3H_2O]^+$ originates from CO_2 loss and the molecular ion $[M]^+$ can be observed at 98 *m/z.* [21,22] Other relevant fragments are 82 *m/z* = $[C_4H_2O_2]^+$ (due to loss of the oxygen atom),[23] carbon monoxide 28 *m/z* = $[CO]^+$, and acetylene 26 *m/z* = $[C_2H_2]^+$, shown in Figure 6.2.

6.3.2 Plasma Ions

For both time-averaged and time-resolved positive plasma ion spectrometry, the instrument was tune on mass 54 *m/z* (for low mass range tuning) and 197 *m/z* (for high mass range tuning).

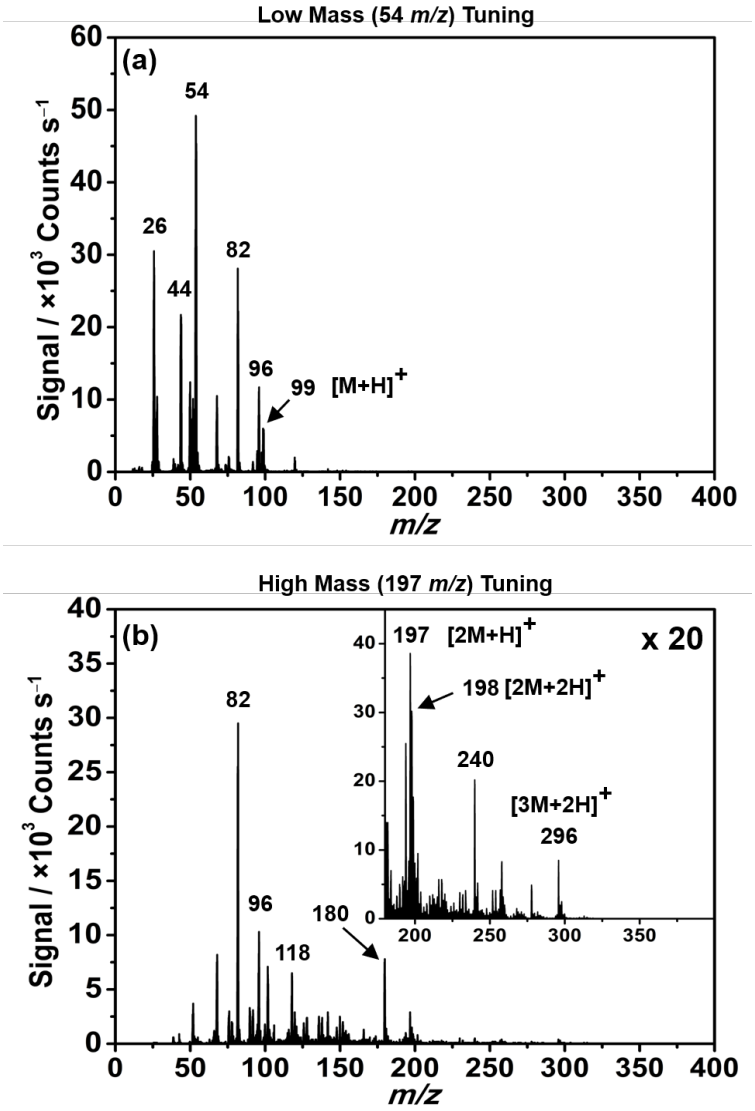

Figure 6.3: Time-averaged positive plasma ion mass spectrum of maleic anhydride pulsed plasma (t_{on} = 50 µs, t_{off} = 6 ms, P_{on} = 7 W, and 0.1 mbar). Mass spectrometer tuning on 54 and 197 *m/z* mass signal. Inset plot was recorded within 185 - 400 *m/z* mass range using the accumulate function.

Time-averaged positive ion mass spectroscopy of maleic anhydride pulsed plasmas showed evidence for plasma polymerisation occurring in the electrical discharge. In the low mass tuning positive ion mass scan (Figure 6.3a), the plasma environment shares similar features with the electron-impact ionisation

mass spectrum (Figure 6.2). Mass signals such as 82 *m/z* = $[C_4H_2O_2]^+$, 54 *m/z* $[C_3H_2O]^+$ (base peak), carbon dioxide 44 *m/z* = $[CO_2]^+$, and acetylene 26 *m/z* = $[C_2H_2]^+$, are still present with significant intensities, with exception of carbon monoxide mass signal (28 *m/z* = $[CO]^+$) which appears to be weaker relatively to the base peak. The molecular ion 98 *m/z* = $[M]^+$ is no longer visible, instead, the doubly deprotonated at 96 *m/z* = $[M-2H]^+$ and protonated 99 *m/z* = $[M+H]^+$ analogous species are present.[15] These ion species are responsible for gas phase plasma initiated polymerisation of maleic anhydride, as they provide excited monomer units, for stepwise polymer chain formation. Plasma polymerisation occurring in the plasma phase is visible in the high mass tuning positive ion mass spectrum, Figure 6.3b (x20 inset plot), where maleic anhydride protonated dimer species 197 *m/z* = $[2M+H]^+$, 198 *m/z* = $[2M+2H]^+$ and trimer species 296 *m/z* = $[3M+2H]^+$ are being generated. In addition to oligomer species, other relevant mass signals are detected; 82 *m/z* = $[C_4H_2O_2]^+$ (base peak), 118 *m/z* = $[C_3H_4O_2]^+$, 180 *m/z* = $[M-H_2O]^+$ (water subtraction) and 240 *m/z* = $[2M+CO_2]^+$ (carbon dioxide addition).

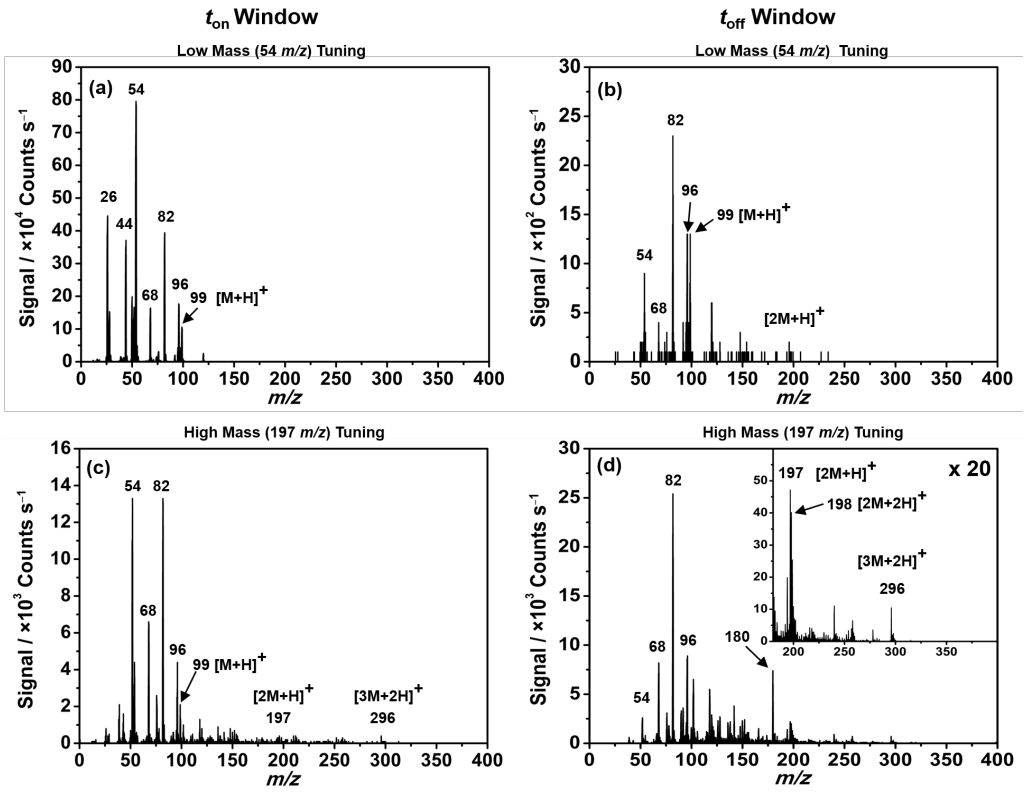

Figure 6.4: Time-resolved positive plasma ion mass spectra of maleic anhydride pulsed plasma (t_{on} = 30 µs, t_{off} = 10 ms, P_{on} = 15 W, and 0.1 mbar).

For time-resolved positive plasma ion mode, different plasma environments are observed for both low and high mass tuning (on-time and off-period). In low mass tuning spectra, ion counting is considerably higher (10^4 counts s^{-1} range) in the t_{on} window due to the greater degree of ionisation during the plasma pulsation, Figure 6.4a, and plasma ion signals range from (26 to 99 *m/z* – low mass range). Conversely, in the t_{off} plasma window ion signals are weaker in intensity (10^2 counts s^{-1} range) as the ions generated in the on-period are progressively decreasing in number, Figure 6.4b. When the spectrometer is operated in high mass tuning mode, the main difference between t_{on} and t_{off} plasma windows is the average mass counting, which is higher during the off-time plasma period, as shown in Figure 6.4d. In fact, large mass signals are recorded in the high range of the mass spectrum, if compared to the plasma on-period (Figure 6.4c). This is a strong indication that high mass species form in great number after the plasma pulse (which is the initiating step), and step-growth plasma polymerisation occurs in the off-time period.

6.3.3 Plasma Radicals

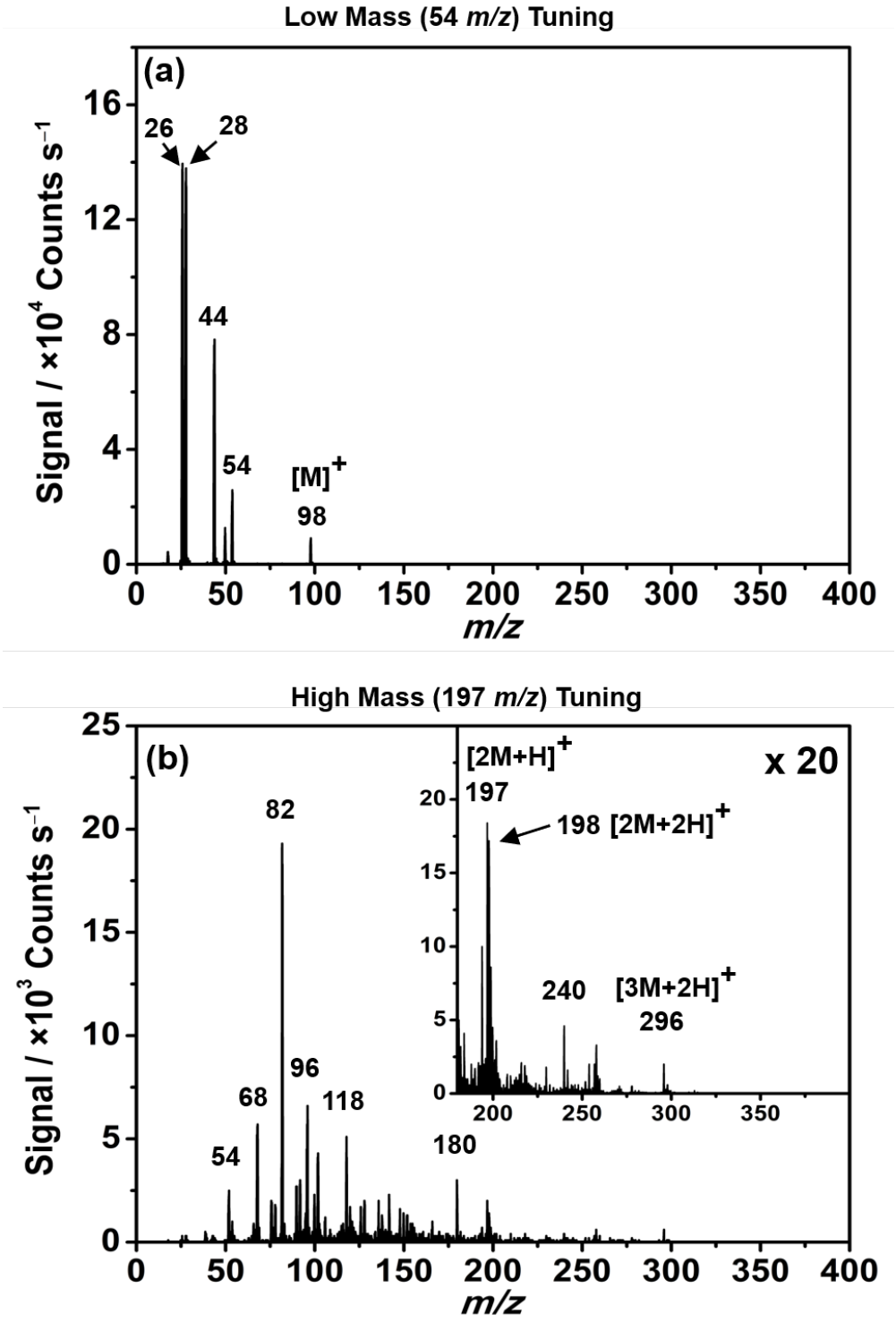

Figure 6.5: Time-averaged electron-impact ionisation mass spectrum of maleic anhydride pulsed plasma (t_{on} = 50 µs, t_{off} = 6 ms, P_{on} = 7 W, and 0.1 mbar).

Low mass tuning electron-impact ionisation mass spectrum, operating in time-averaged mode (Figure 6.5a), shows a very similar mass signal population to the original monomer precursor (Figure 6.2). The most intense mass signals are recorded at 28 *m/z* = $[CO]^+$ and 26 *m/z* = $[C_2H_2]^+$, and other characteristic mass fragments such as; 98 *m/z* = $[M]^+$ (molecular ion). Mass peaks 54 *m/z* = $[C_3H_2O]^+$ and 44 *m/z* = $[CO_2]^+$ are also present, but their signals are not as intense as in the precursor mass spectrum, see Figure 6.2. Similarly, to positive plasma ions (Figure 6.3b), when the spectrometer is tuned on a higher mass (197 *m/z*), high mass signals for radical species become visible (Figure 6.5b). Plasma radical oligomers such as: 197 *m/z* = $[2M+H]^+$, 198 *m/z* = $[2M+2H]^+$ and 296 *m/z* = $[3M+2H]^+$ are being generated as a consequence of plasma activation, together with other high mass plasma radical species, such as; 82 *m/z* = $[C_4H_2O_2]^+$ (base peak), 118 *m/z* = $[C_3H_4O_2]^+$, 180 *m/z* = $[M-H_2O]^+$ and 240 *m/z* = $[2M+CO_2]^+$.

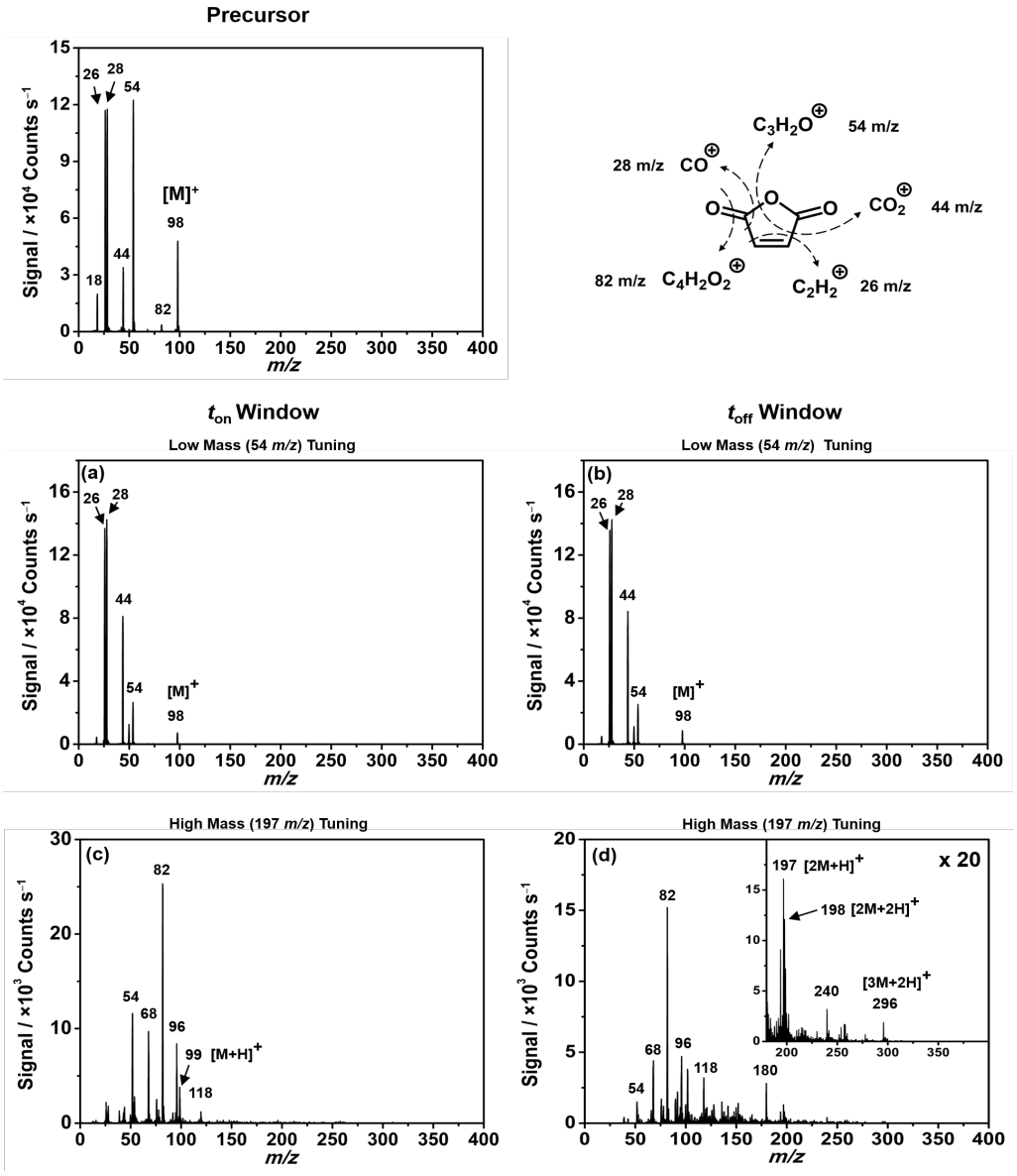

Figure 6.6: Time-resolved electron-impact ionisation mass spectra of maleic anhydride precursor gas (top left) and pulsed plasmas (middle and bottom spectra, with t_{on} = 50 µs, t_{off} = 6 ms, P_{on} = 7 W, and 0.1 mbar).

In time-resolved electron-impact ionisation mode (low mass tuning), the same set of plasma radical species are found to be present in both on-period and off-period, Figure 6.6a and b. The most intense mass signals are recorded at 28 *m/z* = $[CO]^+$ and 26 *m/z* = $[C_2H_2]^+$, while characteristic mass fragments such as; 98 *m/z* = $[M]^+$ (molecular ion), *54 m/z* = $[C_3H_2O]^+$ and 44 *m/z* = $[CO_2]^+$ are also observed.

When the internal ionising source is operated on high mass tuning (197 *m/z*), Figure 6.6c and d, two distinct populations of plasma radicals are observed. During t_{on} window (Figure 6.6c) low mass plasma radicals such as: 82 *m/z* = $[C_4H_2O_2]^+$ (base peak), 68 *m/z* $[C_4H_4O]^+$, 54 *m/z* $[C_3H_2O]^+$ 96 *m/z* = $[M\text{-}2H]^+$, 99 *m/z* = $[M+H]^+$, are generated, as opposed to the off-time period Figure 6.6d inset plot where heavier radicals (118, 180, 240 *m/z*) and protonated oligomer species (197, 198, 296 *m/z*), are detected as a consequence of plasma initiated step-growth polymerisation.

6.4 Discussion

In situ mass spectrometry was employed for the first time as a diagnostic technique to gain an insight on pulsed plasma polymerisation of maleic anhydride mechanism. Maleic anhydride monomer precursor undergoes radical chain growth polymerisation when exposed to short (microsecond time window) pulsed electric discharges followed by extended (millisecond time window) off-time periods. Radical chain growth polymerisation proceeds via the initiation step during the pulsed plasma discharge (t_{on} – microsecond range), where activated species 96 *m/z* = $[M\text{-}2H]^+$, 99 *m/z* = $[M+H]^+$ are generated. Following the initiation step, activated species recombine during the extended off-time window (t_{off} – millisecond range) leading to the formation of radical oligomer species such as; protonated and doubly protonated radical dimers 197 *m/z* = $[2M+H]^+$, 198 *m/z* = $[2M+2H]^+$ and doubly protonated radical trimers 296 *m/z* = $[3M+2H]^+$, as illustrated in Scheme 6.1.

Using short plasma pulses in the microsecond range enables avoiding excessive fragmentation of the maleic anhydride precursor, this allows high selective plasma activation of the double bond, without causing the maleic anhydride ring to open (t_{on}). When a short plasma discharge is followed by a long plasma off-period (t_{off}), favourable collisions between activated maleic anhydride precursor species (96 *m/z*, 99 *m/z*), are more likely to occur giving rise to controlled plasma polymerisation reaction via subsequent addition of activated monomer precursor units.

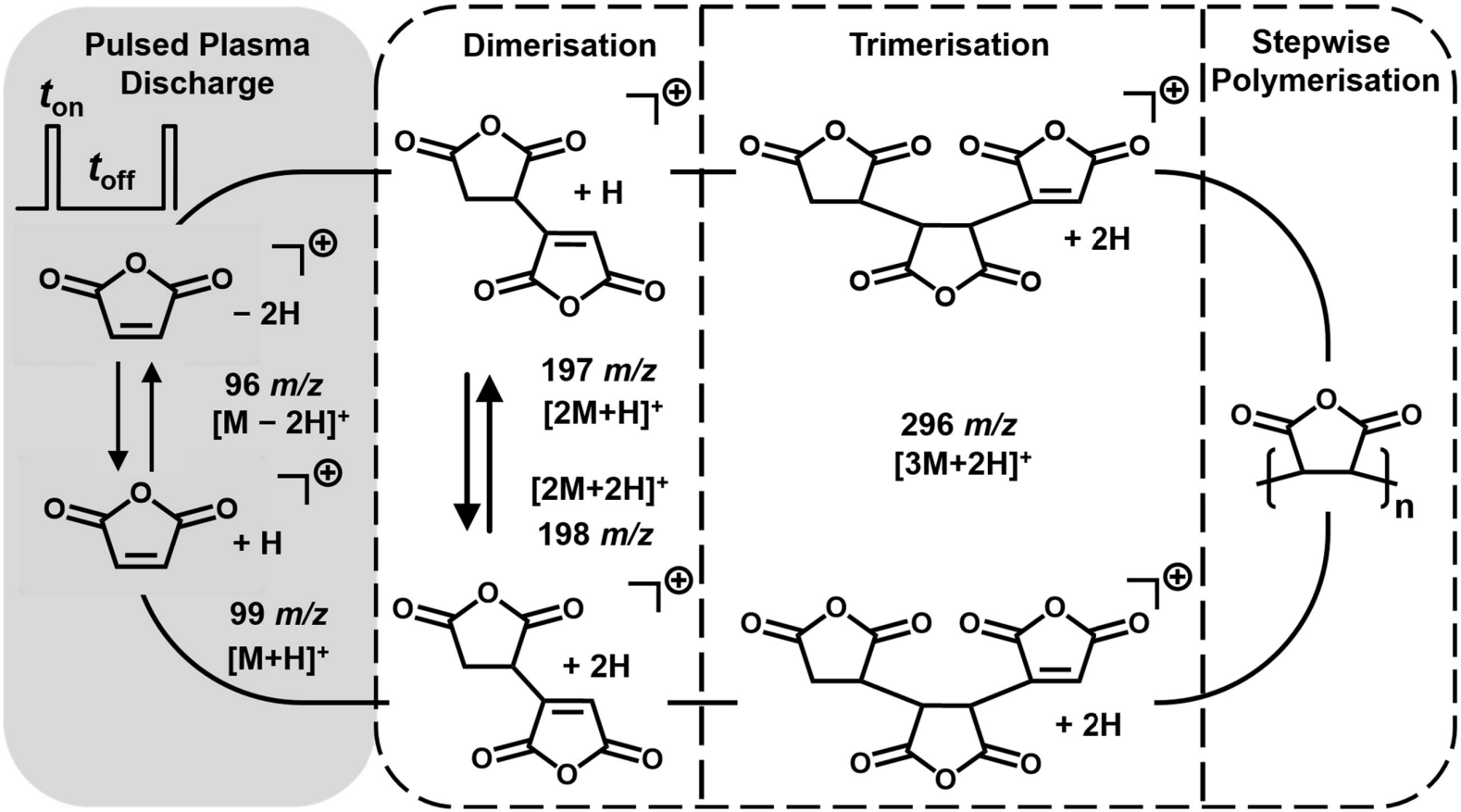

Scheme 6.1: Free radical chain step-growth polymerisation mechanism for maleic anhydride pulsed plasma deposition (a similar mechanism is envisaged for the analogous plasma ion species).

6.5 Conclusions

Pulsed plasmas of maleic anhydride precursors were studied by situ mass spectrometry and polymerisation mechanism was discussed. Short plasma electrical discharges followed by longer plasma off-periods were investigated by time-averaged and time-resolved acquisition modes for both plasma ions and radicals. Maleic anhydride was proven to be a suitable plasma precursor that gives rise to activated species 96 *m/z* = $[M-2H]^+$, 99 *m/z* = $[M+H]^+$ when exposed to short plasma discharges. The plasma polymerisation proceeds by monomer addition with the formation of protonated and doubly protonated radical dimers 197 *m/z* = $[2M+H]^+$, 198 *m/z* = $[2M+2H]^+$ and doubly protonated radical trimers 296 *m/z* = $[3M+2H]^+$.

REFERENCES

1 Trivedi B.C.; Culbertson B.M. Maleic anhydride. Plenum Press, New York 2. 1982.

2 Centi, G.; Trifiro, F.; Ebner, J. R.; Franchetti, V. M. Mechanistic Aspects of Maleic Anhydride Synthesis from C4 Hydrocarbons over Phosphorus Vanadium Oxide. *Chem. Rev.* **1988**, 88, 55–80.

3 Dewar, M. J. S.; Pierini, A. B. Mechanism of the Diels-Alder Reaction . Studies of the Addition of Maleic Anhydride to Furan and Methylfurans. **1984**, 1, 203–208.

4 Lang, J. L.; Pavelich, W. A.; Clarey, H. D. The Homopolymerization of Maleic Anhydride. *J. Polym. Sci.* **1961**, 55, S31–S32.

5 Nagahiro, I.; Nishihara, K.; Sakota, N. Photoinduced Polymerization of Maleic Anhydride in Dioxane. *J. Polym. Sci. Polym. Chem. Ed.* **1974**, 12, 785–792.

6 Klumperman, B. Mechanistic Considerations on Styrene–maleic Anhydride Copolymerization Reactions. *Polym. Chem.* **2010**, 1, 558–562.

7 De Brouwer, H.; Schellekens, M. A. J.; Klumperman, B.; Monteiro, M. J.; German, A. L. Controlled Radical Copolymerization of Styrene and Maleic Anhydride and the Synthesis of Novel Polyolefin-Based Block Copolymers by Reversible Addition–fragmentation Chain-Transfer (RAFT) Polymerization. *J. Polym. Sci. Part A Polym. Chem.* **2000**, 38, 3596–3603.

8 Zweifel, H.; Völker, T. On the Mechanism of Anionic Polymerization of Maleic Anhydride. *Die Makromol. Chemie* **1973**, 170, 141–153.

9 Evenson, S. A. ; Fail, C. A.; Badyal, J. P. S. Surface Esterification of Poly(Ethylene-Alt-Maleic Anhydride) Copolymer. *J. Phys. Chem. B* **2000**, 104, 10608–10611.

10 Ryan, M. E.; Hynes, A. M.; Badyal, J. P. S. Pulsed Plasma Polymerization of Maleic Anhydride. *Chem. Mater.* **1996**, 8, 37–42.

11 Jenkins, A. T. A.; Hu, J.; Wang, Y. Z.; Schiller, S.; Foerch, R.; Knoll, W. Pulsed Plasma Deposited Maleic Anhydride Thin Films as Supports for Lipid Bilayers. *Langmuir* **2000**, *16*, 6381–6384.

12 Teare, D. O. H.; Schofield, W. C. E.; Garrod, R. P.; Badyal, J. P. S. Rapid Polymer Brush Growth by TEMPO-Mediated Controlled Free-Radical Polymerization from Swollen Plasma Deposited Poly(Maleic Anhydride) Initiator Surfaces. *Langmuir* **2005**, 21, 10818–10824.

13 Drews, J.; Goutianos, S.; Kingshott, P.; Hvilsted, S.; Rozlosnik, N.; Almdal, K.; Sorensen, B. F. Plasma Polymerized Thin Films of Maleic Anhydride and 1,2-Methylenedioxybenzene for Improving Adhesion to Carbon Surfaces. *Journal of Vacuum Science & Technology a*. **2007**, 25,1108–1117.
14 Severini, F.; Pegoraro, M.; Ricca, G.; Audisio, G; Dainese, D.; Gallo, R. Synthesis and Characterization of Maleic Anhydride Oligomers. *Brit. Polym. J.* **1990**, 23, 23–28.
15 Mishra, G.; McArthur, S. L. Plasma Polymerization of Maleic Anhydride: Just What Are the Right Deposition Conditions? *Langmuir* **2010**, 26, 9645–9658.
16 Lampitt, R. A.; Crowther, J. M.; Badyal, J. P. S. Switching Liquid Repellent Surfaces. *J. Phys. Chem. B* **2000**, 104, 10329–10331.
17 Drews, J.; Goutianos, S.; Kingshott, P.; Hvilsted, S.; Rozlosnik, N.; Almdal, K.; Sørensen, B. F. Plasma Polymerized Thin Films of Maleic Anhydride and 1,2-Methylenedioxybenzene for Improving Adhesion to Carbon Surfaces. *J. Vac. Sci. Technol. A Vacuum, Surfaces, Film.* **2007**, 25, 1108–1117.
18 Carletto, A.; Badyal, J. P. S. Mechanistic Reaction Pathway for Hexafluoropropylene Oxide Pulsed Plasma Deposition of PTFE-like Films. *J. Phys. Commun.* **2017**, 1, 55024.
19 O'Toole, L.; Short, R. D.; Ameen, A. P.; Jones, F. R. Mass Spectrometry of and Deposition-Rate Measurements from Radiofrequency-Induced Plasmas of Methyl Isoburate, Methyl Methacrylate and N-Buthyl Methacrylate. *J. Chem. Soc. Faraday Trans.* **1995**, 91, 1363–1370.
20 NIST National Institute of Standard and Technology, U.S. Department of Commerce, NIST Mass Spectrometry Data Center. http://webbook.nist.gov/cgi/cbook.cgi?ID=C108316&Mask=200#Mass-Spec (accessed Aug 3, 2017).
21 Karpati, A.; Mandelbaum, A. Studies in Mass spectrometry—XVI. The Striking Difference between the Mass Spectra of Stereoisomeric Cyclic Anhydrides. *Org. Mass Spectrom.* **1971**, 5, 1345–1346.
22 Cooper, C. D.; Compton, R. N. Electron Attachment to Cyclic Anhydrides and Related Compounds. *J. Chem. Phys.* **1973**, 59, 3550–3565.
23 Compton, R. N.; Reinhardt, P. W.; Cooper, C. D. Mass Spectrometry Utilizing Collisional Ionization of Cesium: Maleic Anhydride and Succinic Anhydride. *J.Chem. Phys.* **1974**, 60, 2953–2957.

7 : BUTYL ACRYLATE PULSED PLASMA POLYMERISATION

7.1 Introduction

The use of acrylic monomers employed as plasma precursor species has been reported in numerous studies.[1,2,3,4,5] There are several intrinsic characteristics that make this class of organic compounds particularly suitable for plasma deposition purposes; The main interesting feature offered is the presence of a polymerisable double bond; in fact a C=C π-bond can be rapidly plasma-activated and used to generate initiating sites for monomer-monomer addition plasma polymerisation (conventional step-growth polymerisation). Moreover, acrylates monomers are relatively easy to source due to commercial availability and the organic materials obtained from conventional polymerisation methods, are of enormous technological interest because of their versatility and wide range of potential applications.[6,7,8]

It has been found experimentally that butyl acrylate (Structure 3) vapours undergo pulsed plasma polymerisation to give structurally well-defined polymeric film depositions very similar to poly(butyl acrylate) obtained from conventional polymerisation techniques.[9]

In this chapter, we present and discuss a set of experimental results obtained from average and time-resolved mass spectrometric analysis conducted on ions and radical species generated by butyl acrylate polymerising pulsed plasma systems.

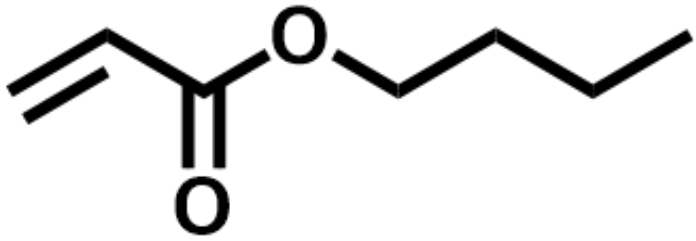

Structure 3: Butyl acrylate monomer structure

7.2 Experimental

Butyl acrylate monomer (Aldrich, 99% purity) was loaded into a monomer tube and freeze-pump-thawed for 5 cycles. Monomer precursors were introduced in the plasma reactor via a fine control needle valve. Prior to each experiment, the plasma reactor was plasma cleaned (50 W oxygen plasma continuous wave), then purged with butyl acrylate monomer at a pressure of 0.1 mbar for 20 min. For pulsed plasmas, an on-period (t_{on}) of 50 μs and an off-period (t_{off}) of 10 ms were used in conjunction with 7 W of continuous wave power input during the on-period (P_{on}).[10,11] Ionised gaseous species (plasma ions) were sampled directly from the electrical discharge through the 200 μm end cap orifice. For time-resolved measurements and detector gating operations, the transit time was calculated using the procedure described in section 2.6 (Chapter 2).

7.3 Results

7.3.1 Butyl Acrylate Electron-Impact Mass Spectrometry

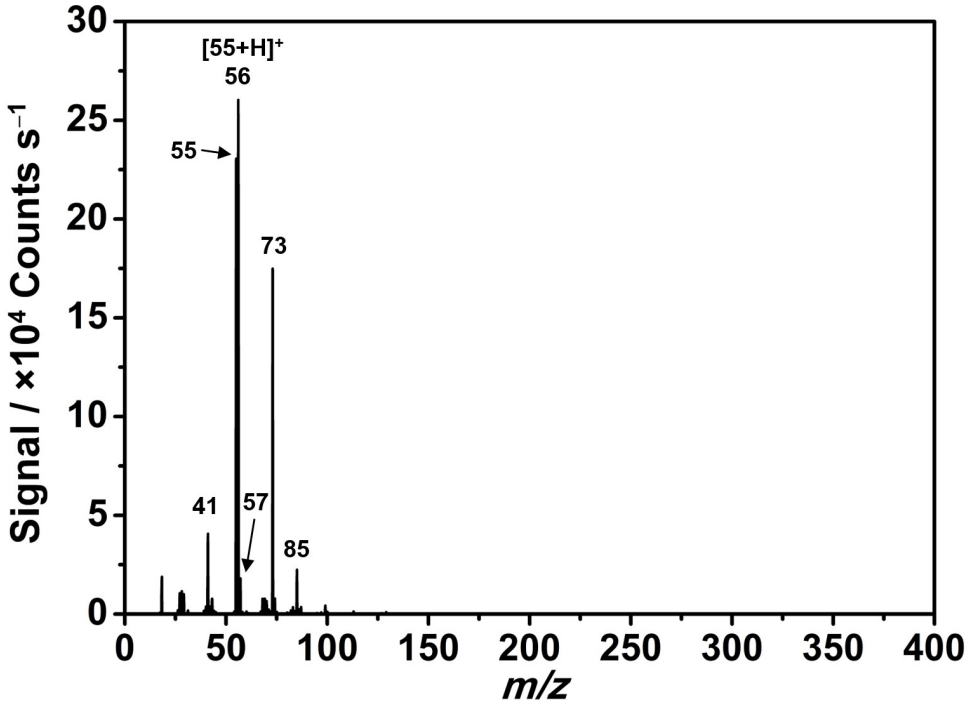

Figure 7.1: 20 eV electron-impact ionisation mass spectrum of butyl acrylate monomer, (0.1 mbar). Mass spectrometer tuning on 56 *m/z*.

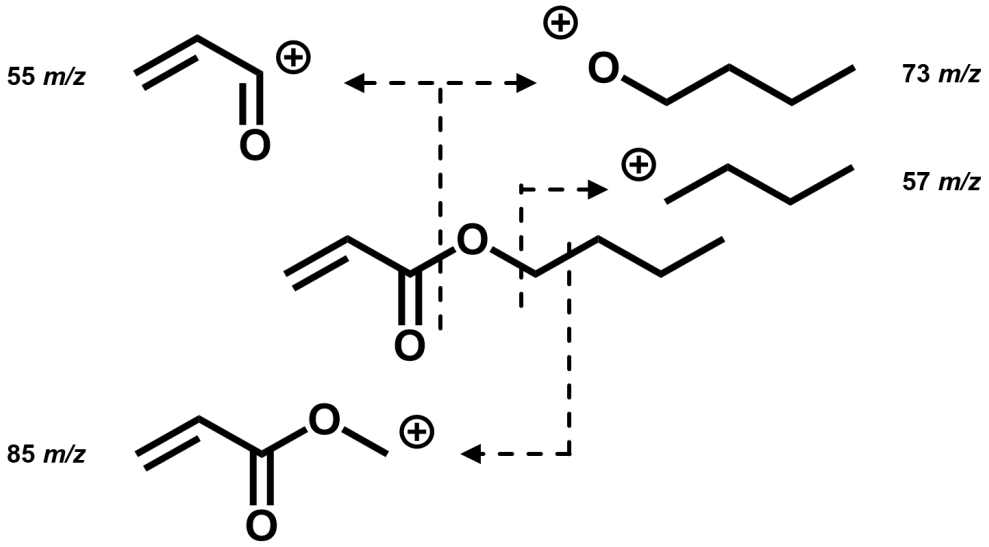

Figure 7.2: Butyl acrylate precursor fragmentation pattern.

The 20 eV electron-impact ionisation mass spectrum of butyl acrylate monomer is characterised by a very intense mass signals at 56 *m/z* = $[55+H]^+$ that originates from the protonated fragment at 55 *m/z*. The butyl group is also visible at 57 *m/z*, Figure 7.1. Acryloyl ion at 85 *m/z* arises from the oxygen-carbon bond cleavage as illustrated in Figure 7.2. Other relevant fragments are observed at 41 *m/z* = $[55\text{-}CH_2]^+$ and 73 *m/z* = $[C_4H_9O]^+$ but no molecular ion signal was detected (128 *m/z* = $[M]^+$). The experimental mass spectrum of butyl acrylate monomer is in good accordance with the fragmentation pattern reported by NIST database.[12]

7.3.2 Plasma Ions

During time-averaged and time-resolved positive plasma ion analysis, the spectrometer was tune on mass 129 *m/z*, (different tunings were performed on a range of different mass signals, with no significant difference observed on the resulting mass spectra).

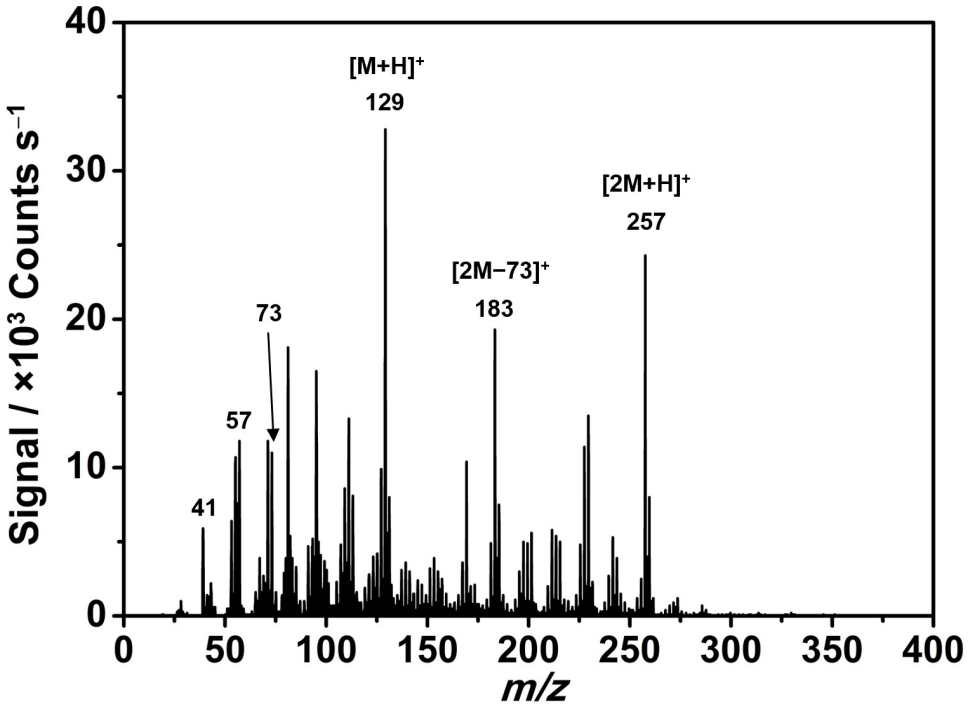

Figure 7.3: Time-averaged positive plasma ion mass spectrum of butyl acrylate pulsed plasma (t_{on} = 50 µs, t_{off} = 10 ms, P_{on} = 7 W, and 0.1 mbar). Mass spectrometer tuning on 129 *m/z* mass signal.

Pulsed plasma polymerisation of butyl acrylate precursor vapours was investigated by time-averaged positive ion mass spectroscopy, Figure 7.3. Mass signals at 41 *m/z,* 57 *m/z* and 73 *m/z* are originated by plasma electron impact fragmentation of the precursor monomer, as observed for the analogous electron-impact ionisation mass spectrum, Figure 7.1. Butyl acrylate protonated dimer species ($[2M+H]^+$), are visible at 257 *m/z*. The presence of these species represents a strong evidence of step-wise polymerisation occurring during the pulsed electrical discharge. Intermediate species are also observed at 183 *m/z* ($[2M-73]^+$). The base peak corresponding to the protonated molecular ion ($[M+H]^+$) is detected at 129 *m/z.*

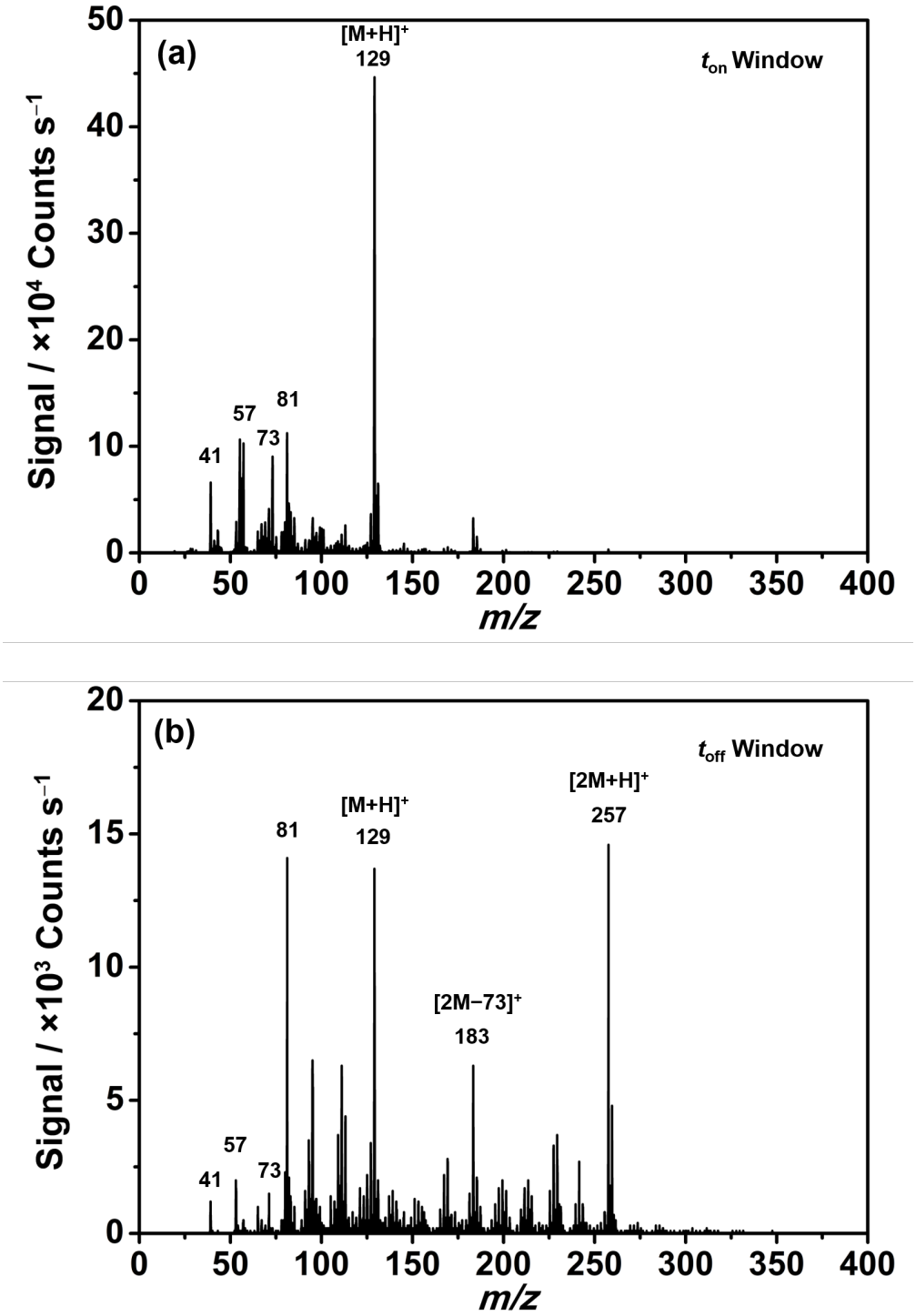

Figure 7.4: Time-resolved positive plasma ion mass spectra of butyl acrylate pulsed plasma t_{on} window (a) and t_{off} window (b) (t_{on} = 50 µs, t_{off} = 10 ms, P_{on} = 7 W, and 0.1 mbar). Mass spectrometer tuning on 129 *m/z* mass signal.

On-time (Figure 7.4a) and off-time (Figure 7.4b) periods were investigated by time-resolved positive plasma ion spectrometry. In the on-time plasma window, the protonated molecular ion 129 *m/z* ($[M+H]^+$) is the predominant mass signal, while other characteristic mass signals are observed at 41 *m/z,* 57 *m/z,* 73 *m/z* but no oligomer species are present during the plasma pulse. The off-time window mass scan shows a different set of positive ion masses, with major peaks found at 81 *m/z,* 129 *m/z* (protonated molecular ion $[M+H]^+$), 183 *m/z* ($[2M-73]^+$) and protonated dimer species (257 *m/z* = $[2M+H]^+$). This strongly suggests that plasma polymerisation by monomer-monomer addition, occurs exclusively in the off-time period. Another major difference between the on-time and off-time period is the overall ion mass counting which falls in the 10^4 count s^{-1} range during the t_{on} window (due to plasma ionisation), and much lower in the subsequent plasma period (t_{off} window – 10^3 count s^{-1}). A further analysis was carried out on consecutive 1 millisecond-long sampling positive ion mass spectra, which were recorded during the off-period, Figure 7.5. In the first microsecond the protonated molecular ion (129 *m/z* = $[M+H]^+$) is the most intense signal (0–1 ms), while dimer species (257 *m/z* = $[2M+H]^+$) are progressively formed in the following microsecond long time windows (1–7 ms), as the overall signal intensity drops throughout the entire duration of the off-time window.

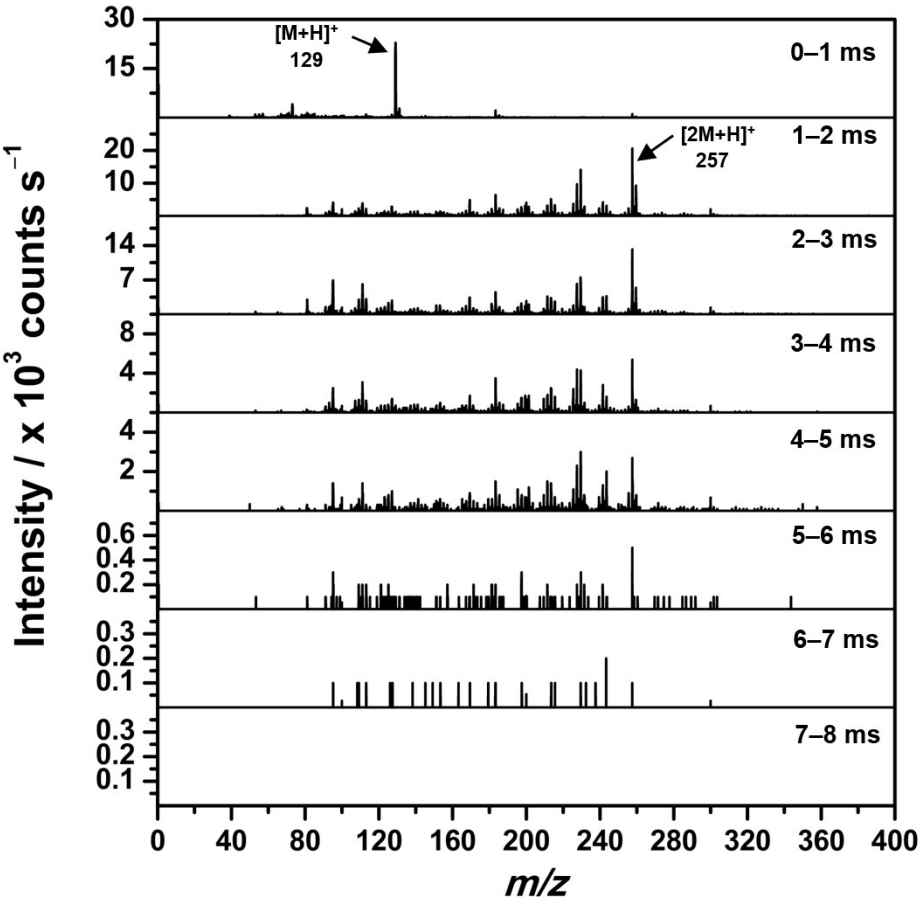

Figure 7.5: Off-period positive ion mass spectra taken during consecutive 1 ms sampling time windows for butyl acrylate pulsed plasma (t_{on} = 50 µs, t_{off} = 10 ms, P_{on} = 7 W, and 0.1 mbar).

7.3.3 Plasma Radicals

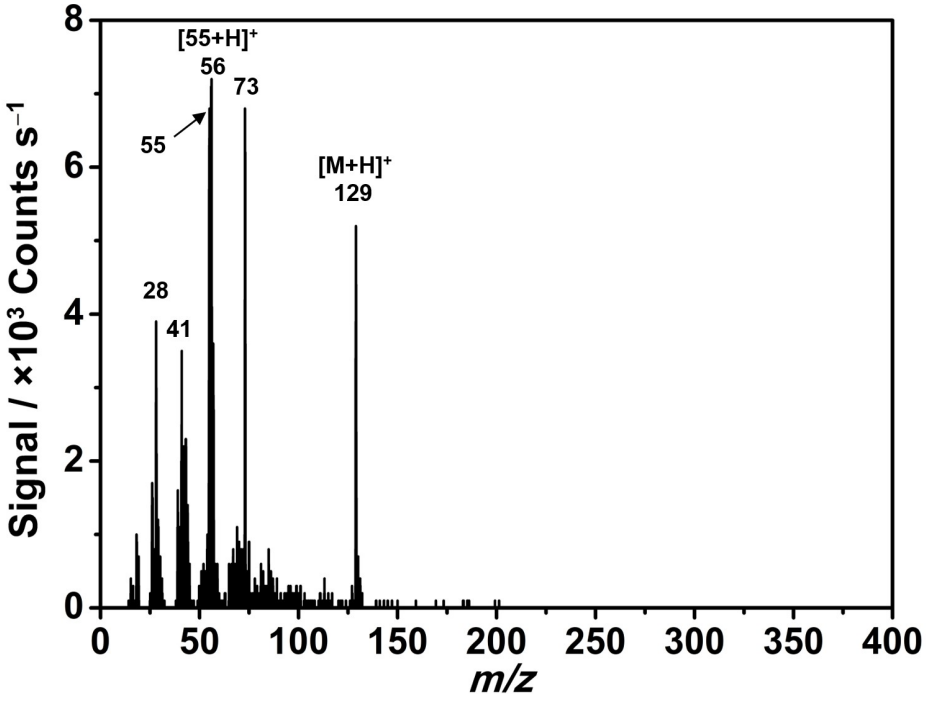

Figure 7.6: Time-averaged electron-impact ionisation mass spectrum of butyl acrylate pulsed plasma (t_{on} = 50 µs, t_{off} = 10 ms, P_{on} = 7 W, and 0.1 mbar).

Time-averaged electron-impact ionisation mass spectrum of butyl acrylate pulsed plasma (shown in Figure 7.6) was employed to investigate plasma radical species produced by pulsed electrical discharges. The main mass signals formed via monomer precursor electron-impact ionisation (20 eV electron energy), are observed at 28 *m/z* = $[CO]^+$, 41 *m/z*, 55 *m/z* = $[57\text{-}2H]^+$, 56 *m/z* = $[57\text{-}H]^+$, 57 *m/z* and 73 *m/z*. The protonated molecular ion signal at 129 *m/z* = $[M+H]^+$ is very intense, indicating that a large amount of protonated butyl acrylate radicals is produced as a potential source of activated species. Although oligomer species are not observed.

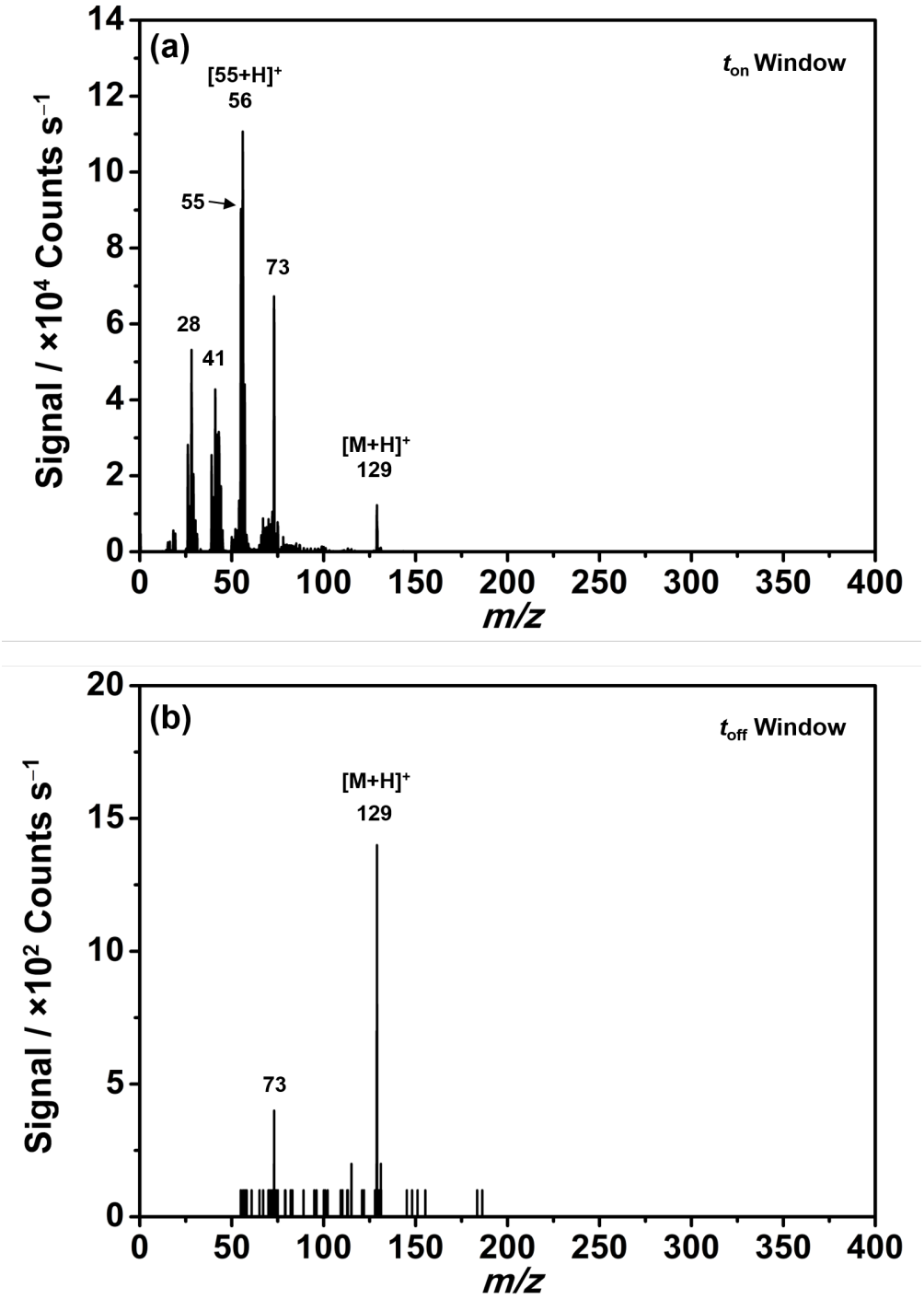

Figure 7.7: Time-resolved electron-impact ionisation mass spectra of butyl acrylate precursor gas (top left) and pulsed plasmas (middle and bottom spectra), with t_{on} = 50 µs, t_{off} = 10 ms, P_{on} = 7 W, and 0.1 mbar.

Time-resolved electron-impact ionisation mode allowed for investigation of plasma radical species formed in the on-time and off-time period. During the plasma discharge (on-time) very intense signals are detected at 28 *m/z* = $[CO]^+$, 41 *m/z*, 55 *m/z* $[57\text{-}2H]^+$, 56 *m/z* $[57\text{-}H]^+$, 57 *m/z* and 73 *m/z* while the protonated molecular ion signal at 129 *m/z* = $[M+H]^+$ appears to be relatively low in intensity, Figure 7.7a. Unlike on-time electron-impact ionisation mode, when the internal ionising source is operated in the off-time period, very weak plasma radical signals for 73 *m/z* and 129 *m/z* = $[M+H]^+$ are detected (Figure 7.7b). The electron-impact mass spectrum falls in the 10^2 count s^{-1} ion counting range. Plasma radical scarcity in the off-time period is confirmed by consecutive 1 millisecond-long positive radical analysis sampling window, Figure 7.8. Radical species of the protonated molecular ion 129 *m/z* = $[M+H]^+$ are only observed in the first millisecond within the off-time, while in the following millisecond-long "time slices" (1–2 ms to 7–8 ms), plasma radical signals are absent.

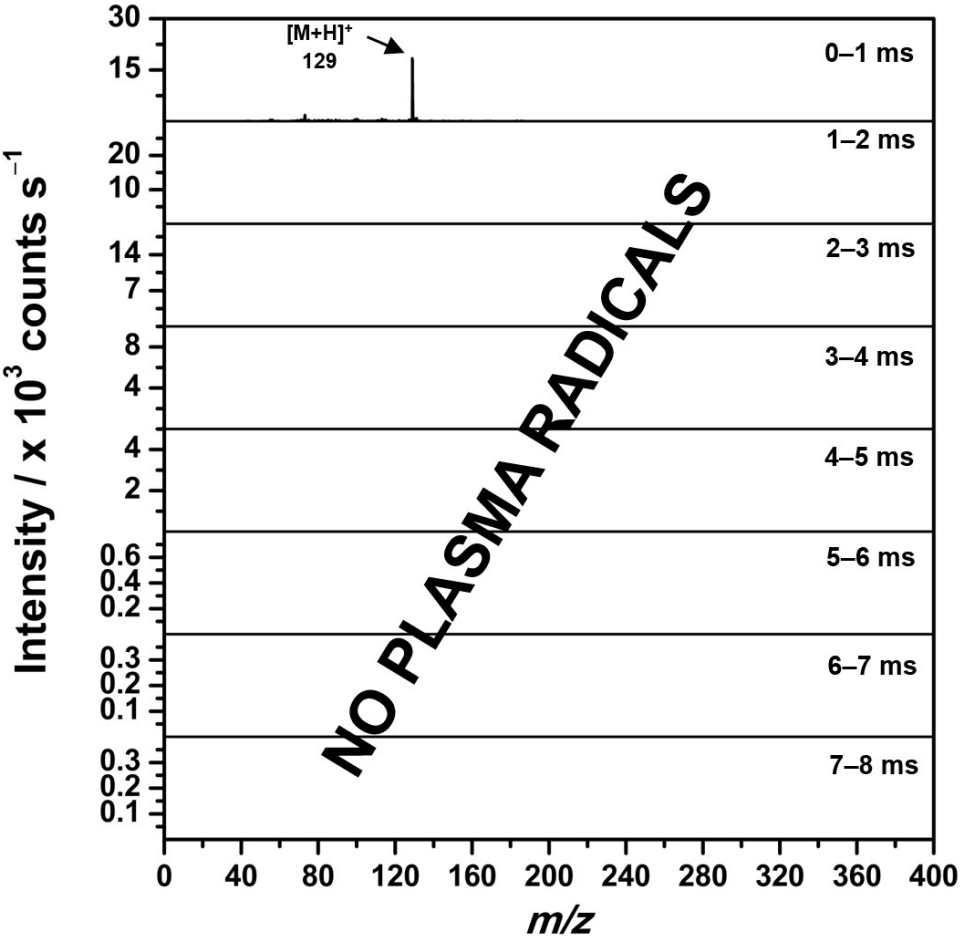

Figure 7.8: Off-period electron-impact ionisation mass spectra taken during consecutive 1 ms sampling time windows for butyl acrylate pulsed plasma (t_{on} = 50 µs, t_{off} = 10 ms, P_{on} = 7 W, and 0.1 mbar).

7.4 Discussion

Both time-averaged and off-time positive plasma ion analysis (Figure 7.3 and Figure 7.4b respectively) recorded high intensity signals of protonated monomer ($[M+H]^+$) and protonated dimer ($[2M+H]^+$) species. These results represent strong evidence for monomer unit addition via double bond opening (π-bond cleavage) with consequent recombination and chain growth by conventional polymerisation mechanism. In this reaction where protonated monomer ions (generated by plasma excitation during the on-time period) are functioning as initiating activated species (Scheme 7.1). Figure 7.5 shows consecutive positive ion mass spectra (1 millisecond-long) sampled from the off-time period. The protonated molecular ion signal (129 *m/z* = $[M+H]^+$) is found to be the most abundant species during the very first time frame (0–1 ms), while dimer species start to form from the second sample (1–2 ms) on.

When plasma radical species were investigated by both time-averaged and time-resolved electron-impact mass spectrometry, no dimer species were observed unlike positive ions. Plasma radicals only form during the on-time window, with mass species ranging from 28 to 129 *m/z*, and 56 *m/z* being the base peak. Off-time analysis showed very low radical concentration overall (10^2 count s^{-1} ion counting range). This was confirmed by consecutive samples during the off-period (Figure 7.8), where the majority of radical species (mostly 129 *m/z* = $[M+H]^+$) were generated at the very beginning (0–1 ms) of the off-time window, with no signal observed in the following time frames. This outcome can be explained by the low stability of secondary radicals formed by acrylates on the reactive sites (double bond).

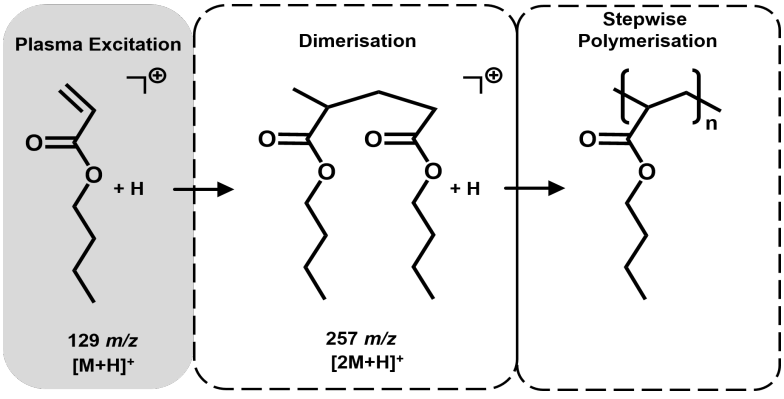

Scheme 7.1: Chain growth polymerisation mechanism for butyl acrylate pulsed plasma deposition of plasma ion species.

7.5 Conclusions

Pulsed plasma polymerisation of butyl acrylate mechanism was investigated by in situ mass spectrometry. Experimental results showed that butyl acrylate vapours exposed to pulsed electrical discharges lead to the formation, in the gas phase, of oligomer ionic species by monomer-monomer addition reaction. Such protonated butyl acrylate dimers (257 *m/z* = $[2M+H]^+$), indicate that the reaction pathway proceeds via subsequent addition of protonated monomer units due to the higher tendency of acrylates to form ions, unlike methacrylates that are more likely to generate radicals. Very low concentrations of plasma radical species were produced in the off-time period, this can be attributed to the relatively lower stability of secondary radicals in acrylates (compared to tertiary radicals of methacrylates). For this reason, it is plausible to assume that the formation of ionic species is more favourable for acrylate precursors.

REFERENCES

1 Coulson, S. R.; Woodward, I. S.; Badyal, J. P. S.; Brewer, S. A.; Willis, C. Ultralow Surface Energy Plasma Polymer Films. *Chem. Mater.* **2000**, *12*, 2031–2038.

2 Tarducci, C.; Schofield, W. C. E.; Badyal, J. P. S.; Brewer, S. A.; Willis, C. Cyano-Functionalized Solid Surfaces. *Chem. Mater.* **2001**, *13*, 1800–1803.

3 Kumar, V.; Pulpytel, J.; Arefi-Khonsari, F. Fluorocarbon Coatings via Plasma Enhanced Chemical Vapor Deposition of 1H,1H,2H,2H-Perfluorodecyl Acrylate-1, Spectroscopic Characterization by FT-IR and XPS. *Plasma Process. Polym.* **2010**, *7*, 939–950.

4 Song, Z.; Tang, J.; Li, J.; Xiao, H. Plasma-Induced Polymerization for Enhancing Paper Hydrophobicity. *Carbohydr. Polym.* **2013**, *92*, 928–933.

5 Loyer, F.; Bengasi, G.; Frache, G.; Choquet, P.; Boscher, N. D. Insights in the Initiation and Termination of Poly(Alkyl Acrylates) Synthesized by Atmospheric Pressure Plasma-Initiated Chemical Vapor Deposition (AP-PiCVD). *Plasma Process. Polym.* **2018**, *15*, 1800027.

6 Swift, G. Acrylic (and Methacrylic) Acid Polymers. In *Encyclopedia of Polymer Science and Technology*; John Wiley & Sons, Inc.: Hoboken, NJ, USA, 2002; Vol. 1, pp 96–124.

7 Voronin, S. a; Zelzer, M.; Fotea, C.; Alexander, M. R.; Bradley, J. W. Pulsed and Continuous Wave Acrylic Acid Radio Frequency Plasma Deposits: Plasma and Surface Chemistry. *J. Phys. Chem. B* **2007**, *111*, 3419–3429.

8 Alexander, M. R.; Duc, T. M. The Chemistry of Deposits Formed from Acrylic Acid Plasmas. *J. Mater. Chem.* **1998**, *8*, 937–943.

9 Schofield, W. C. E.; Badyal, J. P. S. Pulsed Plasma Polymerisation of Butylacrylate for Pressure-Sensitive Adhesion. Plasma Chem. Plasma Process. **2006**, 26, 361–369.

10 Carletto, A.; Badyal, J. P. S. Mechanistic Reaction Pathway for Hexafluoropropylene Oxide Pulsed Plasma Deposition of PTFE-like Films. *J. Phys. Commun.* **2017**, 1, 55024.

11 O'Toole, L.; Short, R. D.; Ameen, A. P.; Jones, F. R. Mass Spectrometry of and Deposition-Rate Measurements from Radiofrequency-Induced Plasmas of Methyl Isoburate, Methyl Methacrylate and N-Buthyl Methacrylate. *J. Chem. Soc. Faraday Trans.* **1995**, 91, 1363–1370.

12 NIST National Institute of Standard and Technology, U.S. Department of Commerce, NIST Mass Spectrometry Data Center. https://webbook.nist.gov/cgi/cbook.cgi?ID=C141322&Type=IR-SPEC&Index=1 (accessed Jan 3, 2019).

8 : CONCLUSIONS

In recent years, pulsed plasma polymerisation techniques have attracted considerable interest for the preparation of highly functionalised plasma polymer films. Pulsed plasma polymerisation allows the preservation of fragile functionality within monomer units allowing the construction and deposition of increasingly elaborated polymer scaffolds. Furthermore, these organic films possess similar properties to the ones obtained by conventional polymerisation. The work carried out during this project has led to a number of relevant observations concerning pulsed plasma deposition methods; our main findings are summarised below.

Time-resolved mass spectrometry is a powerful diagnostic tool to explore the double nature of pulsed polymerising plasmas. It has been shown that, from the mechanistic point of view, there are two distinct reaction regimes within the plasma phase, namely on-periods and off-periods. During each short burst of plasma (on-time window) monomer activation occurs with the consequent generation of reactive species (via ion, or electron bombardment). This is followed by propagation reactions leading to conventional polymerisation during the subsequent off-time window (in the absence of ion, or electron- induced damage). Both behaviours were successfully observed in the gas phase, for hexafluoropropylene oxide, glycidyl methacrylate, maleic anhydride and butyl acrylate.

For pulsed plasma deposition of PTFE-like thin films using hexafluoropropylene oxide precursors, the influence of the duty cycle on plasma generated species was investigated by in situ mass spectrometry. In chapter 4, it was demonstrated that shorter t_{on} values produced longer perfluoroalkyl plasma species. These experimental results are the direct consequence of perfluoroalkyl polymer chain propagation during the off-time (t_{off}) due to lower amount of energetic plasma ion-induced fragmentation. Additionally, the relative concentrations of neutral versus ionic plasma species was found to rise for shorter pulse duty cycles.

Glycidyl methacrylate pulsed plasmas have been investigated using time-resolved in situ mass spectrometry. A further confirmation of the efficiency of pulsed plasma methodologies can be found in the highly selective

step-wise monomer addition polymerisation mechanism observed during low pulsed plasma duty cycles (t_{on} = microseconds timescale, and t_{off} = milliseconds timescale). Analogous results were attained with maleic anhydride precursors, where sequential monomer addition gave rise to a distinct sequence of protonated, doubly protonated radical dimers ($[2M+H]^+$,$[2M+2H]^+$) and doubly protonated radical trimers $[3M+2H]^+$ during the extended off-period window.

Concerning the general mechanism, given that plasmas are usually identified as ionised gaseous systems, and the presence of ions is an essential requirement for creating the plasma state. It reasonable to assume that a direct correlation between the ionisation process and the formation of polymeric organic coatings may exist. However, it is worth to consider that the population of ions in a low pressure plasma is sensibly smaller compared to that of free radicals (for instance, laboratory or industrial glow discharges used for plasma polymerisation of organic monomers, contain nearly a million times more radical species than ions). For this reason, we believe that the plasma polymerisation mechanism is predominantly radical, as radical recombination reactions of activated monomer species are the main responsible for gas phase oligomerisation and the formation of functional organic deposits.

As a final remark, although mass spectrometry employed for diagnostic of reactive plasmas represents a convenient solution to explore the intricate nature of such systems, there are still some limitations. When operating in radical detection mode, plasma radical species must be ionised in order to be detected by the spectrometer (20 eV internal ion source), this operation is an additional source of fragmentation for fragile radical oligomers. As a result, high mass radical species are difficult to detect compared to their ion counterparts (which are generated at lower ionisation energies). Additionally, it has been documented that quadrupole mass filters suffer from poor focussing capabilities for the transmission of large ions, causing a substantial drop in sensitivity at higher masses. In order to fully characterise pulsed polymerising plasma, the use of complementary techniques (i.e. optical spectroscopies, Langmuir probes) would be the best case scenario.